

การศึกษาทางทฤษฎีของการดูดซับไฮโดรเจนบนท่อนาโนคาร์บอนผนังเดี่ยวแบบอาร์มแชร์ (5,5)



นางสาว ขวัญชนก ดลเสมอ

ศูนย์วิทยทรัพยากร

วิทยานิพนธ์นี้เป็นส่วนหนึ่งของการศึกษาตามหลักสูตรปริญญาวิทยาศาสตรมหาบัณฑิต

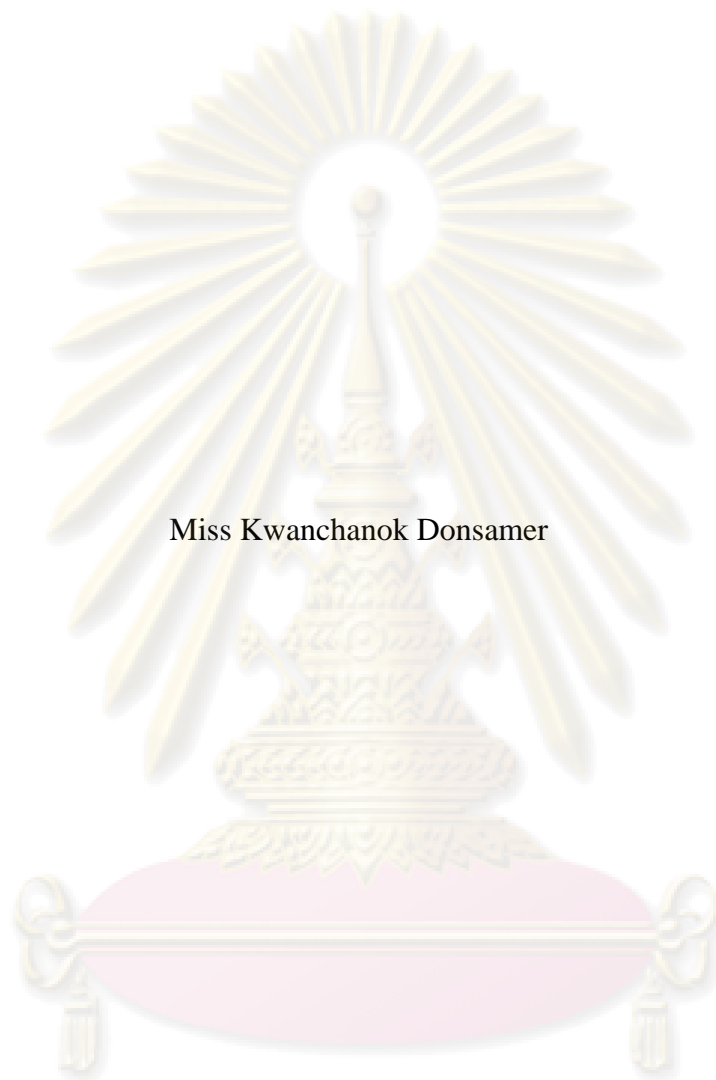
สาขาวิชาปิโตรเคมีและวิทยาศาสตร์พอลิเมอร์

คณะวิทยาศาสตร์ จุฬาลงกรณ์มหาวิทยาลัย

ปีการศึกษา 2551

ลิขสิทธิ์ของจุฬาลงกรณ์มหาวิทยาลัย

THEORETICAL STUDY OF HYDROGEN ADSORPTION ON ARMCHAIR (5,5) SINGLE-
WALLED CARBON NANOTUBES



Miss Kwanchanok Donsamer

A Thesis Submitted in Partial Fulfillment of the Requirements

for the Degree of Master of Science Program in Petrochemistry and Polymer Science

Faculty of Science

Chulalongkorn University

Academic Year 2008

Copyright of Chulalongkorn University

Thesis Title THEORETICAL STUDY OF HYDROGEN ADSORPTION ON ARMCHAIR (5,5) SINGLE-WALLED CARBON NANOTUBES
By Miss Kwanchanok Donsamer
Field of study Petrochemistry and Polymer Science
Thesis Principal Advisor Associate Professor Vithaya Ruangpornvisuti, Dr.rer.nat.

Accepted by the Faculty of Science, Chulalongkorn University in Partial Fulfillment of the Requirements for the Master's Degree

Deputy Dean for Administrative Affairs,
.....*Vimolvan Pimpan*.....Acting Dean, The Faculty of Science
(Associate Professor Vimolvan Pimpan, Ph.D.)

THESIS COMMITTEE

.....*Sirirat Kokpol*.....Chairman
(Associate Professor Sirirat Kokpol, Ph.D.)

.....*Vithaya Ruangpornvisuti*.....Thesis Principal Advisor
(Associate Professor Vithaya Ruangpornvisuti, Dr.rer.nat.)

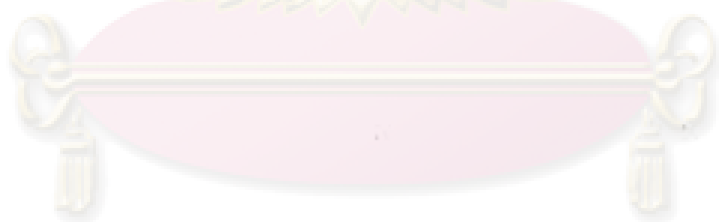
.....*Voravee Hoven*.....Member
(Assistant Professor Voravee Hoven, Ph.D.)

.....*Nuanphun Chantarasiri*.....Member
(Associate Professor Nuanphun Chantarasiri, Ph.D.)

.....*Akapong S.*.....External Member
(Akapong Suwattanamala, Ph.D.)

ขวัญชนก ตลเสมอ: การศึกษาทางทฤษฎีของการดูดซับไฮโดรเจนบนท่อนาโนคาร์บอน
ผนังเดี่ยวแบบอาร์มแชร์ (5,5) (THEORETICAL STUDY OF HYDROGEN
ADSORPTION ON ARMCHAIR (5,5) SINGLE-WALLED CARBON NANOTUBES)
อ. ที่ปรึกษาวิทยานิพนธ์หลัก: รศ.ดร. วิทยา เรืองพรวิสุทธิ์, 83 หน้า.

งานวิจัยนี้ศึกษาการดูดซับทางเคมีของไฮโดรเจนบนท่อนาโนคาร์บอนที่มีโครงสร้าง
สมบูรณ์และบกพร่องแบบ Stone-Wales ของท่อนาโนคาร์บอนชนิดผนังเดี่ยวแบบอาร์มแชร์ (5,5)
แบบปลายปิด (C_{80} , C_{90}) และปลายเปิด ($C_{70}H_{20}$) โดยใช้ทฤษฎีการคำนวณโดยวิธีเดนซิติฟังก์ชัน
ชั้น ศึกษาพลังงานการดูดซับไฮโดรบนท่อนาโนคาร์บอน ที่ใช้โครงสร้างแบบยืดหยุ่นและแบบคงตัว
ศึกษาที่ชนิดการคำนวณแบบ B3LYP และเบสิสเซต 3-21G และ 6-31G(d) และกลไกการดูดซับ
ได้ถูกนำเสนอ จากการคำนวณพบว่าการดูดซับบนท่อนาโนคาร์บอนแบบยืดหยุ่นแข็งแรงมากกว่า
บนท่อนาโนคาร์บอนแบบคงตัว พลังงานการดูดซับไฮโดรเจนแบบปฏิกิริยาแอดดิชัน บนพันธะ C-
C ชนิด I, II และ III บริเวณที่เป็นโครงสร้างบกพร่องแบบ Stone-Wales ระหว่างโครงสร้างแบบ
ยืดหยุ่นไม่แตกต่างกับแบบคงตัว สำหรับท่อแบบปลายเปิดและปลายปิด (C_{90}) และปลายเปิด
($C_{70}H_{20}$) การดูดซับจะบนพันธะ C1-C2 (ชนิด I) พบว่าสูงกว่าบนพันธะ C1-C3 (ชนิด II) ส่วนการ
ดูดซับบนท่อปลายปิด (C_{80}) บนพันธะ C2-C4 (ชนิด III) สูงกว่าบนพันธะชนิดอื่นๆ ส่วนการดูดซับ
บนท่อนาโนคาร์บอนที่โดปด้วยอะตอมโบรอน มีค่าสูงกว่าการดูดซับบนท่อนาโนคาร์บอนปกติ



ศูนย์วิทยทรัพยากร จุฬาลงกรณ์มหาวิทยาลัย

สาขาวิชา ปิโตรเคมีและวิทยาศาสตร์พอลิเมอร์ ลายมือชื่อ นิสิต.....ขวัญชนก ตลเสมอ.....
ปีการศึกษา..... 2551..... ลายมือชื่อ อ.ที่ปรึกษาวิทยานิพนธ์หลัก.....*Prof. Dr. Witaya Ruangsri*

4972234323: PETROCHEMISTRY AND POLYMER SCIENCE PROGRAM

KEY WORD: HYDROGEN STORAGE / CHEMISORPTION / SWCNT/ DFT

KWANCHANOK DONSAMER: THEORETICAL STUDY OF HYDROGEN ADSORPTION ON ARMCHAIR (5,5) SINGLE-WALLED CARBON NANOTUBES. THESIS PRINCIPAL ADVISOR: ASSOC. PROF. VITHAYA RUANGPORNVISUTI, Dr.rer.nat., 83 pp.

The chemisorption of hydrogen molecule on pristine and Stone-Wales defect armchair (5,5) SWCNTs of cap-ended C_{80} , C_{90} and open-ended $C_{70}H_{20}$ has been investigated using density functional theory (DFT) calculations. The adsorption energies of hydrogen molecule on these various SWCNTs of which the structures treated as the flexible and rigid models were obtained at the B3LYP3-21G and B3LYP/6-31G(d) methods and adsorption mechanism were proposed. It was found that adsorption on the SWCNTs as flexible models are stronger than the rigid models. The adsorption energy of hydrogen addition on C-C bond types I, II and III around the Stone-Wales defect area of all the SWCNTs based on the flexible model are hardly different from their pristine SWCNTs. The adsorption energies on the C_1-C_2 bond (type I) are higher than on the C_1-C_3 bond (type II) for the cap-ended C_{90} and open-ended $C_{70}H_{20}$. The adsorption on the cap-ended C_{80} at the C_2-C_4 bond (type III) is higher than on other bond types. In all cases, the adsorption energies on the B-doped SWCNTs are higher than on their corresponding non-doped SWCNTs.

ศูนย์วิทยทรัพยากร
จุฬาลงกรณ์มหาวิทยาลัย

Field of study: Petrochemistry and Polymer Science Student's signature: Kwanchanok Donsamer

Academic year: 2008

Principal Advisor's signature: Vithaya Ruangpornvisuti

ACKNOWLEDGEMENTS

This research was partially supported by the NCE-PPAM (National Center of Excellence for Petroleum, Petrochemicals and Advanced Materials) and NANOTEC, Grant No.NN-B-22-m10-10-49-18, National Science and Technology Development Agency, Thailand.

I would like to express my sincere gratitude to my advisor Associate Professor Dr.Vithaya Ruangpornvisuti for his continuous attention and guidance though the years of my study. I deeply appreciate suggestion and comments of my committee members, Associate Professor Dr. Sirirat Kokpol, Assistant Professor Dr.Voravee Hoven, Associate Professor Dr. Nuanphun Chantarasiri and Dr. Akapong Suwattanamala.

The greatest thanks are extended to Dr. Wichien Sang-aroon and Ms. Raina Wabayor who always assists intensive quantum and computational chemistry details. Moreover, I greatly appreciated the Petrochemistry and Polymer Science Program and Graduate School Chulalongkorn University for research grant.

Finally, I would like to dedicate this to my parents, for their love, understanding and support for me is priceless.



ศูนย์วิจัยทรัพยากร
จุฬาลงกรณ์มหาวิทยาลัย

CONTENTS

	Page
ABSTRACT IN THAI	iv
ABSTRACT IN ENGLISH	v
ACKNOWLEDGEMENTS	vi
CONTENTS	vii
LIST OF FIGURES	x
LIST OF TABLES	xiii
LIST OF ABBREVIATIONS AND SYMBOLS	xv
CHAPTER I INTRODUCTION	1
1.1 Background.....	1
1.2 Carbon nanotubes (CNTs).....	1
1.2.1 Classification of CNTs	3
1.2.1.1 Armchair SWCNT.....	4
1.2.1.2 Zig Zag SWCNT.....	4
1.2.1.3 Chiral SWCNT.....	5
1.2.2 Properties of CNTs	5
1.2.2.1 Physical properties.....	5
1.2.2.2 Chemical properties.....	7
1.2.3 Defect on carbon nanotubes.....	7
1.3 Boron-doped carbon nanotubes.....	8
1.4 Literature reviews.....	9
1.5 Objective.....	11
CHAPTER II THEORETICAL BACKGROUND	12
2.1 Molecular mechanics.....	13
2.2 Electronic structure methods.....	14
2.2.1 Semi-Empirical methods	14
2.2.1.1 AM1 method.....	15
2.2.1.2 PM3 method.....	15

	Page
2.2.2 Ab initio methods.....	16
2.2.3 Density functional methods (DFT) methods.....	17
2.2.4 The Kohn-Sham energy and the Kohn-Sham equations.....	18
2.2.4.1 The Kohn-Sham energy.....	18
2.2.4.2 The Kohn-Sham equations.....	21
2.2.4.3 Hybrid methods.....	22
2.2.5 ONIOM methods.....	23
2.2.5.1 ONIOM energy definition.....	25
2.2.5.2 Treatment of link atoms.....	26
2.3 Basis sets.....	28
2.3.1 Minimal basis sets.....	29
2.3.2 Split valence basis sets	29
2.3.2.1 Polarized basis sets.....	30
2.3.3.2 Diffuse functions.....	31
2.4 Transition state theory	32
2.5 Molecular vibrational frequencies.....	33
CHAPTER III DETAILS OF THE CALCULATIONS.....	35
3.1 Methods of calculations.....	35
3.1.1 Full-structure optimization.....	36
3.1.2 Partial-structure optimization.....	37
3.1.3 ONIOM approach and transition state calculation.....	38
3.1.4 Structure models and ONIOM approach for B-doped SWCNTs	39
3.1.4.1 B-doped pristine SWCNTs.....	40
3.1.4.2 B-doped SW defect SWCNTs.....	41
CHAPTER IV RESULTS AND DISCUSSION	43
4.1 Adsorption of hydrogen on pristine and SW defect SWCNTs.....	43
4.1.1 The full-structure optimization.....	43
4.1.2 The partial-structure optimization.....	50

	Page
4.2 Adsorption mechanism of addition of hydrogen molecule to armchair (5,5) SWCNTs.....	55
4.3 B-doped armchair (5,5) SWCNTs	57
4.3.1 B-doped type I.....	58
4.3.2 B-doped type II.....	61
4.3.3 B-doped type III.....	65
CHAPTER V CONCLUSIONS.....	70
Suggestion for future work.....	71
REFERENCES.....	72
APPENDIX.....	76
APPENDIX A.....	77
VITA.....	83



 ศูนย์วิจัยทรัพยากร
 จุฬาลงกรณ์มหาวิทยาลัย

LIST OF FIGURES

Figure		Page
1.1	Molecular structures of a single-walled carbon nanotube (SWCNT) and of a multi-walled carbon nanotube (MWCNT).....	2
1.2	Molecular structures of (a) cap-ended and (b) open-ended carbon nanotubes.....	2
1.3	Graphene sheet with (n,m) scheme for naming its rolled nanotube.....	3
1.4	Structure of armchair (6,6) SWCNT	4
1.5	Structure of zig zag (10,0) SWCNT	4
1.6	Structure of chiral (8,3) SWCNT.....	5
1.7	Structure of the Stone-Wales (SW) defect compare to the pristine cluster.....	8
2.1	The ONIOM extrapolation scheme for a molecular system partitioned into two (left) and three (right) layers.....	25
2.2	Definition of different atom sets within the ONIOM scheme.....	26
2.3	Schematic illustration of reaction path.....	32
3.1	The atom numbers given in the structures indicate the position where two hydrogen atoms were added at the pristine (a) cap-ended C ₈₀ , (b) C ₉₀ and (c) open-ended C ₇₀ H ₂₀ and the SW defect (d) cap-ended SW-C ₈₀ , (e) SW-C ₉₀ and (f) open-ended SW-C ₇₀ H ₂₀ SWCNTs.....	35
3.2	The atom numbering and C-C bond types of adsorption atoms defined for (a) the pristine and (b) SW defect SWCNTs. These clusters are fractions of their whole structure which our illustrated in Figure 3.1....	36
3.3	Two types of surface defined as high and low levels of theory for the two layer ONIOM approach of pristine (a) cap-ended C ₈₀ , (b) C ₉₀ and (c) open-ended C ₇₀ H ₂₀ , SW defect (d) cap-ended SW-C ₈₀ , (e) SW-C ₉₀ and (f) open-ended SW-C ₇₀ H ₂₀ SWCNTs. Ball type is of area for high level of theory.....	38
3.4	Possibility of doping types for two boron atoms into armchair (5,5) SWCNTs are defined as (a) type I, (b) type II and (c) type III for pristine and (d) type I, (e) type II and (f) type III for SW defect.....	39

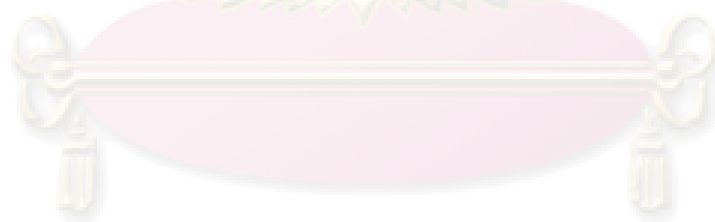
Figure	Page
3.5	40
<p>The atom numbers given in the structures indicate the position where two hydrogen atoms were added at the pristine (a), (d), (g) cap-ended B_2C_{88}, (b), (e), (g) B_2C_{88} and (c), (f), (i) open-ended $B_2C_{68}H_{20}$ B-doped SWCNTs (doping type I (a), (b), (c), doping type II (d), (e), (f), doping type III (g), (h), (i)). Their clear views are located on the right.....</p>	
3.6	41
<p>The atom numbers given in the structures indicate the position where two hydrogen atoms were added at the SW defect (a), (d), (g) cap-ended SW-B_2C_{88}, (b), (e), (g) SW-B_2C_{88} and (c), (f), (i) open-ended SW-$B_2C_{68}H_{20}$ B-doped SWCNTs (doping type I (a), (b), (c), doping type II (d), (e), (f), doping type III (g), (h), (i)). Their clear views are located on the right.....</p>	
4.1	44
<p>Adsorption of double hydrogen-atoms to pristine cap-ended C_{80}, C_{90} and open-ended $C_{70}H_{20}$ on two carbon atoms of bond type I (a),(d),(f) bond type II (b),(e),(g) bond type III (c) and bond length are defined. Their relative energies are at the B3LYP/6-31G(d) and B3LYP/3-21G (in parenthesis), in kcal/mol.</p>	
4.2	45
<p>Adsorption of double hydrogen-atoms to SW defect of cap-ended C_{80}, C_{90} and open-ended $C_{70}H_{20}$ on two carbon atoms of bond type I (a),(d),(f) bond type II (b),(e),(g) bond type III (c) and bond length are defined. Their relative energies are at the B3LYP/6-31G(d) and B3LYP/3-21G (in parenthesis), in kcal/mol.....</p>	
4.3	51
<p>Adsorption of double hydrogen-atoms to rigid structure of pristine cap-ended C_{80}, C_{90} and open-ended $C_{70}H_{20}$ on two carbon atoms of bond type I (a),(d),(f) bond type II (b),(e),(g) bond type III (c) and bond length are defined. Their relative energies are at the B3LYP/6-31G(d) and B3LYP/3-21G (in parenthesis), in kcal/mol.....</p>	
4.4	52
<p>Adsorption of double hydrogen-atoms to rigid structure of SW defect of cap-ended C_{80}, C_{90} and open-ended $C_{70}H_{20}$ on two carbon atoms of bond type I (a),(d),(f) bond type II (b),(e),(g) bond type III (c) and bond length are defined. Their relative energies are at the B3LYP/6-31G(d) and B3LYP/3-21G (in parenthesis), in kcal/mol.....</p>	

Figure	Page	
4.5	Transition-state of structures adsorption process on the pristine (a) cap-ended C_{80} , (b) C_{90} , (c) open-ended $C_{70}H_{20}$ and the SW defect (d) cap-ended SW- C_{80} , (e) SW- C_{90} , (f) open-ended SW- $C_{70}H_{20}$ armchair (5,5) SWCNTs.....	56
4.6	Addition of hydrogen molecule to C–C binding site.....	56
4.7	Adsorption complexes of two hydrogen-atoms adsorbed on various pristine armchair (5,5) B-doped SWCNTs (type I).....	58
4.8	Adsorption complexes of two hydrogen-atoms adsorbed on various Stone-Wales defect armchair (5,5) B-doped SWCNTs (type I).....	59
4.9	Adsorption complexes of two hydrogen-atoms adsorbed on various pristine armchair (5,5) B-doped SWCNTs (type II).....	62
4.10	Adsorption complexes of two hydrogen-atoms adsorbed on various Stone-Wales defect armchair (5,5) B-doped SWCNTs (type II).....	63
4.11	Adsorption complexes of two hydrogen-atoms adsorbed on various pristine armchair (5,5) B-doped SWCNTs (type III).....	66
4.12	Adsorption complexes of two hydrogen-atoms adsorbed on various Stone-Wales defect armchair (5,5) B-doped SWCNTs (type III).....	67

LIST OF TABLES

Table		Page
4.1	Total energy and relative energy of pristine and SW defect SWCNTs calculated at B3LYP/3-21G and B3LYP/6-31G(d) levels of theory.....	46
4.2	Total energy of bare tube at adsorbed form and strain of pristine and SW defect SWCNTs calculated at B3LYP/3-21G and B3LYP/6-31G(d) levels of theory.....	47
4.3	Adsorption energy of hydrogen molecule and two hydrogen atom to pristine and SW defect SWCNTs calculated at B3LYP/3-21G and B3LYP/6-31G(d) levels of theory.....	48
4.4	Pyramidalization angle of pristine and the SW defect armchair (5,5) SWCNTs.....	49
4.5	Total energy and relative energy of rigid structure of pristine and SW defect SWCNTs calculated at B3LYP/3-21G and B3LYP/6-31G(d) levels of theory using frozen models.....	53
4.6	Interaction energy of hydrogen molecule and two hydrogen atoms on rigid structure of pristine and SW-defect SWCNTs calculated at B3LYP/3-21G and B3LYP/6-31G(d) levels of theory using frozen models.....	54
4.7	Activation energies and single imaginary vibrational frequencies of hydrogen molecule adsorbed to pristine and SW defect armchair (5,5) SWCNTs, at the ONIOM(B3LYP/6-31G(d):AM1) and ONIOM(B3LYP/3-21G:AM1) (in parenthesis).....	55
4.8	Adsorption energies of hydrogen molecule and two proton-radicals on various pristine and SW defect armchair (5,5) B-doped SWCNTs (type I).....	60
4.9	Interaction energies of hydrogen molecule and two proton-radicals on various rigid structure of pristine and SW defect armchair (5,5) B-doped SWCNTs (type I).....	61

Table	Page
4.10 Adsorption energies of hydrogen molecule and two proton-radicals on various pristine and SW defect armchair (5,5) B-doped SWCNTs (type II).....	64
4.11 Interaction energies of hydrogen molecule and two proton-radicals on to various rigid structures of pristine and SW defect armchair (5,5) B-doped SWCNTs (type II).....	65
4.12 Adsorption energies of hydrogen molecule and two proton-radicals on various pristine and SW defect armchair (5,5) B-doped SWCNTs (type III).....	68
4.13 Interaction energies of hydrogen molecule and two proton-radicals on to various rigid structure of pristine and SW defect armchair (5,5) B-doped SWCNTs (type III).....	69

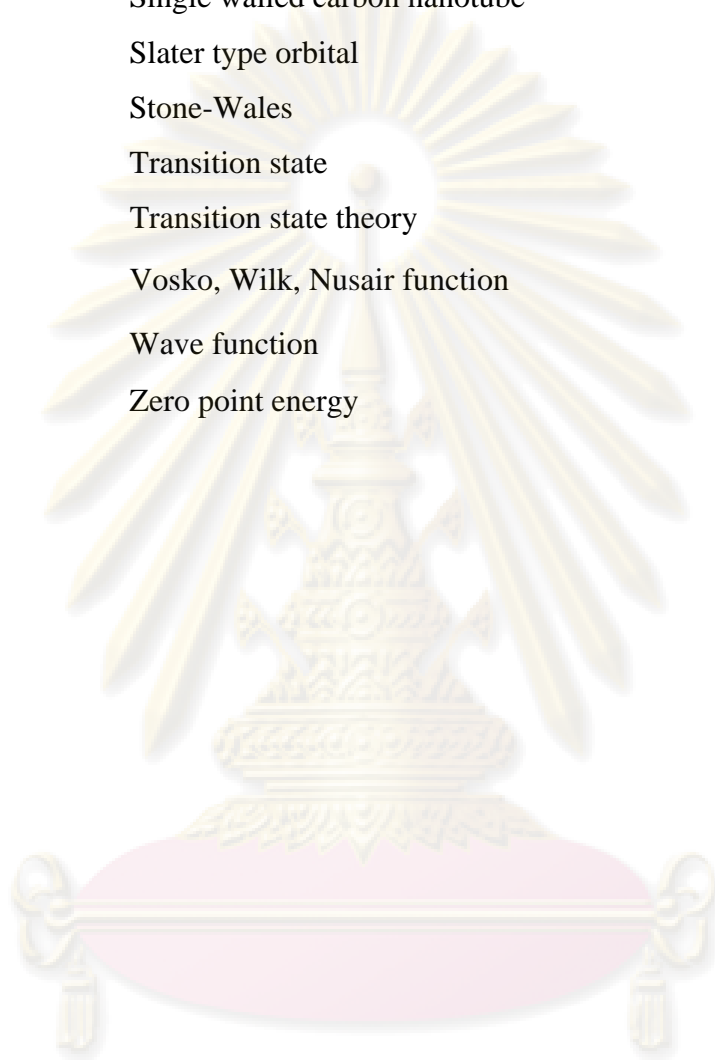


ศูนย์วิทยทรัพยากร
จุฬาลงกรณ์มหาวิทยาลัย

LIST OF ABBREVIATIONS AND SYMBOLS

\AA	Angstrom
AM1	Austin model 1
B3LYP	Beck 3 Lee–Yang–Parr
CNT	Carbon nanotube
d_t	Carbon nanotubes diameter
θ	Chiral angle
Ch	Chiral vector
CNDO	Complete neglect of differential diatomic overlap
DFT	Density functional theory
ρ	Electron density
E	Energy
H	Enthalpy
v_{xc}	Exchange correlation potential
f	Function of the coordinates
G	Gibbs free energy
ρ_r	Ground state electron density
ν_k	Harmonic vibrational frequency
\hat{H}	Hamiltonian operator
HF	Hartree–Fock
INDO	Intermediate neglect of differential diatomic overlap
ν_i	Imaginary vibrational frequencies
Kcal/mol	Kilocalorie per mole
ϵ_i^{KS}	Kohn-Sham energy levels
\hat{h}^{KS}	Kohn-Sham operator
ψ_i^{KS}	Kohn-Sham spatial orbital
E_c^{LYP}	LYP correlation functional
MNDO	Modified neglect of differential overlap
MWCNT	Multi walled carbon nanotube
NDDO	Neglect of differential diatomic overlap

ONIOM	Our N-layer integrated molecular orbital + molecular mechanics
PM3	Parametric number 3
PBCs	Periodic boundary conditions
SWCNT	Single walled carbon nanotube
STO	Slater type orbital
SW	Stone-Wales
TS	Transition state
TST	Transition state theory
E_x^{VWN}	Vosko, Wilk, Nusair function
ψ	Wave function
ZPE	Zero point energy



ศูนย์วิทยทรัพยากร
จุฬาลงกรณ์มหาวิทยาลัย

CHAPTER I

INTRODUCTION

1.1 Background

Hydrogen is considered as an ideal material for alternative energy source. Because hydrogen is the most plentiful element on earth, it is a clean burning fuel that produces neither carbon dioxide nor toxic emissions and can be used for electricity production, transportation, and other energy needs. Hydrogen is not commonly found in its pure form, since it readily combines with other elements and is most commonly found in combination with oxygen in water, and in organic matter including living plants, petroleum, coal, natural gas and other hydrocarbon compounds. One of the major problems faced by the hydrogen economy is the lack of proper storage media of hydrogen. Compress gas or liquid hydrogen are currently being used in hydrogen-fueled vehicles, but they inherently have serious technical drawbacks such as bulky tank size, safety problems, and extra energy cost for liquidation, which should be critical issues for commercial hydrogen storages or in new forms of materials such as metal hydride, carbon nanotubes and chemical hydrides. As the development of hydrogen storage in various systems for the large-scale application of fuel cells, mobiles and automotive uses has been lot of interest, materials research is going on throughout the world with various adsorption mechanisms to increase the storage capacity [1]. The use of SWCNTs as a material for safety and effective storage of hydrogen have been investigated by many experimental [2-7] and theoretical groups [8-12]. In this research, we considered about carbon nanotubes that could be storage hydrogen on it structure.

1.2 Carbon nanotubes (CNTs)

Carbon nanotubes are one allotrope of carbon, pure carbons have only two covalent bonds of sp^2 and sp^3 which sp^2 is a strong bond with in a plane but weak between planes. When sp^2 bonds come together carbon atoms are form hexagonal ring gives graphite sheet generated. The tube can be rolled-up from graphene sheet.

Carbon nanotubes have simulated a widespread research interest in recent year due to their high tensile strength, ultra-high stiffness, high current carrying capacity and high thermal conducting. As shown in Figure 1.1, two types of carbon nanotubes exist in nature is single-walled carbon nanotubes (SWCNTs), have only one single layer of graphene sheet rolled into cylindrical shape while multi-walled carbon nanotubes (MWCNTs) have more than two layers [13].

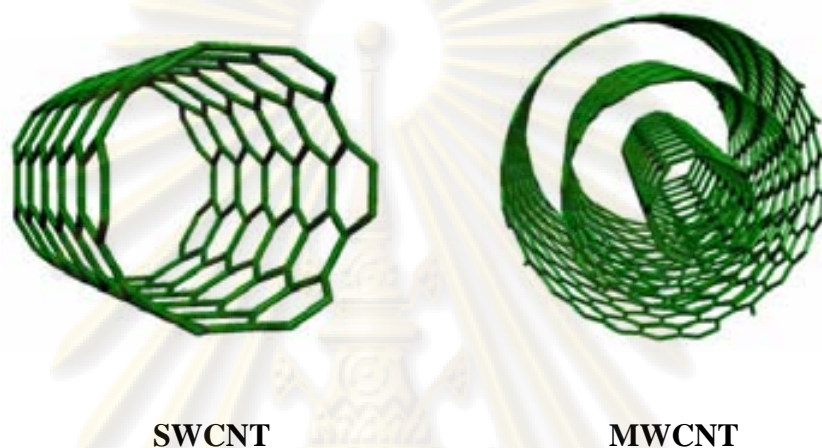


Figure 1.1 Molecular structures of a single-walled carbon nanotube (SWCNT) and of a multi-walled carbon nanotube (MWCNT).

Termination at the edge of carbon nanotube can defined into two type: if the edges of the nanotubes were terminated by hydrogen atoms called open-ended and if the edges of the nanotubes is capped with half of a fullerene molecule called cap-ended as shown Figure 1.2.

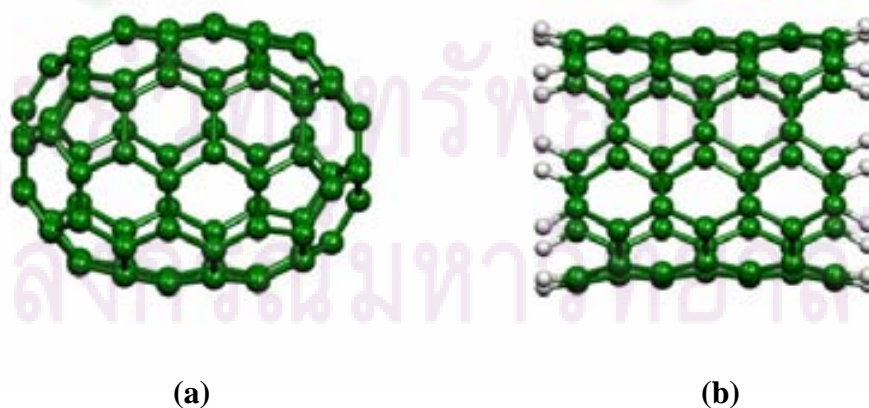


Figure 1.2 Molecular structures of (a) cap-ended and (b) open-ended carbon nanotubes.

1.2.1 Classification of CNTs

The way the graphene sheet is wrapped is represented by a pair of indices (n,m) called the chiral vector (C_h) , $C_h = na_1 + ma_2$ (n,m) . The unit vectors of the unit cell is a_1 and a_2 , the integers n and m denote the number of unit vectors along two directions in the honeycomb crystal lattice of graphene, that vary in accordance with the size of the carbon nanotubes diameter (d_t) and its chiral angle (θ) as shown in equations 1.1 and 1.2, where $a = 2.46 \text{ \AA}$ is the lattice constant of a graphene layer. The carbon nanotubes is formed by connecting A and A' point. Due to the way they rolled-up in Figure 1.3, there are three types of carbon nanotubes [13].

$$d_t = a\sqrt{n^2 + m^2 + nm} \quad (1.1)$$

$$\cos \theta = \frac{2n + m}{2\sqrt{n^2 + m^2 + nm}} \quad (1.2)$$

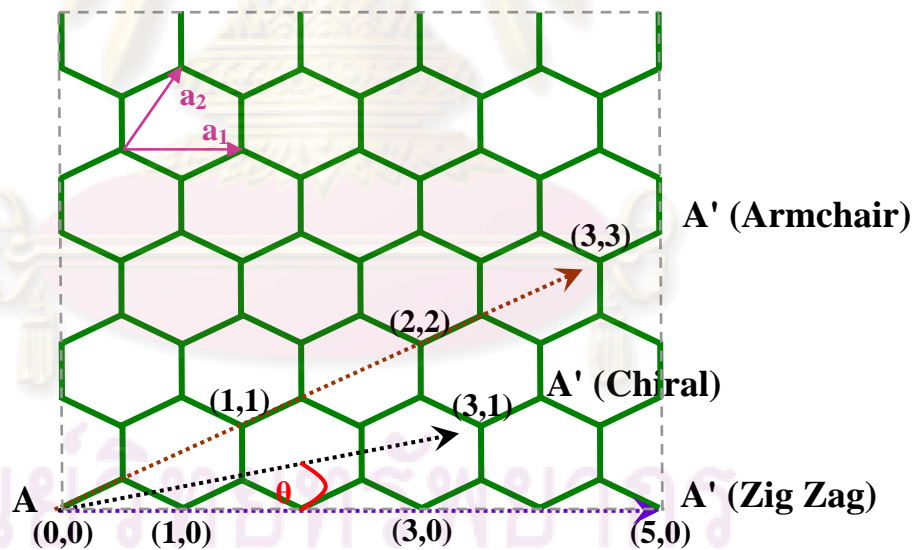


Figure 1.3 Graphene sheet with (n,m) scheme for naming its rolled nanotube.

1.2.1.1 Armchair SWCNT

An armchair nanotube has a chiral vector where $n = m$, therefore $C_h = (n, n)$ and chiral angle is 30° . The symmetrical classification of an armchair nanotube is an achiral nanotube. Achiral means the nanotube has a structure that is a mirror image of the original one.

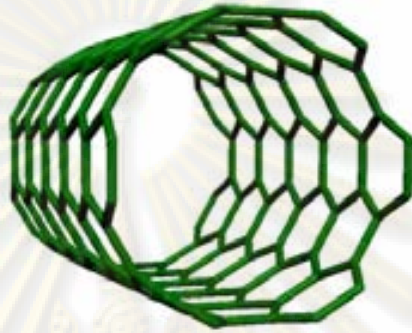


Figure 1.4 Structure of armchair (6,6) SWCNT.

1.2.1.2 Zig Zag SWCNT

A zigzag nanotube has a chiral vector where $m = 0$, therefore $C_h = (n, 0)$ and chiral angle is 0° . The symmetrical classification of a zigzag nanotube is an achiral nanotube, the same as an armchair nanotube. Achiral means the nanotube has a structure that is a mirror image of the original one.

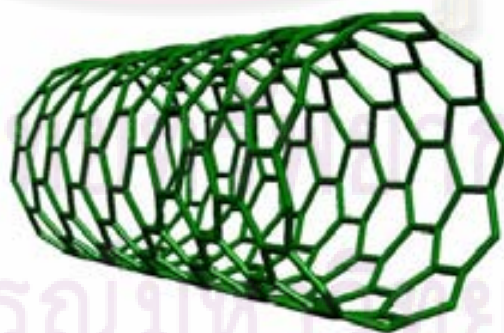


Figure 1.5 Structure of zigzag (10,0) SWCNT.

1.2.1.3 Chiral SWCNT

A chiral nanotube has general n and m values, therefore $C_h = (n, m)$ and chiral angle is between 0° and 30° . The symmetrical classification of a chiral nanotube is a chiral nanotube. Chiral means the nanotube has a spiral symmetry, which does not give it an identically structured mirror image.

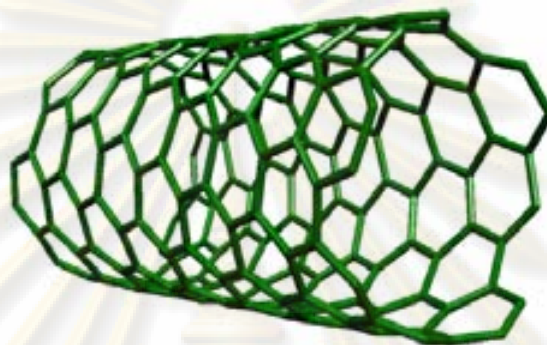


Figure 1.6 Structure of chiral (8,3) SWCNT.

1.2.2 Properties of CNTs

Their ability quickly adsorbs high densities of hydrogen at room temperature and atmospheric pressure. The interaction of hydrogen and single-walled carbon nanotubes is between the Van der Waals force of the single-walled carbon nanotubes and chemical bonds of the hydrogen molecule (as opposed to being due to hydrogen dissociation).

1.2.2.1 Physical properties

The strength of the sp^2 carbon-carbon bonds gives carbon nanotubes amazing mechanical properties. Carbon nanotubes have two types of bonds. Along the cylinder wall the σ bonds form the hexagonal network, which is found in graphite in its pure form. The π bonds point perpendicular to the nanotubes surface. This bonding structure, which is stronger than the sp^3 bonds found in diamond, provides the molecules with their unique strength. A single-walled carbon nanotube is stronger than that steel with the same weight. The Young's Modulus of SWCNT is up to 1000 GPa, which is 5 times greater than steel (230 GPa) while the density is only 1.3 g/cm^3 .

The tensile strength, or breaking strain of nanotubes can be up to 63 GPa which is higher than steel. That means that materials made of carbon nanotubes are lighter and more durable. In addition, the thermal conductivity of carbon nanotubes is 2000 W/m.K which is five times greater than that of copper (400 W/m.K). These properties coupled with the lightness of carbon nanotubes, gives them great potential in applications such as aerospace. There may be other applications due to these properties, such as car bumpers, and strong wires. Nanotubes also have a very high aspect ratio. The lengths of carbon nanotubes are usually around 1 μm , while the diameter for SWCNT is only 1 nm (50 nm for MWCNT). This property makes carbon nanotubes to use full for tips of electron probes and nanowires [14].

Another advantage of carbon nanotubes is their behaviour under compression. Unlike carbon fibres, which fracture easily under compression, carbon nanotubes form kink-like ridges that can relax elastically when the stress is released. As a result, nanotubes not only have the desirable properties of carbon fibres, but are also much more flexible and they can be compressed without fracture. Such excellent mechanical properties could lead to applications in their own right, or in conjunction with other desirable properties.

Especially notable is the fact that nanotubes can be metallic or semiconductor character depending on diameter and chirality of the tubes. There are two basic approaches to calculate the electronic energy bands of a material. The idea of the free-electron approximation is that the electrons in a crystal move essentially as free particle. Due to symmetry and unique electronic structure of graphene, the structure of a nanotube strongly affects its electronic properties. For a given (n,m) nanotube, if $2n + m = 3q$ (where q is an integer), then the semiconductor is metallic, otherwise the nanotube is a semiconductor. Thus all armchair ($n=m$) nanotubes are metallic. At the same time, carbon nanotubes have been studied to make switches and transistors, which would be much smaller than the silicon chips currently used. The wires made by carbon nanotubes are capable of currents that are 100 times greater than metal wires, making carbon nanotubes useful in the production of flat panels [13].

1.2.2.2 Chemical Properties

It has been indicated that carbon nanotubes can interact with different types of compounds. The development of efficient methodologies for the chemical modification of carbon nanotube has simulated the preparation of soluble carbon nanotube that can be employed in several biological applications. SWCNTs have a large specific surface area exhibited very good adsorption properties lead to given their capacity for adsorption, such as adsorbing the gaseous molecule on the surface. The adsorption properties provide the opportunities for applications, such as gases storage [15]. These SWCNT structures contain a number of different adsorption sites with different adsorption potential. Both experimental and theoretical chemistry were studied the physisorption and chemisorption of carbon dioxide, nitrogen, oxygen and water [13,16], methane and krypton [17] with carbon nanotubes. Recently, carbon nanotubes have been reported as supports for catalyst. Another property of carbon nanotubes is their ability to quickly adsorb high densities of hydrogen at room temperature and atmospheric pressure [7]. The experimental and simulation adsorptions for studies of hydrogen storage in carbon nanotubes have been reviewed by Darkrim *et al.* [18].

1.2.3 Defect on carbon nanotubes

Perfect graphene sheets and carbon nanotubes are known to have high chemical stability and unique physical properties resulting from the strong π -interactions of their hexagonal networks. Carbon nanotubes are not found to form perfect structures which due to the presence of defect such as vacancies, Stone-Wales (SW) defect, pentagons and heptagons and dopants, are believed to have a pivotal role in tailoring the physical and chemical properties of graphenes and carbon nanotubes. Indeed, a number of recent theoretical investigations revealed the higher chemical reactivity of Stone-Wales defects than that of PS in the sidewalls of zigzag $(n,0)$ single-wall carbon nanotubes (SWNTs) and planar graphenes (polycyclic graphite fragments). However, the chemical reactivity of Stone-Wales defects in the sidewalls of armchair (n,n) SWNTs has not been examined theoretically before now.

SW defect which defined as a 5-7-7-5 (C₁₆) cluster model as shown in Figure 1.7, is a topological defects play a dominant role in creating new structure of carbon nanotubes [19,20]. Stone-Wales defect is one of the most important topological defects in carbon nanotubes, consisting of two pentagon-heptagon pairs can be created by a 90° rotation of a C-C bond in a hexagonal ring network of the carbon nanotubes (SW-transformation) [21]. Due to the presence of structural defect believed that which will affect to the hydrogen storage capacity in carbon nanotubes. This result may prove to be an interesting one that needs more attention on the aspect of chemisorption in SWCNTs with various structures [22].

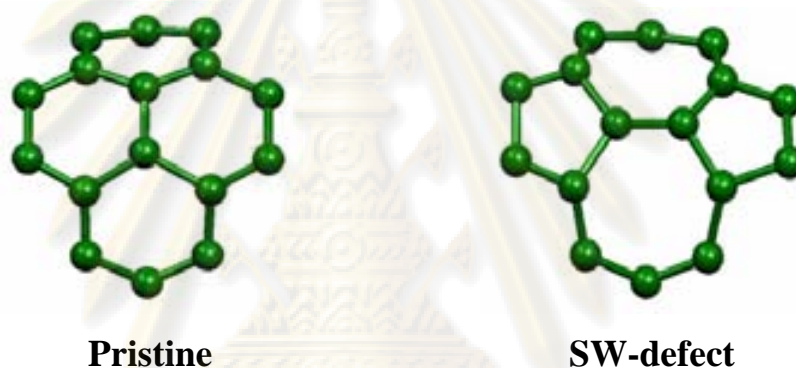


Figure 1.7 Structure of the Stone-Wales (SW) defect compare to the pristine cluster.

1.3 Boron-doped carbon nanotubes

Researchers have conducted numerous experiments and simulation aimed at developing their adsorption capacity of carbon nanotubes. Most of the work has involved pure carbon nanotubes. These are inert systems, their outer walls are not reactive and they show great mechanical stability. Doping carbon nanotubes is one of choice to increase adsorption energy.

When a foreign atom is inserted in the nanotube lattice, its symmetry is altered and its structure and properties immediately change. Many research report about doping various atoms into carbon nanostructure. Boron is a hard refractory material a little like diamond. Boron is the first that comes to mind as a dopant. However, both boron and carbon are chemical elements and they are in the same row of the periodic

table but carbon is not a common element on earth while boron is readily available in nature. Therefore, B-doped carbon nanotubes have been investigated in many report [23,24] and boron doped carbon nanotubes are needs to enhance the hydrogen molecule binding energy.

1.4 Literature review

Many experimental and theoretical groups have investigated the use of SWCNTs as material for the safe and effective storage of hydrogen.

In 2000, Wu *et al.* [25] synthesised the multi-walled carbon nanotubes from the catalytic decomposition of CO and CH₄ on powder Co/La₂O₃ catalysts. TEM and HR-TEM, XRD and TGA were used to characterize carbon nanotubes. It was found that the size of the nanotubes was controllable by adjusting the composition of the catalysts and the crystallinity could be improved by annealing. The carbon nanotubes produced from CO were found to be able to uptake a certain amount of hydrogen under ambient conditions, whereas graphite powders were unable. It was suggests that the carbon nanotubes may be a promising material that can be used for hydrogen storage under ambient conditions.

In 2005, Bettinger [26] investigated the reactivity of SW-defect compared to the pristine side walls of (5,5) and (10,10) SWCNTs for methylene group addition to the ten C-C junctions resulting from SW rotations of the two unique bonds using density functional theory (PBE/6-31G(d)//PBE/3-21) imposing periodic boundary conditions (PBCs). It was found that the methylene additions are exothermic and at least one of the junctions associated with the SW defects is more highly reactive than the pristine tubes while some of the bonds show higher reactivity than those in the perfect tubes, others are less reactive.

In 2005, Zhou *et al.* [24] studied the doping effects of B and N on atomic and molecular adsorption of hydrogen in SWNTs using density functional theory (DFT) calculations. The adsorption of molecular and atomic hydrogen was compared in pristine and B, or N doped SWCNTs when hydrogen atom is adsorbed on top of C or B or N atoms. The results shown that in case of hydrogen molecular adsorption, both B- and N-doping decrease the adsorption energies in SWNTs. However, the B and N doping effects are different on the hydrogen atomic adsorption. The B-doping

increases the hydrogen atomic adsorption energies both in zigzag and armchair nanotubes while the N-doping decreases the hydrogen atomic adsorption energies.

In 2006, Zhou and Zhao [27] using DFT computations with periodic boundary conditions (PBC) studied the differences between hydrogen adsorption in boron nitride (BN) compared with in carbon nanotubes. The physisorption of hydrogen on BN nanotubes is less favorable energetically than on carbon nanotubes and chemisorption of hydrogen molecules on pristine BN nanotubes is endothermic, means that perfect BN nanotubes are not good candidates for hydrogen storage.

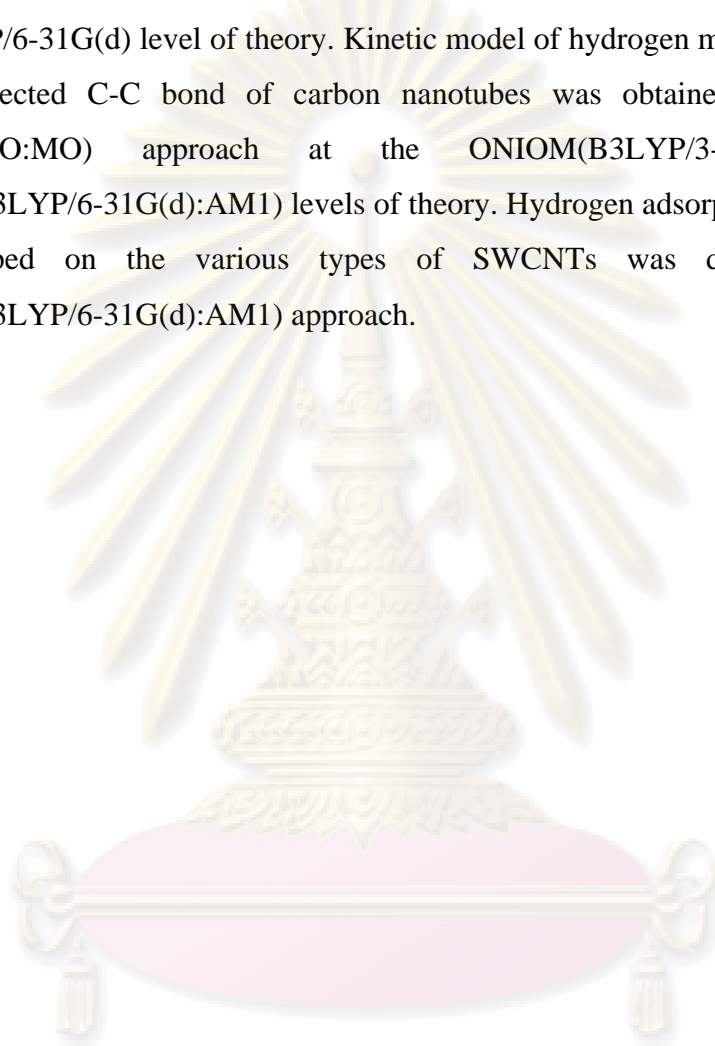
In 2007, Gayathri and Geetha [28] proposed that the Pentagon-Octagon defects have an important contribution to the physisorption mechanism between hydrogen molecule and single walled carbon nanotubes of different sizes and types, the presence of structural defects will increase the hydrogen storage capacity in carbon nanotubes by using the DFT calculations.

In 2007, Dinadayalane *et al.* [29] investigated the SW defect formation with two different orientations in armchair (5,5) SWCNTs in order to compare between the circumferential C-C bond rotation and axial C-C bond rotation in generating SW defect and how the SW defect formation energy varies by changing the defect position, using Hatree-Fock and MP2 and DFT methods with B3LYP hybrid functional using 3-21G and 6-31G(d) basis sets. The calculated results suggested that the formation energies computed at the B3LYP/6-31G(d) level are in good agreement with those obtained at the MP2/6-31G(d) level and 90° rotation of an axial C-C bond is slightly more preferred than the circumferential C-C bond in forming the SW defect in (5,5) SWCNTs. The presence of five membered ring at the edge is not favored in SW defect SWCNTs.

In this year, Dinadayalane and Kaczmarek [30] studied by DFT at the B3LYP/6-31G(d) level of theory. Investigate the structure and reaction energies from the chemisorption of a single hydrogen atom and of the preference for binding positions in the chemisorption of two hydrogen atom considering (3,3), (4,4), (5,5) and (6,6) armchair SWCNTs of 9- and 15-carbon atom layers. They proposed that chemisorption of one and two hydrogen atoms decreases as the diameter of the armchair nanotubes increases and two hydrogen atoms prefer to bind at adjacent positions compared to alternate carbon sites of armchair nanotubes. The present study indicates that changing the length of the nanotubes has a significant effect on the reaction energy of hydrogen chemisorption.

1.5 Objective

In this work, we have studied the chemisorption of hydrogen on pristine and SW-defect armchair (5,5) single-walled carbon nanotubes of cap-ended C_{80} , C_{90} and open-ended $C_{70}H_{20}$ using density functional theory (DFT) method with B3LYP/3-21G and B3LYP/6-31G(d) level of theory. Kinetic model of hydrogen molecule adsorption on the selected C-C bond of carbon nanotubes was obtained by two-layered ONIOM(MO:MO) approach at the ONIOM(B3LYP/3-21G:AM1) and ONIOM(B3LYP/6-31G(d):AM1) levels of theory. Hydrogen adsorption on two-boron atoms doped on the various types of SWCNTs was done by use of ONIOM(B3LYP/6-31G(d):AM1) approach.



ศูนย์วิจัยทรัพยากร
จุฬาลงกรณ์มหาวิทยาลัย

CHAPTER II

THEORETICAL BACKGROUND

All chemists use models. Beginning chemistry students use plastic models to help them understand and visualize the structures of molecules. Recently, both students and experienced researchers have begun to use chemical drawing programs for the same purpose.

In a similar way, computational chemistry simulates chemical structures and reactions numerically, based in full or in part on the fundamental laws of physics. It allows chemists to study chemical phenomena by running calculations on computers rather than by examining reactions and compounds experimentally. Some methods can be used to model not only stable molecules, but also short-lived, unstable intermediates and even transition state. In this way, they can provide information about molecules and reactions which is impossible to obtain through observation. Computational chemistry is therefore both an independent research area and a vital adjacent to experimental studies.

There are two broad areas within computational chemistry devoted to the structure of molecules and their reactivity: molecular mechanics and electronic structure theory. They both perform the same basic types of calculations:

- Computing the energy of a particular molecular structure (spatial arrangement of atoms or nuclei and electrons). Properties related to the energy may also be predicted by some methods.
- Performing geometry optimization, which located the lowest energy molecular structure in close proximity to the specified starting structure. Geometry optimization depend primarily on the gradient of the energy-the first derivative of the energy with the respect to atomic positions.
- Computing the vibrational frequencies of molecules resulting from intratomic motion within the molecule. Frequencies depend on the second derivative of the energy with respect to atomic structure, and frequency calculations may also predict other properties which depend on second derivatives. Frequency calculations are not possible or practical for all computational chemistry methods [31].

2.1 Molecular Mechanics

Molecular mechanics simulations use the laws of classical physics to predict the structures and properties of molecules. There are many different molecular mechanics methods. Each one is characterized by its particular force field. A force field has these components.

- A set of equations defining how the potential energy of a molecule vary with the locations of its component atoms.
- A series of atom types, defining the characteristics of an element within specific chemical context. Atom types prescribe different characteristics and behavior for an element depending upon its environment. For example, carbon atom in a carbonyl is treated differently than one bonded to three hydrogens. The atom types depend on hybridization, charge and the type of the other atoms to which it is bonded.
- One or more parameter sets that fit the equations and atom types to experimental data. Parameter sets define force constants, which are value used in the equations to relate atomic characteristics to energy component and structural data such as bond lengths and angles.

Molecular mechanics calculations don't explicitly treat the electrons in a molecule system. Instead, they perform computations based upon the interactions among the nuclei. Electronics effects are implicitly included in force fields through parameterization. This approximation makes molecular mechanics computations quite inexpensive computationally, and allows them to be used for very large systems containing many thousands of atoms. However, it also carries several limitations as well. Among the most important these:

- Each force field achieves good results only for a limited class of molecules, related to those for which it was parameterized. No force field can be generally used for all molecular systems of interests.
- Neglect of electrons means that molecular mechanics methods cannot treat chemical problems where electronic effects predominate. For example, they cannot describe processes which involve bond formation or bond breaking.

Molecular properties which depend on subtle electronic details are also not reproducible by molecular mechanics methods [31].

2.2 Electronic structure methods

Electronic Structure Methods use the laws of quantum mechanics rather than classical physics as the basis for their computations. Quantum mechanics states that the energy and other related properties of a molecule may be obtained by solving the Schrödinger equation (2.1):

$$\mathbf{H}\Psi = \mathbf{E}\Psi \quad (2.1)$$

For any but the smallest systems, however, exact solutions to the Schrödinger equation are not computationally practical. Electronic structure methods are characterized by their various mathematical approximations to its solution. There are two major classes of electronic structure methods [31]:

2.2.1 Semi-empirical methods

Semi-Empirical methods are simplified versions of Hartree-Fock theory using empirical (identical to derived from experimental data) corrections in order to improve performance. These methods are usually referred to through acronyms encoding some of the underlying theoretical assumptions. The most frequently used methods the Neglect of Differential Diatomic Overlap (NDDO) integral approximation, Intermediate Neglect of Differential Diatomic Overlap (INDO) and Complete Neglect of Differential Diatomic Overlap (CNDO). A number of additional approximations are made to speed up calculations and a number of parameterized corrections are made in order to correct for the approximate quantum mechanical model. How the parameterization is performed characterizes the particular Semi-Empirical method, as Modified Neglect of Differential Overlap (MNDO), Austin Model 1 (AM1), Parametric Number 3 (PM3). The parameterization is performed such that the calculated energies are expressed as heats of formations instead of total energies [32].

2.2.1.1 AM1 method

Austin Model 1 (AM1) is a semi-empirical method for the quantum calculation of molecular electronic structure. AM1 is an attempt to improve the MNDO model by reducing the repulsion of atoms at close separation distances. The core-core repulsion was modified by introducing attractive and repulsive Gaussian functions centered at internuclear points. That the core-core repulsions was modified to overcome the tendency of MNDO to overestimate repulsions between atoms separated by about their van der Waals distances. The core-core repulsion of AM1 has the form.

$$V_{nn}(A, B) = V_{nn}^{MNDO}(A, B) + \frac{Z_A Z_B}{R_{AB}} \times \left(\sum_k a_{kA} e^{-b_{kA}(R_{AB} - c_{kA})^2} + \sum_k a_{kB} e^{-b_{kB}(R_{AB} - c_{kB})^2} \right) \quad (2.2)$$

where the core-core repulsion of MNDO model has the form.

$$V_{nn}^{MNDO}(A, B) = Z_A Z_B \langle s_A s_B | s_A s_B \rangle \left(1 + e^{-\alpha_A R_{AB}} + e^{-\alpha_B R_{AB}} \right) \quad (2.3)$$

Where, α exponent is taking as fitting parameters. The core repulsion energy is here a function of both the electron-electron repulsion integral $\langle s_A s_A, s_B s_B \rangle$. Here, k is between 2 and 4 depending on the atom, R_{AB} being the internuclear separation and Z_A being the effective core charge including the nuclear charge and all core electrons. It should be noted that the Gaussian functions more or less were added as patches onto the underlying parameters, which explains why different number of Gaussians are used for each atom.

2.2.1.2 PM3 method

Parametric Number 3 (PM3) is a variation of AM1, differing mainly in how the parameterization is done, two parameterization of MNDO-type methods, MNDO and AM1, had been carried out, and PM3 was at first called MNDO-PM3, meaning MNDO parameteric method 3. All parameters could then be optimized simultaneously, including the two-electron terms, and a significantly larger training

set with several hundred data could be employed. In this parameterization, the AM1 expression for the core-core repulsions was kept, except only 2 Gaussian were assigned to each atom. These Gaussian parameters were included as an integral part of model, and allowed to vary freely. In a sense it has the best set of parameter for the given set of experimental data. The optimization process, however, still required some human intervention, in selecting experimental data and assigning appropriate weight factors to each of data. PM3 has been parameterized for the elements, H, Li, C, N, O, F, Mg, Al, Si, P, S, Cl, Zn, Ga, Ge, etc, parameter for many of the transition metals are also being developed under the name PM3, which includes d-orbitals. The PM3 set of parameters are determined exclusively from geometrical data, since there are very few reliable energetic data available for transition metal compound.

2.2.2 Ab initio method

Unlike either molecular mechanics or semi-empirical methods, use no experimental parameters in their computations. Instead, their computations are based solely on the laws of quantum mechanics-the first principles referred to in the name ab initio-and on the values of a small number of physical constants:

- The speed of light
- The masses and charges of electrons and nuclei
- Planck's constant

The simplest kind of ab initio is Hartree-Fock (HF) approximation. Semi-empirical and ab initio methods differ in the trade-off made between computational cost and accuracy of result. Semi-empirical calculations are relative inexpensive and provide reasonable qualitative descriptions of molecular systems are fairly accurate quantitative predictions of energies and structures for systems where good parameter sets exist. In contrast, ab initio computations provide high quality quantitative predictions for broad range of systems. They are not limited to any specific class of system. Early ab initio programs were quite limited in the size of system they could be handle. However, this is not true for modern ab initio programs. On a typical workstation, Gaussian can compute the energies and related properties for systems containing a dozen heavy atoms in just a few minutes. It can handle jobs of up to a

few hundred atoms, and it can predict the structures of molecules having as many as one hundred atoms on the same size computer system. Corresponding larger systems can be handled on supercomputer systems based upon their specific CPU performance characteristics [31].

2.2.3 Density functional theory (DFT) method

A third class of electronic structure methods have come into wide use, Density Functional Theory (DFT) Method. These DFT methods are similar to ab initio methods in many ways. DFT calculations require about the same amount of computation resources as Hartree-Fock theory, the least expensive ab initio method.

DFT methods are attractive because they include the effects of electron correlation-the fact that electrons in a molecular system react to one another's motion and attempt to keep out of one another's way-in their model. Hartree-Fock calculations consider this effect only in an average sense-each electron sees and reacts to an averaged electron-density-while methods including electron correlation account for the instantaneous interactions of pairs of electrons with opposite spin. This approximation causes Hartree-Fock results to be less accurate for some types of systems. Thus, DFT methods can provide the benefits of some more expensive ab initio methods at essentially Hartree-Fock cost.

DFT is based not on the wavefunction, but rather on the electron probability density function or electron density function, commonly called simply the electron density or charge density, designated by $\rho(x, y, z)$. The most common implementation of density functional theory is through the Kohn-Sham method. Within the framework of Kohn-Sham DFT, the intractable many-body problem of interacting electrons in a static external potential is reduced to a tractable problem of non-interacting electrons moving in an effective potential. DFT is among the most popular and versatile methods available in computational chemistry. Comparing with the wave mechanics approach, it seems clear that the energy functional may be divided into three parts, kinetic energy, $T[\rho]$, attraction between the nuclei and electrons, $V_{ne}[\rho]$, and electron-electron repulsion, $V_{ee}[\rho]$ (the nuclear-nuclear repulsion is a constant in the Born-Oppenheimer approximation). Furthermore, with reference to Hartree-Fock theory, the $V_{ee}[\rho]$ term may be divided into a Coulomb and Exchange part, $J[\rho]$ and $K[\rho]$, implicitly including correlation energy in all terms the $V_{ne}[\rho]$ and $J[\rho]$ functionals are

given by their classical expression, where the factor of $\frac{1}{2}$ in $J[\rho]$ allows the integration to run over all space for both variables [33].

$$V_{ne}[\rho] = \sum_a \int \frac{Z_a \rho(r)}{|R_a - r|} dr \quad (2.4)$$

$$J[\rho] = \frac{1}{2} \iint \frac{\rho(r)\rho(r')}{|r - r'|} dr dr' \quad (2.5)$$

Early attempts at deducing functionals for the kinetic and exchange energies considered a non-interacting uniform electron gas.

The foundation for the use of the DFT methods in computational chemistry was the introduction of orbitals by Kohn and Sham. The basic idea in the Kohn and Sham formalism is splitting the kinetic energy functional into two parts, one of which can be calculated exactly, and a small correlation term.

2.2.4 The Kohn-Sham energy and the Kohn-Sham equations

The first Kohn-Sham theorem tells us that it is worth looking for a way to calculate molecular properties from the electron density. The second theorem suggests that a variation approach might yield a way to calculate the energy and electron density (the electron density, in turn, could be used to calculate other properties). The two basic ideas behind the Kohn-Sham approach to DFT are, (1) to express the molecular energy as a sum of terms, only one of which, a relatively small term, involves the unknown functional. Thus even moderately large errors in this term will not introduce large errors into the total energy (2) to use an initial guess of the electron density ρ in the Kohn-Sham equations to calculate an initial guess of the Kohn-Sham orbitals. The final Kohn-Sham orbitals are used to calculate an electron density that in turn is used to calculate the energy.

2.2.4.1 The Kohn-Sham energy

The ideal energy is that of an ideal system, a fictitious non-interacting reference system, defined as one in which the electrons do not interact and in which

the ground state electron density ρ_r is exactly the same as in our real ground state system, $\rho_r = \rho_0$. The electronic energy of the molecule is the total internal “frozen-nuclei” energy can be found by adding the internuclear repulsions, and the 0 K total internal energy by further adding the zero-point energy.

The ground state electronic energy of our real molecule is the sum of the electron kinetic energy, the nucleus-electron attraction potential energies, and the electron-electron repulsion potential energies and each is a functional of the ground-state electron density

$$E_0 = \langle T[\rho_0] \rangle + \langle V_{ne}[\rho_0] \rangle + \langle V_{ee}[\rho_0] \rangle \quad (2.6)$$

Focusing on the middle term, the nucleus-electron potential energy is the sum over all $2n$ electrons of the potential corresponding to attraction of an electron for all the nuclei A

$$\langle V_{ne} \rangle = \sum_{i=1}^{2n} \sum_{\text{nuclei A}} -\frac{Z_A}{r_{iA}} = \sum_{i=1}^{2n} v(r_i) \quad (2.7)$$

where $v(r_i)$ is the external potential for the attraction of electron i to the nuclei. The density function ρ can be introduced into $\langle V_{ne} \rangle$ by using that

$$\int \Psi \sum_{i=1}^{2n} f(r_i) \Psi dt = \int \rho(r) f(r) dr \quad (2.8)$$

Where $f(r_i)$ is a function of the coordinates of the $2n$ electrons of a system and Ψ is the total wavefunction from equations (2.7) and (2.8), invoking the concept of expectation

value $\langle V_{ne} \rangle = \left\langle \Psi \left| \hat{V}_{ne} \right| \Psi \right\rangle$, and since $\hat{V} = V_x$, and get,

$$E_0 = \int \rho_0(r) v(r) dr + \langle T[\rho_0] \rangle + \langle V_{ee}[\rho_0] \rangle \quad (2.9)$$

that can not known the function in $\langle T[\rho_0] \rangle$ and $\langle V_{ee}[\rho_0] \rangle$. The Kohn and Sham to introduced the idea of a reference system of non-interacting electrons. Let us to define the quantity $\Delta\langle T[\rho_0] \rangle$ as the deviation of the real kinetic energy from that of the reference system.

$$\Delta\langle T[\rho_0] \rangle \equiv \langle T[\rho_0] \rangle - \langle T_r[\rho_0] \rangle \quad (2.10)$$

Let us next define $\Delta\langle V_{ee} \rangle$ as the deviation of the real electron-electron repulsion energy from classical charged-cloud coulomb repulsion energy. This classical electrostatic repulsion energy is the summation of the repulsion energies for pairs of infinitesimal volume elements $\rho(r_1)dr_1$ and $\rho(r_2)dr_2$ separated by distance r_{12} , multiplied by one-half. The sum infinitesimals is and integral and so

$$\Delta\langle V_{ee}[\rho_0] \rangle = \langle V_{ee}[\rho_0] \rangle - \frac{1}{2} \iint \frac{\rho_0(r_1)\rho_0(r_2)}{r_{12}} dr_1 dr_2 \quad (2.11)$$

Actually, the classical charged-cloud repulsion is somewhat inappropriate foe electrons in that smearing an electron out into a cloud forces it to repel itself, as any two regions of the cloud interact repulsively. This physically incorrect electro self-interacting will be compensated for by a good exchange-correlation functional can be written as

$$E_0 = \int \rho_0(r)v(r)dr + \langle T_r[\rho_0] \rangle + \frac{1}{2} \iint \frac{\rho_0(r_1)\rho_0(r_2)}{r_{12}} + \Delta\langle T[\rho_0] \rangle + \Delta\langle V_{ee}[\rho_0] \rangle \quad (2.12)$$

The sum of the kinetic energy deviation from the reference system and the electron-electron repulsion energy deviation from the classical system is called the exchange-correlation energy, E_{xc}

$$E_{xc}[\rho_0] \equiv \Delta\langle T[\rho_0] \rangle + \Delta\langle V_{ee}[\rho_0] \rangle \quad (2.13)$$

The $\Delta\langle T \rangle$ term represents the kinetic correlation energy of the electrons and the $\langle \Delta V_{ee} \rangle$ term the potential correlation energy and the exchange energy, although exchange and correlation energy in DFT do not have exactly.

2.2.4.2 The Kohn-Sham equations

The Kohn-Sham equations are a theorem obtained by utilizing the variation principle, which the second Hohenberg-Kohn theorem assures applies to DFT. We use the fact that the electron density of the reference system, which is the same as that of our real system, is given by

$$\rho_0 = \rho_r = \sum_{i=1}^{2n} |\psi_i^{KS}(1)|^2 \quad (2.14)$$

where the ψ_i^{KS} are the Kohn-Sham spatial orbital. Substituting the above expression for the orbitals into the energy and varying E_0 with respect to the ψ_i^{KS} subject to the constraint that these remain orthonormal lead to the Kohn-Sham equations, procedure is similar to that used in deriving the Hartree-Fock equations,

$$\left[-\frac{1}{2} \nabla_i^2 - \sum_{\text{nuclei } A} \frac{Z_A}{r_{iA}} + \int \frac{\rho(r_2)}{r_{12}} dr_2 + v_{xc}(1) \right] \psi_i^{KS}(1) = \epsilon_i^{KS} \psi_i^{KS}(1) \quad (2.15)$$

where ϵ_i^{KS} are the Kohn-Sham energy levels and $v_{xc}(1)$ is the exchange correlation potential, arbitrarily designated here for electron number 1, since the Kohn-Sham equations are a set of one-electron equations with the subscript i running from 1 to n , over all the $2n$ electron in the system. The exchange correlation potential is defined as the functional derivative of $E_{xc}[\rho_0(r)]$ with respect to $\rho(r)$

$$v_{xc}(r) = \frac{\delta E_{xc}[\rho(r)]}{\delta \rho(r)} \quad (2.16)$$

We need the derivative v_{xc} for the Kohn-Sham equations, and the exchange-correlation function itself for the energy equation. The Kohn-Sham equations can be written as

$$\hat{h}^{KS} \psi_i^{KS}(\mathbf{r}) = \varepsilon_i^{KS} \psi_i^{KS}(\mathbf{r}) \quad (2.17)$$

The Kohn-Sham operator \hat{h}^{KS} is defined by equation (2.15). The difference between DFT method is the choice of the functional from of the exchange-correlation energy. Functional forms are often designed to have a certain limiting behavior, and fitting parameters to known accurate data. Which functional is the better will have to be settled by comparing the performance with experiments or high-level wave mechanics calculations [34].

2.2.4.3 Hybrid methods

Hybrid functional augment the DFT exchange-correlation energy with a term calculated from Hartree-Fock theory. The Kohn-Sham orbitals are quit similar to the HF orbitals, give an expression, based on Kohn-Sham orbitals, for the HF exchange energy

$$E_x^{HF} = - \sum_{i=1}^n \sum_{j=1}^n \left\langle \psi_i^{KS}(\mathbf{r}_1) \psi_i^{KS}(\mathbf{r}_2) \left| \frac{1}{r_{ij}} \right| \psi_i^{KS}(\mathbf{r}_2) \psi_j^{KS}(\mathbf{r}_1) \right\rangle \quad (2.18)$$

Since the Kohn-Sham Slater determinant is an exact representation of the wavefunction of the noninteracting electron reference system, E_x^{HF} is the exact exchange energy for a system of noninteracting electron with electron density equal to real system. Including in a LSDA gradient-corrected DFT expression for E_{xc} ($E_{xc} = E_x + E_c$) a weighted contribution of the expression for E_x^{HF} give a FH/DFT exchange-correlation functional, commonly called a Hybrid DFT functional. The most popular Hybrid functional at present is based on an exchange-energy functional developed by Becke, and modified Steven *et al.* by introduction of the LYP correlation-energy

functional. This exchange-correlation functional, called the Becke3 LYP or B3LYP functional is

$$E_{xc}^{B3LYP} = (1 - a_0 - a_x)E_x^{LSDA} + a_0E_x^{HF} + a_xE_x^{B88} + (1 - a_c)E_x^{VWN} + a_cE_c^{LYP} \quad (2.19)$$

Here E_x^{LSDA} is the kind accurate pure DFT LSDA non-gradient-corrected exchange functional, E_x^{HF} is the Kohn-Sham orbitals based HF exchange energy functional, E_x^{B88} is the Becke 88 exchange functional

$$E_x^{B88} = E_x^{LDA} + \Delta E_x^{B88} \quad (2.20)$$

$$\Delta E_x^{B88} = -\beta\rho^{1/3} \frac{x^2}{1 + 6\beta x \sinh^{-1} x} \quad (2.21)$$

The β parameter is determined by fitting to known atomic data and x is a dimension gradient variable. The E_x^{VWN} is the Vosko, Wilk, Nusair function (VWN) can be written

$$E_x^{VWN} = E_x^{LDA} (1 + ax^2 + bx^4 + cx^6)^{1/5} \quad (2.22)$$

$$x = \frac{|\nabla\rho|}{\rho^{4/3}} \quad (2.23)$$

which forms part of the accurate functional for the homogeneous electron gas of the LDA and LSDA, and E_c^{LYP} is the LYP correlation functional. The parameters a_0 , a_x and a_c are those that give the best fit of the calculated energy to molecular atomization energies. This is thus gradient-corrected hybrid functional [34].

2.2.5 ONIOM method

ONIOM (Our N-layer Integrated molecular Orbital + molecular Mechanics) method was developed in Morokuma group [35], allows the user to partition a chemical system into layers, which can then each be treated at a different level of theory are applied to different parts of a molecule. A molecule system can be divided

into up to three layers and the three layers do not have to be inclusive, provides a possibility to achieve such high accuracy calculation on a large molecular system. The active part of the reaction is considered in the “model” system and is treated with both at “high” and “low” levels of molecular Orbital calculation, whereas the entire “real” system is treated only at the “low” level of molecular Orbital calculation, and then they are integrated to define the ONIOM total energy of the “real” system. ONIOM is a computationally efficient tool for the study of chemical reactions involving large molecular systems.

An obvious solution to problem is the partitioning of the system into two or more parts or layers, where the interesting or difficult part of the system (the inner layer) is treated at a high level of theory and the rest of the system (the outer layer) is treated at a low level of theory. These hybrid methods differ mainly in two aspects.

First, there are different ways to treat the boundary region of the different parts of the molecule. If there is no covalent bond between the layers, there is no special boundary region. However, if one is interested in the accurate description of a particular region of a large organic molecule or a macromolecule, covalent bonds have to be cut in order to generate the inner model system. This process leaves dangling bonds at the border of inner layer, which have to be saturated in order to avoid a chemically unrealistic model. Therefore, so-called link atom usually hydrogen atom are use.

The second crucial aspect in all the hybrid schemes is the interaction between the inner and outer part of the system. If the total energy $E(X-Y)$ of the entire system $X-Y$ (inner region X , outer region Y) is defined as

$$E(X-Y) = E_{high}(X) + E_{low}(Y) + E_{inner\ layer}(X,Y) \quad (2.24)$$

with $E_{inner\ layer}(X,Y)$ being a separate interaction energy between the two layers, this may be referred to as a connection scheme. On the other hand, if the total $E(X-Y)$ is calculated according to

$$E(X-Y) = E_{low}(X-Y) - E_{low}(X) + E_{high}(X) \quad (2.25)$$

In the latter case there is no necessity for a special interaction Hamiltonian, since the interaction between the two layers is consistently treated at the low level of theory. Obviously, both approaches are equivalent, if

$$E_{low}(Y) + E_{inner\ layer}(X,Y) = E_{low}(X-Y) - E_{low}(X) \quad (2.26)$$

i.e. if $E_{inner\ layer}(X,Y)$ corresponds to the exact interaction energy at the respectively low level.

2.2.5.1 ONIOM energy definition

The basic of ONIOM can be explained easily when it is considered as an extrapolation scheme in a two-dimensional space, spanned by the size of the system on one axis and the level of theory on the other axis.

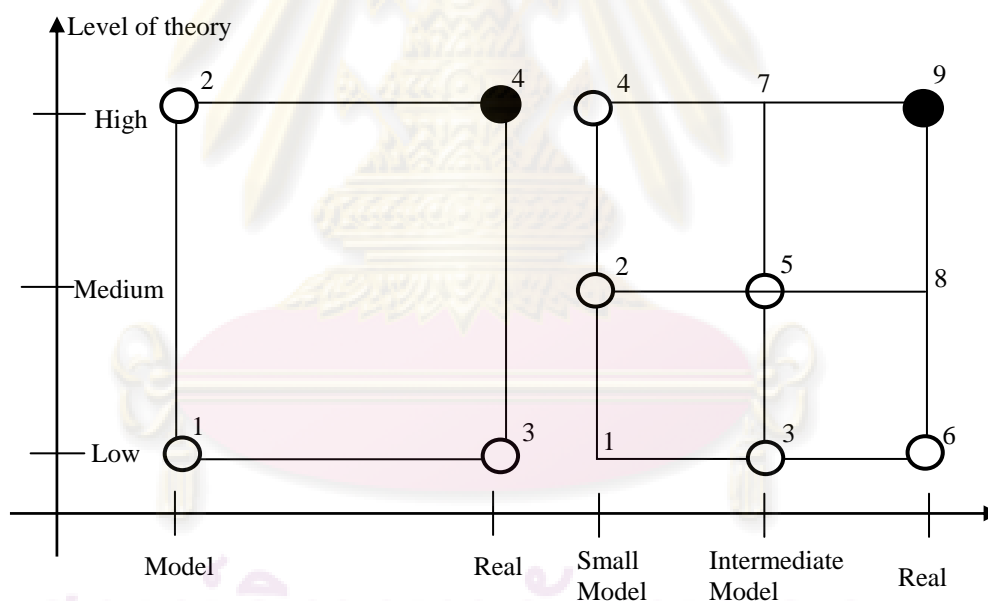


Figure 2.1 The ONIOM extrapolation scheme for a molecular system partitioned into two (left) and three (right) layers.

Figure 2.1 shows the extrapolation procedure schematically to describe the real system at the highest level of theory, the approximation of the target E_4 (point 4) in a system partitioned into the two-layer ONIOM or E_9 (point 9) in a system consisting of three layers. In the case of two layers, in extrapolated energy E_{ONIOM2} is then defined as

$$E_{ONIOM2} = E_3 - E_1 + E_2 \quad (2.27)$$

where E_3 is the energy of the entire (real) system calculated at low level method and E_1 and E_2 are the energies of the model system determined at the low and high level of theory, respectively. E_{ONIOM2} is an approximation to the true energy of the real system E_4

$$E_4 = E_{ONIOM2} + D \quad (2.28)$$

Thus, if the error D of the extrapolation procedure is the constant for two different structures, their relative energy ΔE_4 will be evaluated corrected by using the ONIOM energy ΔE_{ONIOM2} .

For a system partitioned into three different layers, the expression for the total energy ΔE_{ONIOM3} as an approximation for E_9 reads

$$E_{ONIOM3} = E_6 - E_3 + E_5 - E_2 + E_4 \quad (2.29)$$

Since the evaluation of E_1 does not require much computational effort, its value can be used to determine the effect of the three-layer approach as compared to a two-layer partitioning with points 1, 4, and 6. If the energy difference between the two-layer and three-layer extrapolation is constant, a two layer partitioning with the intermediate layer omitted would give comparably accurate result.

2.2.5.2 Treatment of link atoms

As mentioned before, an important and critical feature of all combination schemes is the treatment of the link atoms, as illustrated in Figure 9. The methodology in the case of three-layer ONIOM is exactly the same and will not be discussed explicitly.

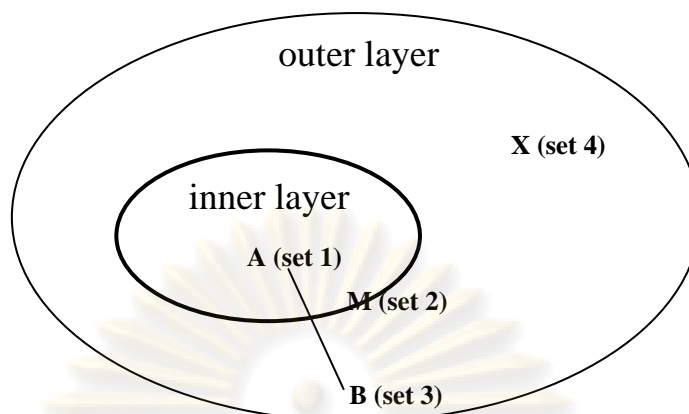


Figure 2.2 Definition of different atom sets within the ONIOM scheme.

Figure 2.2 shows the model system equal to inner layer + link atoms and real system equal to inner layer + outer layer. The atoms present both in the model system and real system are called set 1 atom and their coordinates are denoted by R_1 . The set 2 atoms are the artificially introduced link atoms. They only occur in the model system and their coordinates are described by R_2 . In the real system there are replaced by the atoms described by R_3 . Atoms that belong to the outer layer and are not substituted by atoms are called set 4 atoms with the coordinates R_4 . The geometry of the real system is thus described by R_1 , R_3 and R_4 and they are the independent coordinates for the ONIOM energy

$$E_{\text{ONIOM}} = E_{\text{ONIOM}}(R_1, R_3, R_4) \quad (2.30)$$

In order to generate the model system, described by R_1 and the link atoms R_2 , defined R_2 as function of R_1 and R_3

$$R_2 = f(R_1, R_3) \quad (2.31)$$

The explicit functional form of the R_2 dependency can be chosen arbitrarily. However, considering the fact that the link atoms are introduced to mimic the corresponding covalent bonds of the real system, they should follow the movement of the atoms they replace. If atom A belong to set 1 and atom B belong to set 3, the set 2 link atom is

placed onto the bond axis A-B in terms of internal coordinates choose the same bond angle for set 2 atom as for set 3. Therefore, in the model calculations the link atoms are always aligned along the bond vectors of the real system. For the exact position r_2 of a single H atom along an A-B bond ($r_2 - r_1$), introduced a fixed scale factor (or distance parameter) g . Hence,

$$r_2 = r_1 + g(r_3 - r_1) \quad (2.32)$$

If the A-B bond distance $|r_3 - r_1|$ changes during a geometry optimization, the A-H bond distance $|r_2 - r_1|$ also changes.

2.3 Basis set

A basis set is the mathematical description of the orbitals within a system (which in turn combine to approximate the total electronic wavefunction) used to perform the theoretical calculation. Larger basis sets more accurately approximate the orbitals by imposing fewer restrictions on the locations of the electrons in space. In the true quantum mechanical picture, electrons have a finite probability of existing anywhere in space; this limit corresponds to the infinite basis set expansion in the chart we looked at previously.

Standard basis sets for electronic structure calculations use linear combinations of Gaussian functions to form the orbitals. Gaussian offers a wide range of pre-defined basis sets, which may be classified by the number and types of basis functions that they contain. Basis sets assign a group of basis functions to each atom within a molecule to approximate its orbitals. These basis functions themselves are composed of a linear combination of Gaussian functions.

Slater functions are good approximations to atomic wavefunctions and would be the natural choice for ab initio basis functions, were it not for the fact that the evaluation of certain two-electron integrals requires excessive computer time if Slater functions are used. Actually, things a little more complicated. A single Gaussian is poor approximations to the nearly ideal description of an atomic wavefunctions that a Slater functions provides. The solution to the problem of this poor functions behaviour is to use several Gaussians to approximate a Slater functions. In the

simplest version of this basis, n Gaussian functions are superimposed with fixed coefficients to form one- Slater type orbital (STO) [34].

An individual molecular orbital is defined as

$$\phi_i = \sum_{\mu=1}^N c_{\mu i} \chi_{\mu} \quad (2.33)$$

where the coefficients $c_{\mu i}$ are known as the molecular orbital expansion coefficients. The basis functions $\chi_1 \dots \chi_N$ are also chosen to be normalized.

2.3.1 Minimal Basis Sets

Minimal Basis Sets contain the minimum number of basis functions needed for each atom.

A minimal basis set consists of one Slater functions for each inner-shell and valence-shell atomic orbitals of each atom. The essential idea of the minimal basis set is that we select one basis function for every atomic orbital that is required to describe the free atom. Several minimal basis sets are in common use, but by far the most common are the STO-nG basis sets, $n = 3, 4, 5,$ and 6 . The individual GTOs are called primitive orbitals, while the combined functions are called contracted functions. The STO-nG basis sets are available for almost all elements in the periodic table.

The STO-3G basis set introduces us to the concept of contracted shell in constructing contracted Gaussian from primitive Gaussian. The Gaussian of a contraction shell share common exponents. Example carbon has one s shell and sp shell. This means that the $2s$ and $2p$ Gaussians share common α exponents (which differ from those of the $1s$ functions). Consider the contracted Gaussians.

$$\phi(2s) = d_{1s} e^{-\alpha_{1s} r} + d_{2s} e^{-\alpha_{2s} r} + d_{3s} e^{-\alpha_{3s} r} \quad (2.34)$$

$$\phi(2p_x) = d_{1p_x} e^{-\alpha_{1p} r} + d_{2p_x} e^{-\alpha_{2p} r} + d_{3p_x} e^{-\alpha_{3p} r} \quad (2.35)$$

$$\phi(2p_y) = d_{1p_y} e^{-\alpha_{1p} r} + d_{2p_y} e^{-\alpha_{2p} r} + d_{3p_y} e^{-\alpha_{3p} r} \quad (2.36)$$

$$\phi(2p_z) = d_{1p_z} e^{-\alpha_{1p} r} + d_{2p_z} e^{-\alpha_{2p} r} + d_{3p_z} e^{-\alpha_{3p} r} \quad (2.37)$$

2.3.2 Split valence basis sets

The first way that a basis set can be made larger is to increase the number of basis functions per atom. Split valence basis set, such as 3-21G and 6-31G(d), have two (or more) sizes of basis functions for each valence orbital.

A split-valence basis set uses two (or more) GTOs for each valence atomic orbital but only one GTO for each inner-shell (core) atomic orbital. A split-valence basis set is minimal for inner-shell atomic orbitals and double zeta for the valence atomic orbitals. Split-valence basis sets are called valence double zeta (VDZ), valence triple zeta (VTZ), according to the number of GTOs used for each valence atomic orbitals.

3-21G (pronounced “three two one jee”) The valence functions are split into one basis function with two GTOs, split each valence orbitals into two part, an inner shell and an outer shell, and one with only one GTO. The core orbitals are each represented by one basis functions, each composed of three Gaussian.

6-31G (pronounced “six three one jee”) The core consists of six primitives in inner-shell GTOs which are not split, while the valence orbitals are described by one orbital constructed valence-shell atomic orbitals from three primitive GTOs and one that is a primitive GTO.

2.3.2.1 Polarized basis sets

Split valence basis sets allow orbitals to change size, but not to change shape. Polarized Basis Sets remove this limitation by adding orbitals with angular momentum beyond what is required for the ground state to the description of each atom. So far, the only polarized basis sets we’ve used is 6-31G(d). Its name indicates that it is the 6-31G basis set with d functions added to heavy atoms. This basis set is becoming very common for calculations involving up-to medium sized systems. This basis set is also known as 6-31G*. Another popular polarized basis sets is 6-31G(d,p), also known as 6-31G**, which adds p functions to hydrogen atoms in addition to the d functions on heavy atoms.

To each of these basis sets can be add polarization functions (*). Polarization functions are indicated after the G, with a separate designation for heavy atom those beyond helium. Sometime it is helpful to have polarization functions on

the hydrogens as well, a 6-31G* basis with three 2p functions on each H and He atom is called the 6-31G** (or 6-31G(d,p)). Thus, H and He atom have a 1s orbital represented by an inner 1s' and outer 1s' basis function, making two basis function. To 6-31G* basis is identical 6-31G(d) is valence zeta polarized basis set that adds to the 6-31G set six d-type Cartesian-Gaussian polarization functions, each composed of three Gaussian of inner and one Gaussian of outer, no each of Li through Ca and ten f-orbitals Cartesian-Gaussian polarization functions on each of the atoms Sc through Zn.

6-31G(d) basis set for carbon atom, has a 1s function represented by six Gaussian, and inner 2s, 2p_x, 2p_y and 2p_z (2s' 2p_x', 2p_y', 2p_z') function, each composed of three Gaussian, and an outer 2s, 2p_x, 2p_y and 2p_z (2s'' 2p_x'', 2p_y'', 2p_z'') function, each composed of one Gaussian, and six 3d functions, making a lot of 15 functions. That can be summarized is (1s, 2s' 2p', 2p', 2p', 2s'', 2p'', 2p'', 2p'', 3d, 3d, 3d, 3d, 3d, 3d).

2.3.2.2 Diffuse functions

In some cases the normal basis functions are not adequate. This is particular the case in excited states and in anions where the electronic density is spread out more over the molecule. This model has correctly by using some basis functions which themselves are more spread out. This means that small exponents are added to GTOs. These additional basis functions are called diffuse functions. The diffuse functions added to the 6-31G basis set as follows:

6-31+G added a set of diffuse s and p orbitals to the atoms in the first and second rows.

Diffuse functions can be added along with polarization functions also. Some examples of these functions are 6-31+G*, 6-31++G*, 6-31+G** and 6-31++G** basis sets.

2.4 Transition State Theory

Transition state theory (TST) assumes that a reaction proceeded from one energy minimum to another *via* an intermediate maximum. The transition state is the configuration which divides the reactant and product parts of surface. For example, a molecule which has reached the transition state is continuing to product. The geometrical configuration of the energy maximum is called the transition structure. Within standard TST, the transition state and transition structure are identical, but this is not necessarily for more refined models. The direction of reaction coordinate is started from the reactant to product along a path where the energies are as low as possible and the TS is the point where the energy has a maximum. In the multidimensional case, TS is a first-order point on the potential energy surface as a maximum in the reaction coordinate direction and a minimum along all other coordinates, shown in Figure 2.3 [34].

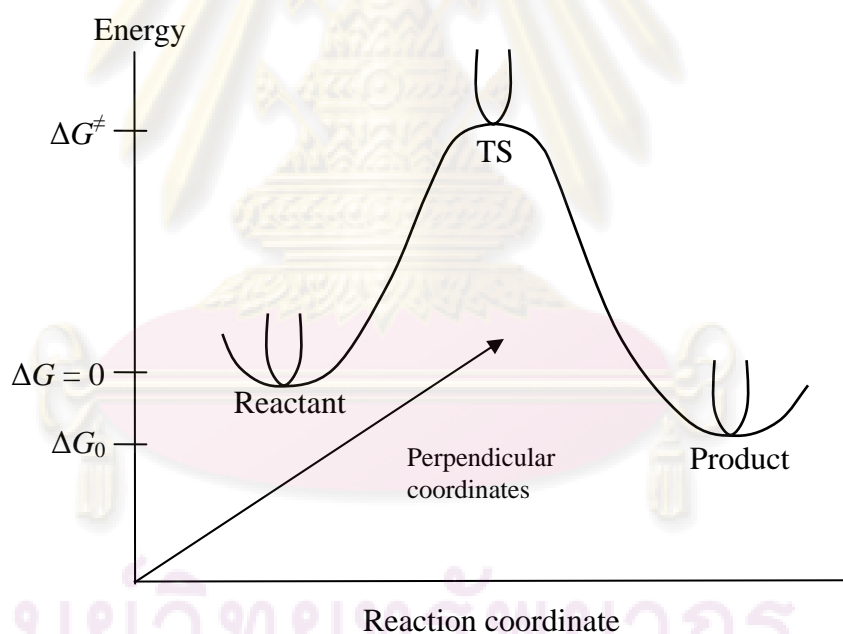


Figure 2.3 Schematic illustration of reaction path.

2.5 Molecular vibrational frequencies

The total molecular energy E is approximately the sum of translation, rotational, vibrational, and electronic energies. In the harmonic oscillator approximation, the vibrational energy of an N -atom molecule is the sum of $3N-6$ normal mode vibrational energies ($3N-5$ for a linear molecule):

$$E_{vib} \approx \sum_{k=1}^{3N-6} \left(\nu_k + \frac{1}{2} \right) h\nu_k \quad (2.38)$$

where ν_k is the harmonic vibrational frequency for the k is the normal mode and each vibrational quantum number ν_k has the possible values 0, 1, 2, ..., independent of the value of the order vibrational quantum numbers.

The harmonic vibrational frequencies of a molecule are calculated as follows.

(1) Solve the electronic Schrödinger equation $(\hat{H}_{el} + V_{NN})\psi_{el} = U\psi_{el}$ for several molecular geometries to find the equilibrium geometry of the molecule. (2) Calculate the set of second derivatives $(\partial^2 U / \partial X_i \partial X_j)_e$ of the molecular electronic energy U with respect to the $3N$ nuclear Cartesian coordinates of a coordinate system with origin at the center of mass. (3) Form the mass-weighted force-constant matrix elements

$$F_{ij} = \frac{1}{(m_i m_j)^{1/2}} \left(\frac{\partial^2 U}{\partial X_i \partial X_j} \right)_e \quad (2.39)$$

Where i and j each go from 1 to $3N$ and m_i is the mass of the atom corresponding to coordinate X_i . (4) Solve the following set of $3N$ linear equations in $3N$ unknowns

$$\sum_{j=1}^{3N} (F_{ij} - \delta_{ij} \lambda_k) l_{jk} = 0 \quad i = 1, 2, \dots, 3N \quad (2.40)$$

In this set of equations, δ_{ij} is the Kronecker delta, and λ_k and the l_{jk} 's are as-yet unknown parameters whose significance will be seen shortly. In order that this set

of homogeneous equations has a nontrivial solution, the coefficient determinant must vanish

$$\det(F_{ij} - \delta_{ij}\lambda_k) = 0 \quad (2.41)$$

This determinant is of order $3N$ and when expanded gives a polynomial whose highest power of λ_k is λ_k^{3N} . The molecular harmonic vibrational frequencies are then calculated from

$$\nu_k = \lambda_k^{1/2} / 2\pi \quad (2.42)$$

Six of the λ_k values found by solving will be zero, yielding six frequencies with value zero, corresponding to the three translational and three rotational degrees of freedom of the molecule. The remaining $3N-6$ vibrational frequencies are the molecular harmonic vibrational frequencies [36].



ศูนย์วิทยทรัพยากร
จุฬาลงกรณ์มหาวิทยาลัย

CHAPTER III

DETAILS OF THE CALCULATIONS

3.1 Structure models for SWCNTs and definition of their C-C bond types

C-C bond types (I, II and III) of pristine and SW defect armchair (5,5) SWCNTs of cap-ended C_{80} , C_{90} and open-ended $C_{70}H_{20}$ are defined as shown in Figures 3.1 and 3.2.

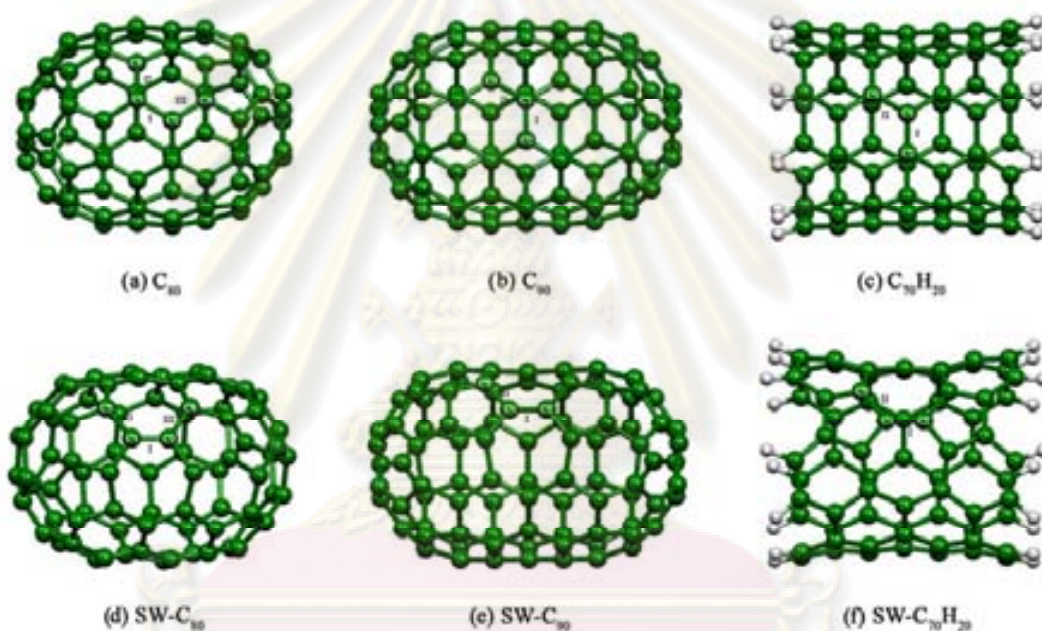


Figure 3.1 Selected atomic numbering and definition of C-C bond types (I, II and III) for armchair (5,5) SWCNTs of the pristine (a) cap-ended C_{80} , (b) C_{90} and (c) open-ended $C_{70}H_{20}$ and the SW defect (d) cap-ended SW- C_{80} , (e) SW- C_{90} and (f) open-ended SW- $C_{70}H_{20}$ SWCNTs.

The chemisorption of two hydrogen atoms at two adjacent carbons of C-C bond (types I, II and III) on outer wall of SWCNT (exohedral addition) is considered here because it has been reported to be more favorable than addition on the inner wall of SWCNT (endohedral addition) and two hydrogen atoms favor binding at adjacent positions [30,37]. The positions where two hydrogen atoms have been added on the sidewalls are designated by labeled carbon atoms and bond types as defined in Figure 3.2.

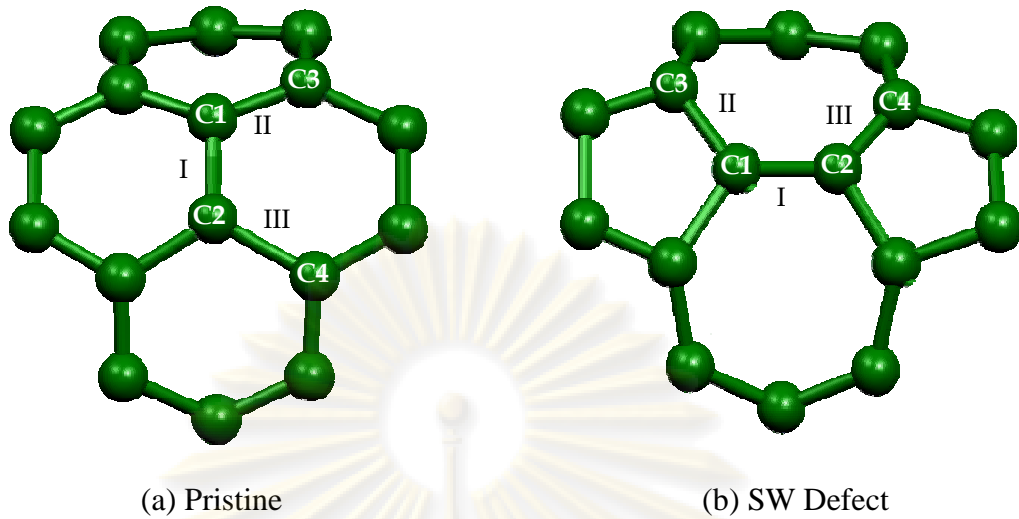


Figure 3.2 The atom numbering and C-C bond types of adsorption atoms defined for (a) the pristine and (b) SW defect SWCNTs. These clusters are fractions of their whole structure which our illustrated in Figure 3.1.

Figure 3.2 is just to clarify adsorption atoms and their C-C bond types. Their whole structures shown in Figure 3.1 are structure models for all studied SWCNTs.

3.1.1 Full structure optimization

Two hydrogen atoms were added simultaneously at the C-C bond type position for each structure as defined in Figure 3.1. When hydrogen adsorbed on the SWCNTs, structure of them were adjusted to the most stable structure. Hence strain energy occur when movement of structure of the SWCNTs arise. Adsorption energy of double hydrogen-atoms based on a hydrogen-molecule, $\Delta E_{\text{ads}}(\text{H}_2)$ and based on double proton-radicals ($\Delta E_{\text{ads}}(2\text{H}^\bullet)$) adsorbed on the flexible structure of SWCNTs are computed using equations (3.1) and (3.2), respectively. Strain energies (ΔE_{st}) of adsorption structures of SWCNTs are computed by using equation (3.3).

$$\Delta E_{\text{ads}}(\text{H}_2) = E_{2\text{H}/\text{SWCNT}} - (E_{\text{H}_2} + E_{\text{strained-SWCNT}}) \quad (3.1)$$

$$\Delta E_{\text{ads}}(2\text{H}^\bullet) = E_{2\text{H}/\text{SWCNT}} - (2E_{\text{H}^\bullet} + E_{\text{strained-SWCNT}}) \quad (3.2)$$

$$\Delta E_{st} = E_{\text{strained-SWCNT}} - E_{\text{isolated-SWCNT}} \quad (3.3)$$

$E_{2H/SWCNT}$ denotes the total energy of two hydrogen atoms chemisorbed on SWCNTs; E_{H_2} and E_H denotes the energies of hydrogen molecule and hydrogen atom; $E_{isolated-SWCNT}$ and $E_{strained-SWCNT}$ denotes the energies of bare tube and bare tube at adsorb form of the armchair (5,5) SWCNTs. The adsorption energy ΔE_{ads} can also be considered as the hydrogen chemisorption energy.

3.1.2 Partial structure optimization

Based on the rigid model of the SWCNTs interacts with a molecule of hydrogen gas was treated, adsorption-state structures of two atoms of the hydrogen molecule adsorbed on the C-C binding atoms of the isolated-SWCNT form of the frozen SWCNTs structure (no movement of the SWCNTs) has been optimized. Interaction energy of double hydrogen-atoms based on a hydrogen-molecule, $\Delta E'_{int}(H_2)$ and adsorption energy based on double proton-radicals ($\Delta E'_{ads}(2H^\bullet)$) on the frozen models are computed using equations (3.4) and (3.5) which $\Delta E_{st} = 0$.

$$\Delta E'_{int}(H_2) = E_{2H/SWCNT} - (E_{H_2} + E_{isolated-SWCNT}) \quad (3.4)$$

$$\Delta E'_{ads}(2H^\bullet) = E_{2H/SWCNT} - (2E_{H^\bullet} + E_{isolated-SWCNT}) \quad (3.5)$$

ศูนย์วิทยทรัพยากร
จุฬาลงกรณ์มหาวิทยาลัย

3.1.3 ONIOM approach and transition state calculation

For investigation of adsorption process of hydrogen molecule at two adjacent carbons, the two-layer ONIOM approach was employed and their two layers are defined as shown in Figure 3.2. The hydrogen adsorption process takes place on the SWCNT via TS transition state can be written as shown in equation (3.6). Figure 3.3 shows that the ball atoms are treated as the high-level layer and their remain atoms are treated as the low-level layer. In this work, the ONIOM (high:low) approach of the ONIOM(B3LYP/3-21G:AM1) and ONIOM(B3LYP/6-31G(d):AM1) were employed. Therefore, the activation energy ($\Delta^\ddagger E$) of hydrogen adsorption on the SWCNT can be computed using equation (3.7).



$$\Delta^\ddagger E = E_{\text{TS}} - (E_{\text{H}_2} + E_{\text{isolated-SWCNT}}) \quad (3.7)$$

All minima and transition states were confirmed by real and single imaginary vibrational frequencies, respectively.

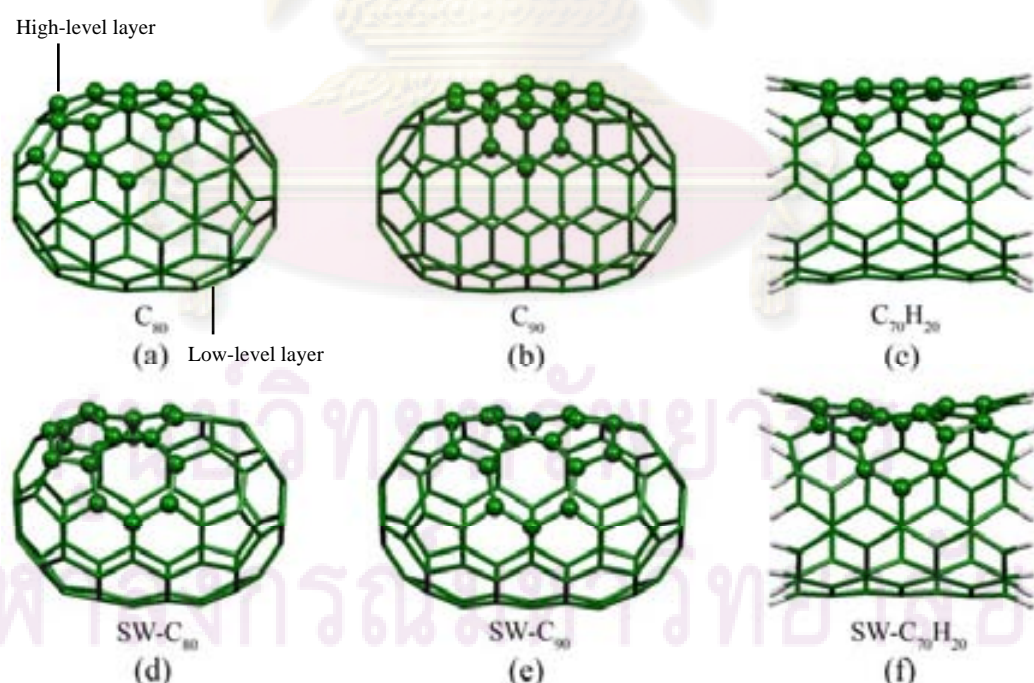


Figure 3.3 Two types of surface defined as high and low levels of theory for the two layer ONIOM approach of pristine (a) cap-ended C_{80} , (b) C_{90} and (c) open-ended $\text{C}_{70}\text{H}_{20}$, SW defect (d) cap-ended SW-C_{80} , (e) SW-C_{90} and (f) open-ended $\text{SW-C}_{70}\text{H}_{20}$ SWCNTs. Ball type is of area for high level of theory.

3.1.4 Structure models and ONIOM approach for B-doped SWCNTs

Structure models for B-doped SWCNTs are defined as follows. Two boron atoms were doped into the armchair (5,5) SWCNTs. Their possible types of stable structures can therefore be classified into three types for pristine and SW defect SWCNTs, respectively, as shown in Figure 3.4.

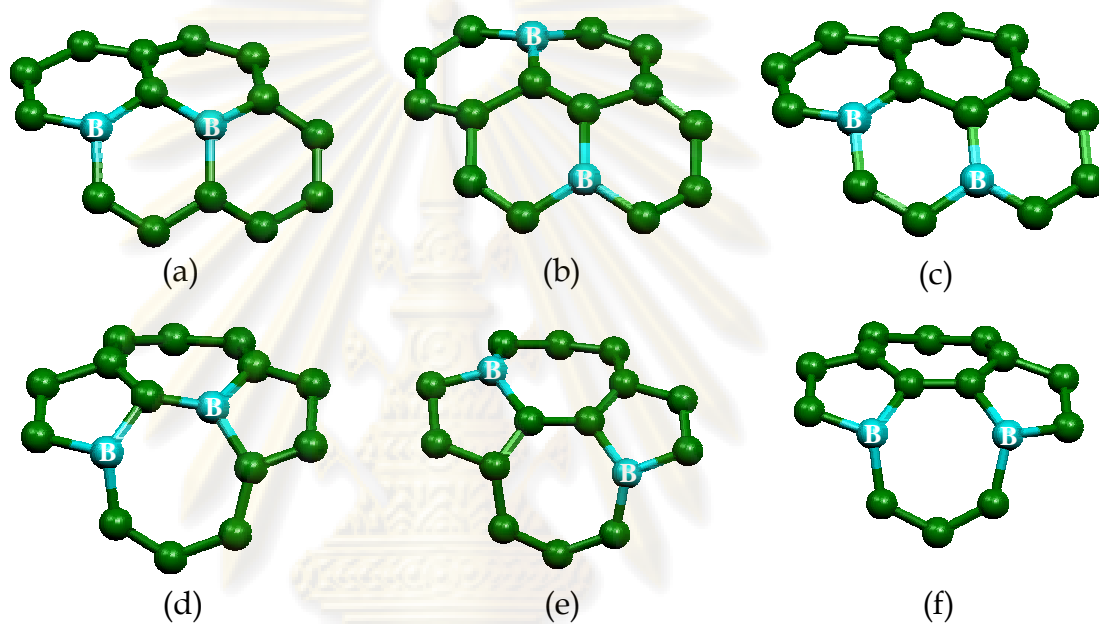


Figure 3.4 Possibility of doping types for two boron atoms into armchair (5,5) SWCNTs are defined as (a) type I, (b) type II and (c) type III for pristine and (d) type I, (e) type II and (f) type III for SW defect.

ศูนย์วิทยทรัพยากร
จุฬาลงกรณ์มหาวิทยาลัย

3.1.4.1 B-doped pristine SWCNTs

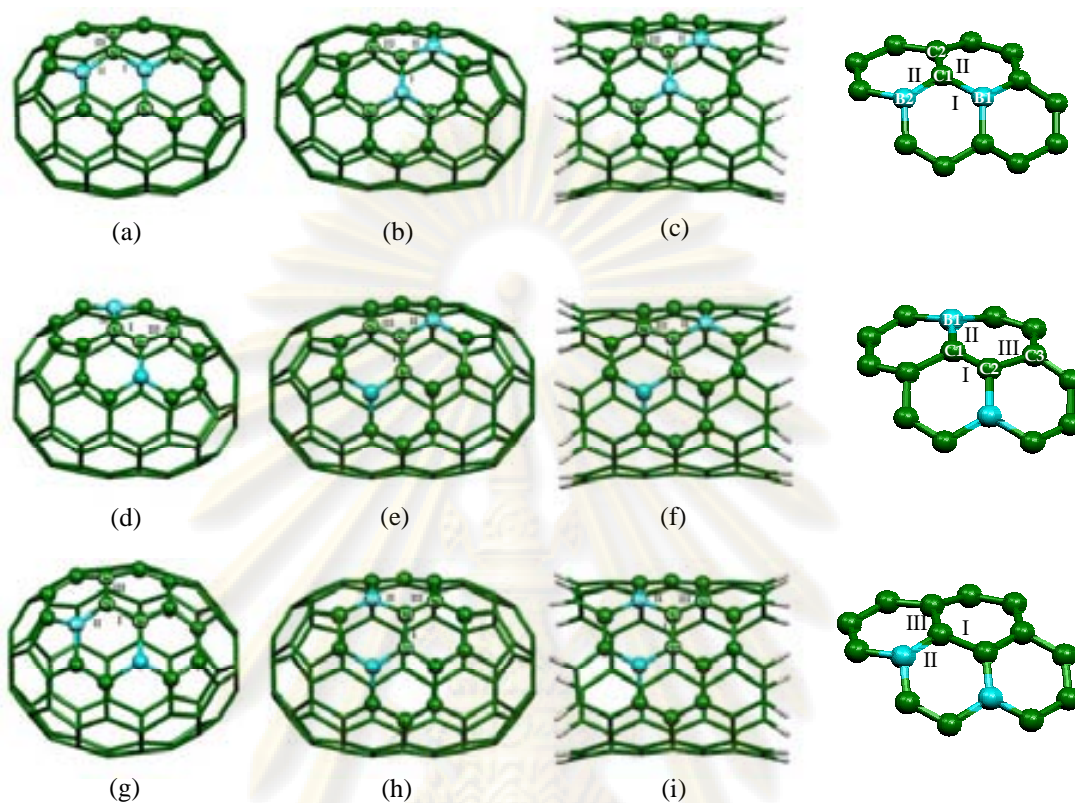


Figure 3.5 The atom numbers given in the structures indicate the position where two hydrogen atoms were added at the pristine (a), (d), (g) cap-ended B_2C_{88} , (b), (e), (g) B_2C_{88} and (c), (f), (i) open-ended $B_2C_{68}H_{20}$ B-doped SWCNTs (doping type I (a), (b), (c), doping type II (d), (e), (f), doping type III (g), (h), (i)). Their clear views are located on the right.

ศูนย์วิทยทรัพยากร
จุฬาลงกรณ์มหาวิทยาลัย

3.1.4.2 B-doped SW defect SWCNTs

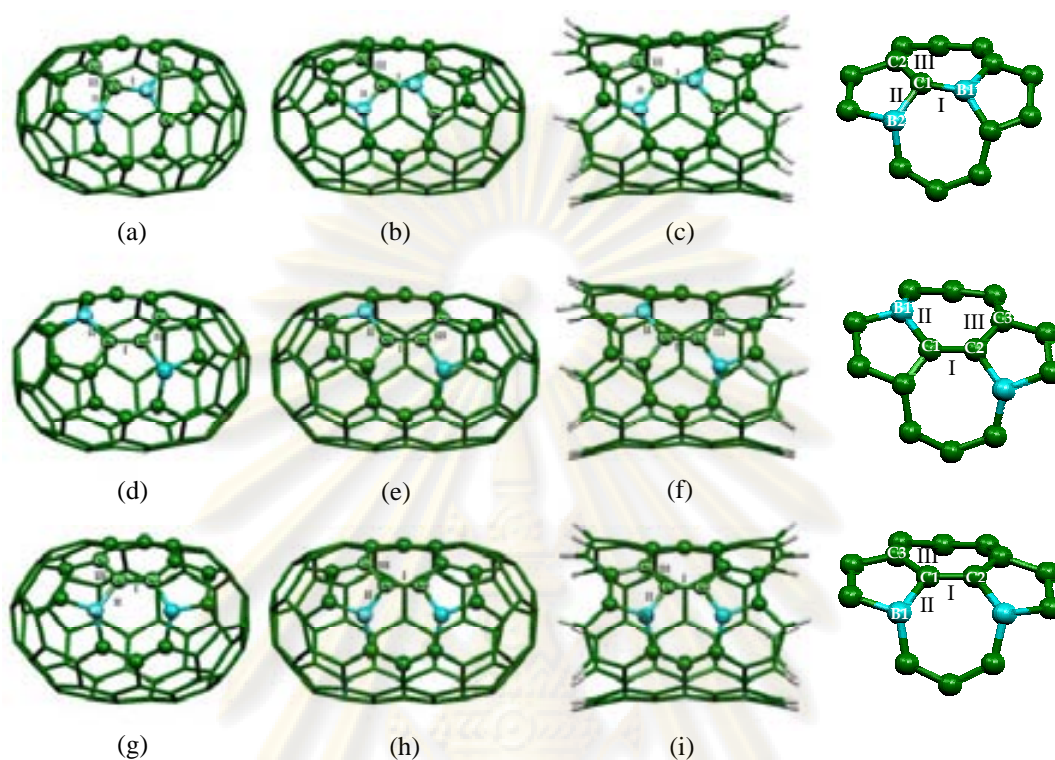


Figure 3.6 The atom numbers given in the structures indicate the position where two hydrogen atoms were added at the SW defect (a), (d), (g) cap-ended SW-B₂C₈₈, (b), (e), (g) SW-B₂C₈₈ and (c), (f), (i) open-ended SW-B₂C₆₈H₂₀ B-doped SWCNTs (doping type I (a), (b), (c), doping type II (d), (e), (f), doping type III (g), (h), (i)). Their clear views are located on the right.

ศูนย์วิทยทรัพยากร
จุฬาลงกรณ์มหาวิทยาลัย

Adsorption energy of double hydrogen–atoms based on a hydrogen–molecule, $\Delta E_{\text{ads}}(\text{H}_2)$ and based on double proton–radicals ($\Delta E_{\text{ads}}(2\text{H}^\bullet)$) adsorbed on the flexible structure of SWCNTs are defined as shown in equations (3.8) and (3.9), respectively. $E_{2\text{H}/\text{B-doped-SWCNT}}$ denotes the total energy of two hydrogen atoms chemisorbed on B-doped SWCNTs.

$$\Delta E_{\text{ads}}(\text{H}_2) = E_{2\text{H}/\text{B-doped-SWCNT}} - (E_{\text{H}_2} + E_{\text{strained-B-doped-SWCNT}}) \quad (3.8)$$

$$\Delta E_{\text{ads}}(2\text{H}^\bullet) = E_{2\text{H}/\text{B-doped-SWCNT}} - (2E_{\text{H}^\bullet} + E_{\text{strained-B-doped-SWCNT}}) \quad (3.9)$$

Interaction energy of double hydrogen–atoms based on a hydrogen–molecule, $\Delta E_{\text{int}}(\text{H}_2)$, and based on double proton–radicals ($\Delta E_{\text{ads}}(2\text{H}^\bullet)$) on the frozen models of SWCNTs are computed using equations (3.10) and (3.11), respectively.

$$\Delta E'_{\text{int}}(\text{H}_2) = E_{2\text{H}/\text{B-doped-SWCNT}} - (E_{\text{H}_2} + E_{\text{isolated-B-doped-SWCNT}}) \quad (3.10)$$

$$\Delta E'_{\text{ads}}(2\text{H}^\bullet) = E_{2\text{H}/\text{B-doped-SWCNT}} - (2E_{\text{H}^\bullet} + E_{\text{isolated-B-doped-SWCNT}}) \quad (3.11)$$

All calculations were performed with the GAUSSIAN 03 program [38]. The MOLDEN 4.2 program [39] was utilized to display the molecular structure, monitor the geometrical parameters and observe the molecular geometry convergence via the Gaussian output files. The molecular graphics of all related species were generated with the MOLEKEL 4.3 program [40].

ศูนย์วิทยทรัพยากร
จุฬาลงกรณ์มหาวิทยาลัย

CHAPTER IV

RESULTS AND DISCUSSION

4.1 Adsorption of hydrogen on pristine and SW defect armchair (5,5) SWCNTs

4.1.1 The full-structure optimization

The full-structure optimizations of bare tubes of pristine and the SW defect armchair (5,5) SWCNTs of cap-ended C_{80} , C_{90} and open-end $C_{70}H_{20}$ were carried out at the B3LYP/3-21G and B3LYP/6-31G(d) levels of theory. Total energies of the isolated form of the bare tubes are given in Table A1. Based on full-structure optimizations, adsorption complexes of various SWCNTs with hydrogen molecule were computed by the B3LYP/3-21G and B3LYP/6-31G(d) levels of theory. The adsorption configurations of double hydrogen-atoms on pristine and the SW defect of cap-ended C_{80} , C_{90} and open-end $C_{70}H_{20}$ are shown in Figures 4.1 and 4.2, respectively. The total energies and relative energies of complex conformers of complexes between two hydrogen-atoms on various pristine and SW defect SWCNTs are given in Table 4.1. Relative stabilities of adsorption complexes of two hydrogen-atoms on each type of pristine SWCNTs are in orders: $2H/C_{80_III} > 2H/C_{80_II} > 2H/C_{80_I}$ for C_{80} , $2H/C_{90_I} > 2H/C_{90_II}$ for C_{90} and $2H/C_{70}H_{20_I} > 2H/C_{70}H_{20_II}$ for $C_{70}H_{20}$ tubes and relative stabilities of adsorption complexes of two hydrogen-atoms on each type of SW defect SWCNTs are in orders: $2H/SW-C_{80_III} > 2H/SW-C_{80_II} > 2H/SW-C_{80_I}$ for SW- C_{80} , $2H/SW-C_{90_I} > 2H/SW-C_{90_II}$ for SW- C_{90} and $2H/SW-C_{70}H_{20_I} > 2H/SW-C_{70}H_{20_II}$ for SW- $C_{70}H_{20}$ tubes.

When hydrogen atoms adsorbed on the SWCNTs. Total energies of the bare tubes of adsorbed-form of all complex conformers and their strain energies, computed at the B3LYP/3-21G and B3LYP/6-31G(d) levels are shown in Table 4.2. The strain energies computed at the B3LYP/3-21G and B3LYP/6-31G(d) levels are very slightly different. The strain energies based on the B3LYP/6-31G(d) level are within the range of 22.60 to 44.72 kcal/mol for C_{80} , 47.38 to 49.70 kcal/mol for C_{90} and 56.30 to 60.85 kcal/mol for $C_{70}H_{20}$.

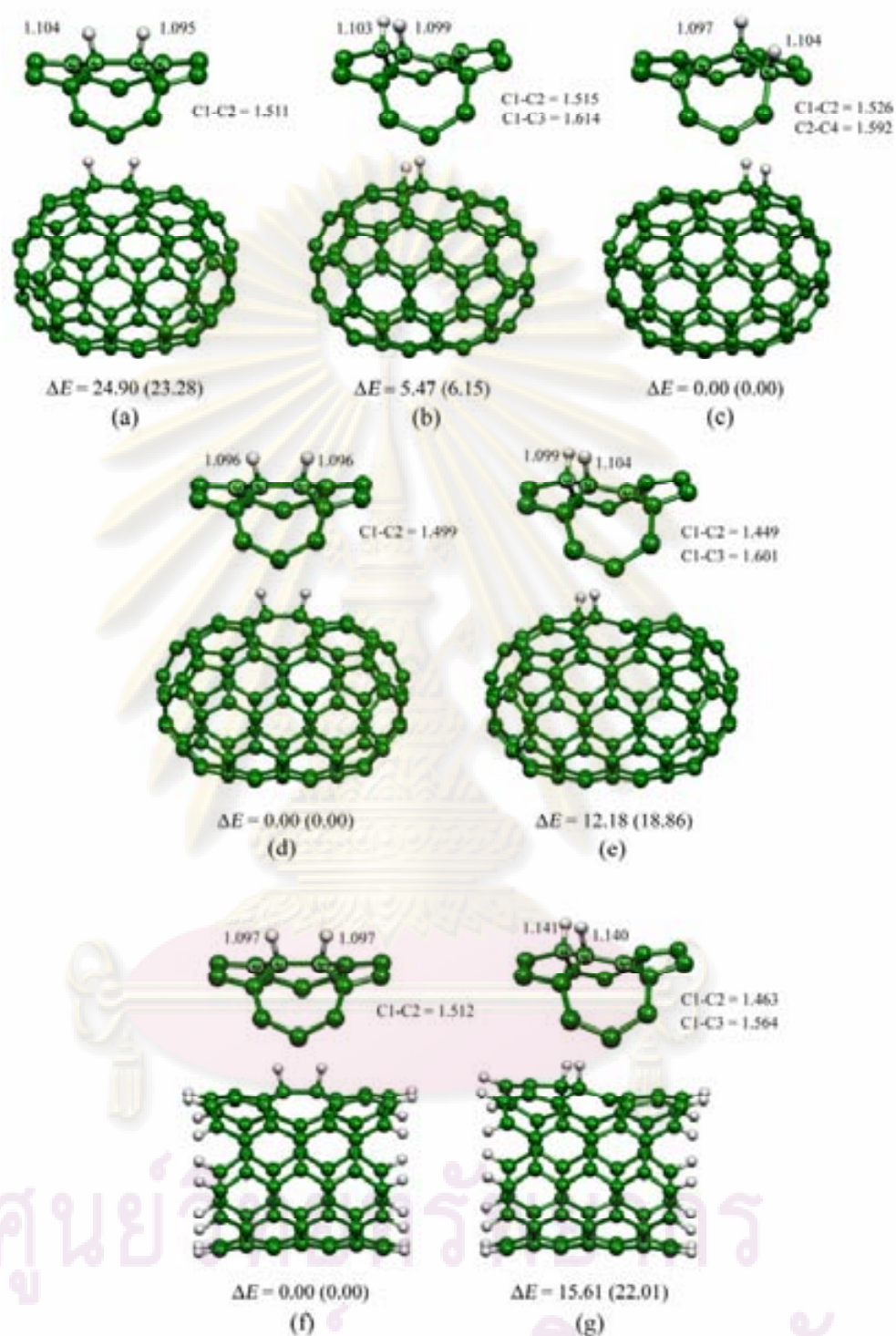


Figure 4.1 Adsorption of double hydrogen-atoms to pristine cap-ended C_{80} , C_{90} and open-ended $C_{70}H_{20}$ on two carbon atoms of bond type I (a), (d), (f) bond type II (b), (e), (g) bond type III (c) and bond length are defined. Their relative energies are at the B3LYP/6-31G(d) and B3LYP/3-21G (in parenthesis), in kcal/mol. Their clear views are located on the top.

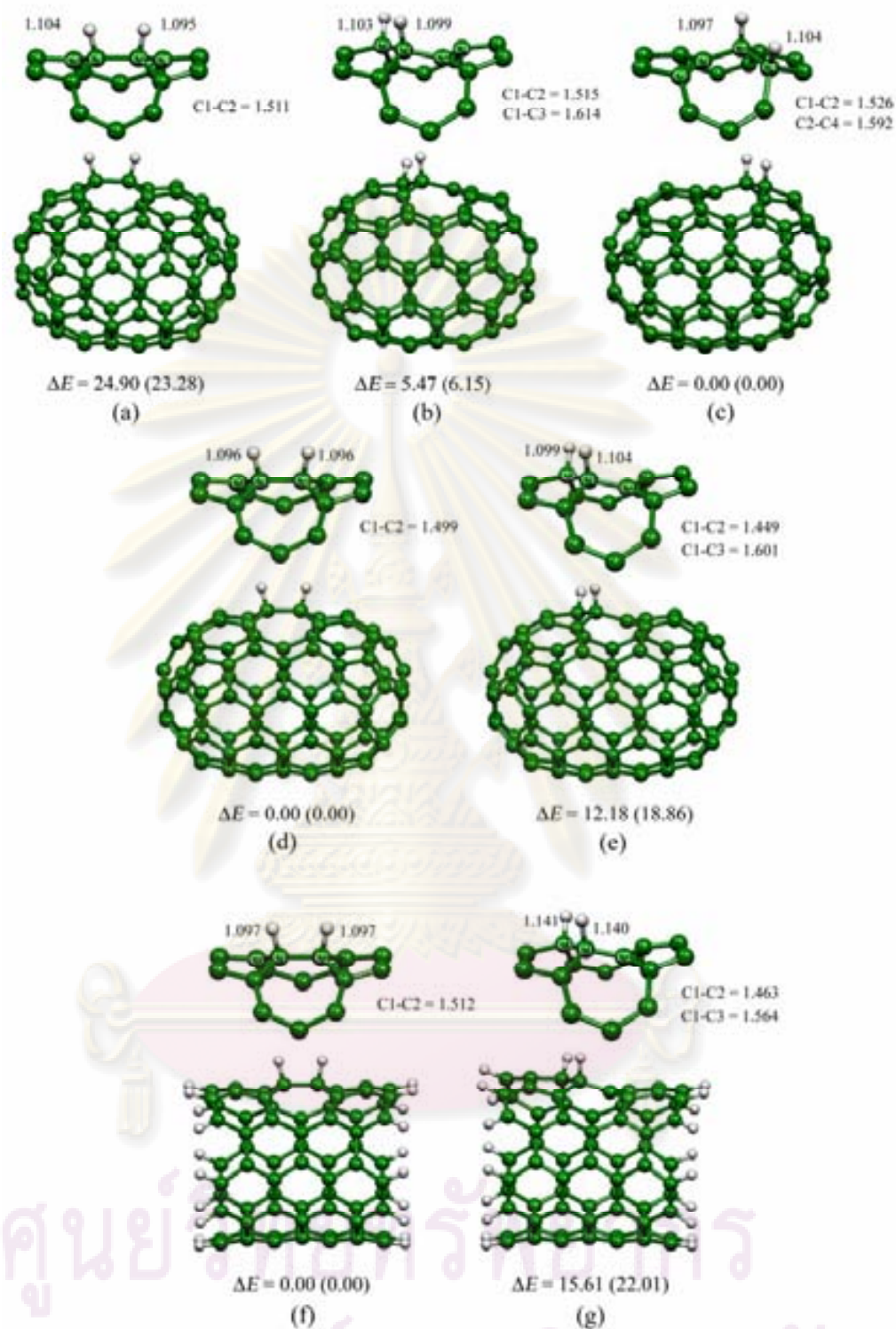


Figure 4.2 Adsorption of double hydrogen-atoms to SW defect of cap-ended C_{80} , C_{90} and open-ended $C_{70}H_{20}$ on two carbon atoms of bond type I (a), (d), (f) bond type II (b), (e), (g) bond type III (c) and bond length are defined. Their relative energies are at the B3LYP/6-31G(d) and B3LYP/3-21G (in parenthesis), in kcal/mol. Their clear views are located on the top.

The data provided in Figures 4.1 and 4.2 indicated that the chemisorptions of two hydrogen atoms significantly altered the C-C bond lengths of SWCNTs in the vicinity of addition sites. This is due to the change in hybridization of the carbon atoms from sp^2 to sp^3 at the adsorption sites. Bond lengths of C-C bonds in bare tubes of pristine SWCNTs are in range 1.40 to 1.46 Å and bond lengths of C-C bonds in bare tubes of SW defect SWCNTs are in range 1.33 to 1.48 Å (as shown in Figures 4.3 and 4.4). While fully optimization presents many of the bond distances are longer than 1.5 Å for both perfect and SW defect SWCNTs, which represents typical bond length of sp^2 - sp^3 C-C single bonds. This indicated weakening of the C-C bonds in the region of hydrogen chemisorption.

Not only difference in bond lengths between C-C bond lengths is determined, the bond lengths of newly formed C-H bonds in the H-chemisorbed on both pristine and SW defect SWCNTs are found to be about 1.1 Å.

Table 4.1 Total energy and relative energy of hydrogen adsorption complexes on pristine and SW-defect SWCNTs calculated at B3LYP/3-21G and B3LYP/6-31G(d) levels of theory

Complexes:	Total Energy (E_{total}) ^a		Relative energy (ΔE_{rel}) ^b	
	B3LYP/3-21G	B3LYP/6-31G(d)	B3LYP/3-21G	B3LYP/6-31G(d)
<i>Pristine:</i>				
2H/C _{80-I} ^c	-3032.662781	-3049.554948	20.70	15.92
2H/C _{80-II}	-3032.651644	-3049.537959	27.69	26.58
2H/C _{80-III}	-3032.695773	-3049.580318	0.00	0.00
2H/C _{90-I}	-3411.686483	-3430.685909	0.00	0.00
2H/C _{90-II}	-3411.673170	-3430.674637	8.35	7.07
2H/C ₇₀ H _{20-I}	-2665.893189	-2680.709746	0.00	0.00
2H/C ₇₀ H _{20-II}	-2665.890677	-2680.707065	1.58	1.68
<i>SW Defect:</i>				
2H/SW-C _{80-I} ^c	-3032.512020	-3049.401319	23.28	24.90
2H/SW-C _{80-II}	-3032.539307	-3049.432281	6.15	5.47
2H/SW-C _{80-III}	-3032.549114	-3049.440992	0.00	0.00
2H/SW-C _{90-I}	-3411.534948	-3430.536802	0.00	0.00
2H/SW-C _{90-II}	-3411.504896	-3430.517386	18.86	12.18
2H/SW-C ₇₀ H _{20-I}	-2665.799244	-2680.622668	0.00	0.00
2H/SW-C ₇₀ H _{20-II}	-2665.764170	-2680.597798	22.01	15.61

^a In a.u.

^b In kcal/mol.

^c Adsorption site is on the C-C bond of type I.

Table 4.2 Total energy of bare tube at adsorbed form and strain of pristine and SW-defect SWCNTs calculated at B3LYP/3-21G and B3LYP/6-31G(d) levels of theory

Complexes:	$E_{\text{total}}^{\text{a}}$		$E_{\text{strain}}^{\text{b}}$	
	B3LYP/3-21G	B3LYP/6-31G(d)	B3LYP/3-21G	B3LYP/6-31G(d)
<i>Pristine:</i>				
2H/C ₈₀ -I ^c	-3031.416761	-3048.315243	50.68	44.87
2H/C ₈₀ -II	-3031.428453	-3048.314958	43.34	45.05
2H/C ₈₀ -III	-3031.432356	-3048.322067	40.89	40.59
2H/C ₉₀ -I	-3410.447300	-3429.450068	43.18	44.18
2H/C ₉₀ -II	-3410.433271	-3429.442686	51.98	48.81
2H/C ₇₀ H ₂₀ -I	-2664.658638	-2679.481516	43.71	43.82
2H/C ₇₀ H ₂₀ -II	-2664.636463	-2679.460492	57.62	57.02
<i>SW Defect:</i>				
2H/SW-C ₈₀ -I ^c	-3031.270744	-3048.165643	47.02	44.72
2H/SW-C ₈₀ -II	-3031.293380	-3048.189933	32.82	29.48
2H/SW-C ₈₀ -III	-3031.299607	-3048.200899	28.91	22.60
2H/SW-C ₉₀ -I	-3410.299094	-3429.303650	48.88	48.98
2H/SW-C ₉₀ -II	-3410.296621	-3429.302509	50.43	49.70
2H/SW-C ₇₀ H ₂₀ -I	-2664.563150	-2679.386037	53.48	56.30
2H/SW-C ₇₀ H ₂₀ -II	-2664.557894	-2679.378772	56.78	60.85

^a In a.u.

^b In kcal/mol.

^c Adsorption site is on the C-C bond of type I.

Adsorption energies of two hydrogen atoms compared with the hydrogen molecule and proton-radicals on the various armchair (5,5) SWCNTs are shown in Table 4.3. Based on the B3LYP/6-31G(d) level, it shows the adsorption energies on C-C bond types (I, II and III) of SWCNTs as following remarks.

For adsorption on the pristine SWCNTs adsorption energies are within the range of -29.82 to -51.94 kcal/mol for C₈₀, -35.43 to -37.88 kcal/mol for C₉₀, -33.10 to -44.61 kcal/mol for C₇₀H₂₀. For adsorption on the SW defect SWCNTs adsorption energies are within the range of -37.77 to -41.96 kcal/mol for SW-C₈₀, -24.72 to -36.19 kcal/mol for SW-C₉₀, -27.32 to -38.37 for SW-C₇₀H₂₀.

The most stable adsorption configurations of both pristine and SW defect are the adsorption complexes of two hydrogen-atoms on C1-C3 bond for C₈₀, C2-C3 for SW-C₈₀, C1-C2 for C₉₀ and SW-C₉₀, C1-C3 for C₇₀H₂₀ and C1-C2 for the SW-C₇₀H₂₀ SWCNTs. The C₈₀ curvature causes the less stable for the C1-C2 bond of C₈₀ and the C1-C3 bond of SW-C₈₀.

As we cannot differentiate the adsorption energies of hydrogen on the pristine and SW defect armchair (5,5) SWCNTs, therefore used of the pyramidalization angle (θ_p) of adsorption carbon atom which obtained from the π -orbital axis vector (POAV) as a tool to describe the adsorption energy. POAV is defined as that vector which makes equal angles ($\theta_{\sigma\pi}$) to the three σ -bonds at a conjugated carbon atom, and the pyramidalization angle is obtained as $\theta_p = (\theta_{\sigma\pi} - 90)^\circ$. It was found that the carbon atoms with large values of θ_p exhibit high reactivity. Pyramidalization angle are shown in Table 4.4.

Tables 4.3 and 4.4 show that the curvatures in terms of θ_p , of adsorption carbon atoms on any SWCNTs donot correlate within their corresponding adsorption energies.

Table 4.3 Adsorption energy of hydrogen molecule and two hydrogen atom to pristine and SW-defect SWCNTs calculated at B3LYP/3-21G and B3LYP/6-31G(d) levels of theory

Complexes:	$\Delta E_{\text{ads}} (\text{H}_2)^a$		$\Delta E_{\text{ads}} (2\text{H}\cdot)^a$	
	B3LYP/3-21G	B3LYP/6-31G(d)	B3LYP/3-21G	B3LYP/6-31G(d)
<i>Pristine:</i>				
2H/C _{80-I} ^b	-47.32	-40.30	-157.75	-150.08
2H/C _{80-II}	-32.99	-29.82	-143.43	-139.59
2H/C _{80-III}	-58.24	-51.94	-168.67	-161.71
2H/C _{90-I}	-43.03	-37.88	-153.46	-147.65
2H/C _{90-II}	-43.48	-35.43	-153.91	-145.21
2H/C _{70H_{20-I}}	-40.12	-33.10	-150.56	-142.87
2H/C _{70H_{20-II}}	-52.46	-44.61	-162.90	-154.39
<i>SW Defect:</i>				
2H/SW-C _{80-I} ^b	-44.34	-37.77	-154.78	-147.55
2H/SW-C _{80-II}	-47.26	-41.96	-157.70	-151.73
2H/SW-C _{80-III}	-49.51	-40.54	-159.94	-150.32
2H/SW-C _{90-I}	-40.94	-36.19	-151.37	-145.96
2H/SW-C _{90-II}	-23.63	-24.72	-134.07	-134.49
2H/SW-C _{70H_{20-I}}	-41.09	-38.37	-151.53	-148.15
2H/SW-C _{70H_{20-II}}	-22.38	-27.32	-132.81	-137.10

^a In kcal/mol.

^b Adsorption site is on the C-C bond of type I.

Table 4.4 Pyramidalization angle of pristine and the SW defect armchair (5,5) SWCNTs

Complexes:	Adsorption atom	θ_p^a	Adsorption atom	θ_p^a
<i>Pristine:</i>				
2H/C _{80-I} ^b	C1	16.79	C2	16.79
2H/C _{80-II}	C1	15.65	C3	15.65
2H/C _{80-III}	C2	18.30	C3	15.95
2H/C _{90-I}	C1	14.46	C2	14.46
2H/C _{90-II}	C1	16.95	C3	15.62
2H/C _{70H_{20-I}}	C1	15.19	C2	15.19
2H/C _{70H_{20-II}}	C1	18.20	C3	17.66
<i>SW defect:</i>				
2H/SW-C _{80-I} ^b	C1	13.89	C2	12.43
2H/SW-C _{80-II}	C1	14.64	C3	18.28
2H/SW-C _{80-III}	C2	16.40	C3	16.59
2H/SW-C _{90-I}	C1	12.20	C2	12.20
2H/SW-C _{90-II}	C1	14.42	C3	15.24
2H/SW-C _{70H_{20-I}}	C1	11.42	C2	11.42
2H/SW-C _{70H_{20-II}}	C1	17.11	C3	15.39

^a In Å.

^b Adsorption site is on the C–C bond of type I.

ศูนย์วิทยทรัพยากร
จุฬาลงกรณ์มหาวิทยาลัย

4.1.2 The partial-structure optimization

The structures of adsorption complexes of hydrogen on the pristine and SW defect armchair (5,5) SWCNTs based on the rigid structure model are shown in Figures 4.3 and 4.4, respectively. They show that the C-H bond length for all adsorption complexes are longer than their corresponding structures obtained by the full-structure optimization.

Total energies and the relative stabilities of adsorption complexes of two hydrogen-atoms on the SWCNTs are shown in Table 4.5. Due to structure based on isolated form of the SWCNTs, therefore no strain of their adsorption-state structure is found. Relative stabilities of adsorption complexes of two hydrogen-atoms on each type of pristine SWCNTs are in orders: $2\text{H}/\text{C}_{80_III} > 2\text{H}/\text{C}_{80_II} > 2\text{H}/\text{C}_{80_I}$ for C_{80} , $2\text{H}/\text{C}_{90_I} > 2\text{H}/\text{C}_{90_II}$ for C_{90} and $2\text{H}/\text{C}_{70\text{H}_{20_I}} > 2\text{H}/\text{C}_{70\text{H}_{20_II}}$ for $\text{C}_{70\text{H}_{20}}$ and relative stabilities of adsorption complexes of two hydrogen-atoms on each type of SW defect SWCNTs are in orders: $2\text{H}/\text{SW-C}_{80_III} > 2\text{H}/\text{SW-C}_{80_II} > 2\text{H}/\text{SW-C}_{80_I}$ for SW- C_{80} , $2\text{H}/\text{SW-C}_{90_I} > 2\text{H}/\text{SW-C}_{90_II}$ for SW- C_{90} and $2\text{H}/\text{SW-C}_{70\text{H}_{20_I}} > 2\text{H}/\text{SW-C}_{70\text{H}_{20_II}}$ for SW- $\text{C}_{70\text{H}_{20}}$.

ศูนย์วิทยทรัพยากร
จุฬาลงกรณ์มหาวิทยาลัย

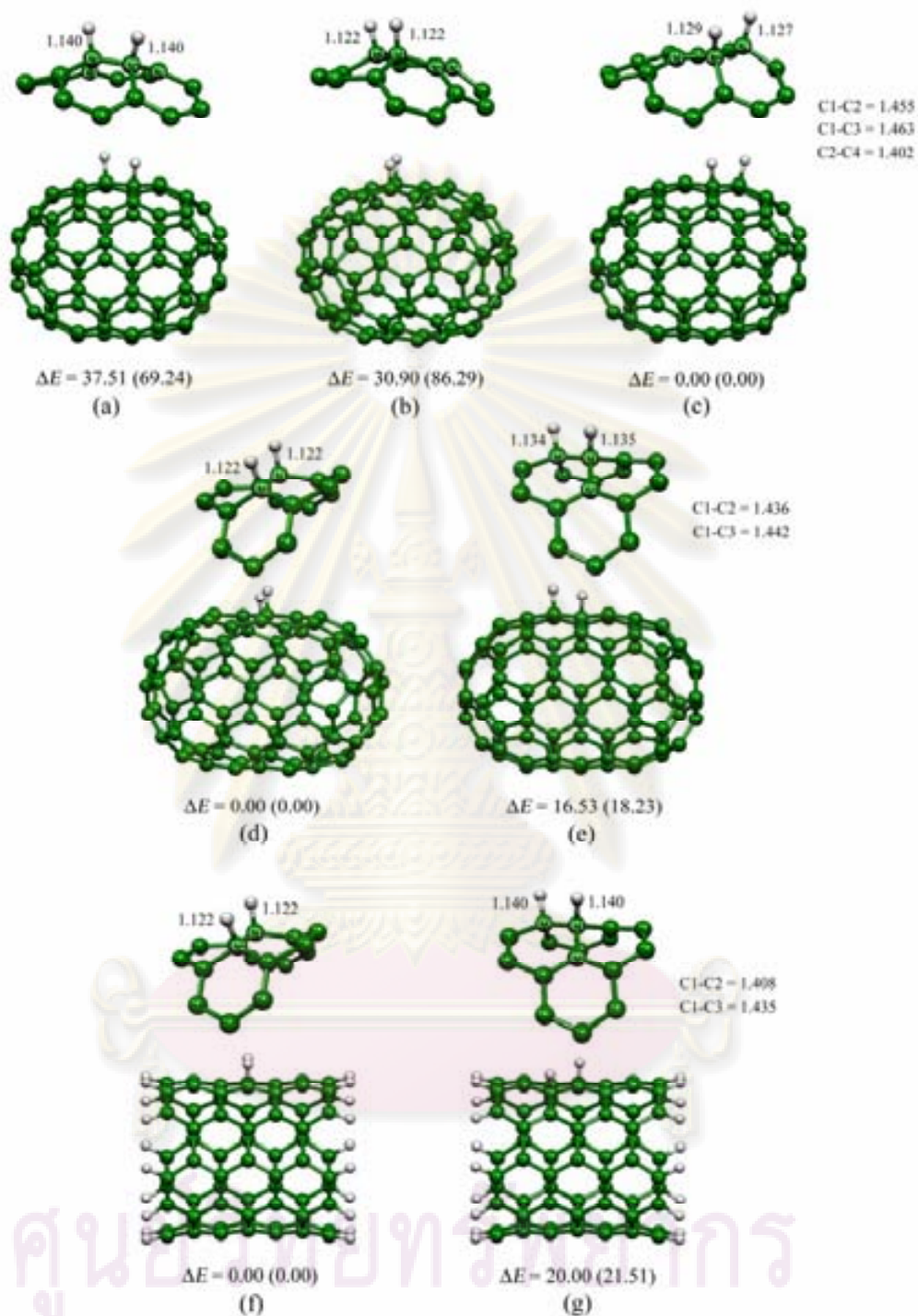


Figure 4.3 Adsorption of double hydrogen-atoms to rigid structure of pristine cap-ended C₈₀, C₉₀ and open-ended C₇₀H₂₀ on two carbon atoms of bond type I (a), (d), (f) bond type II (b), (e), (g) bond type III (c) and bond length are defined. Their relative energies are at the B3LYP/6-31G(d) and B3LYP/3-21G (in parenthesis), in kcal/mol. Their clear views are located on the top.

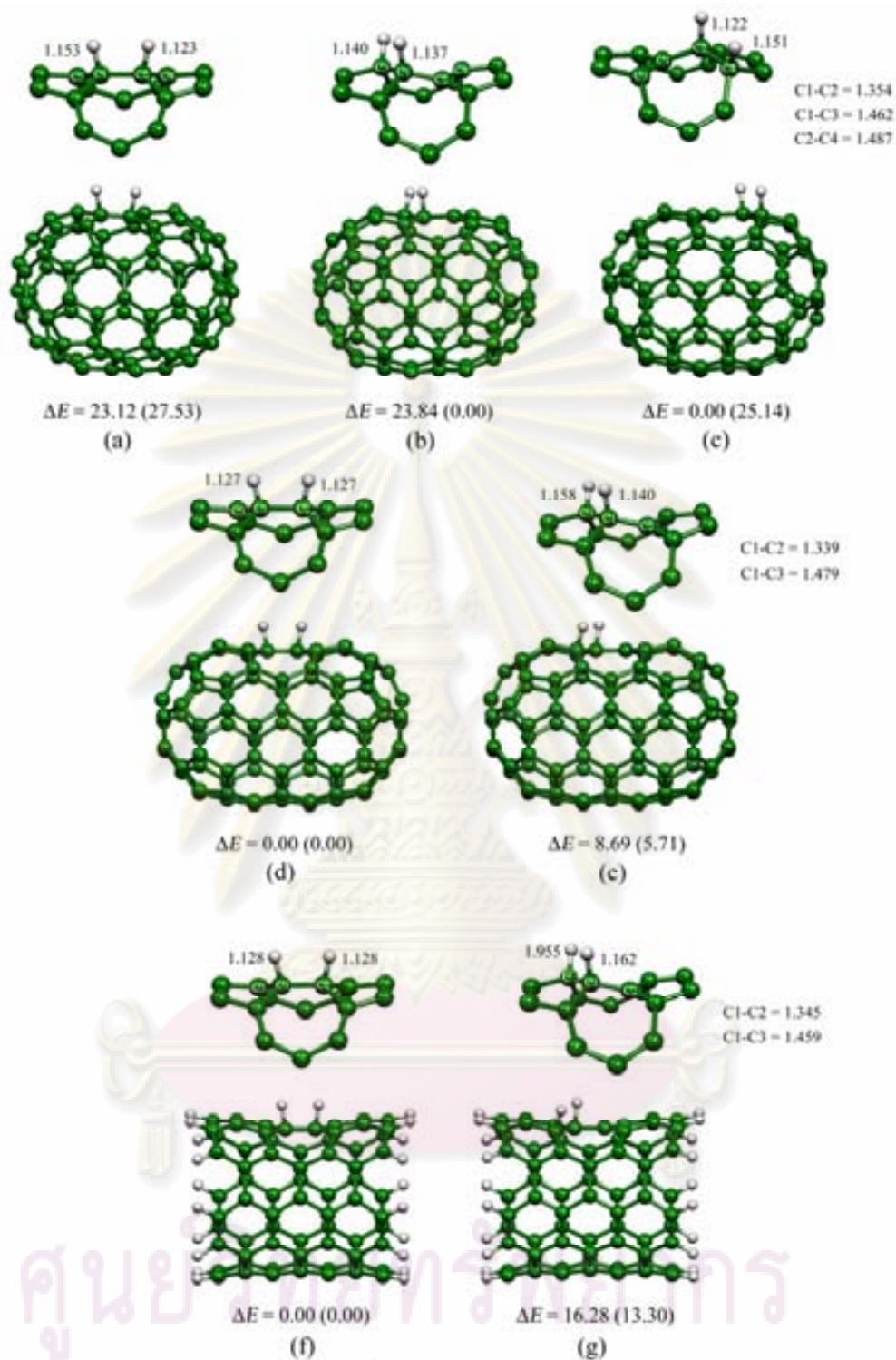


Figure 4.4 Adsorption of double hydrogen–atoms to rigid structure of SW defect of cap-ended C_{80} , C_{90} and open-ended $C_{70}H_{20}$ on two carbon atoms of bond type I (a), (d), (f) bond type II (b), (e), (g) bond type III (c) and bond length are defined. Their relative energies are at the B3LYP/6-31G(d) and B3LYP/3-21G (in parenthesis), in kcal/mol. Their clear views are located on the top.

Table 4.5 Total energy and relative energy of rigid structure of pristine and SW-defect SWCNTs calculated at B3LYP/3-21G and B3LYP/6-31G(d) levels of theory using frozen models

Complexes:	Total Energy (E_{total}) ^a		Relative energy (ΔE_{rel}) ^b	
	B3LYP/3-21G	B3LYP/6-31G(d)	B3LYP/3-21G	B3LYP/6-31G(d)
<i>Perfect:</i>				
2H/C _{80-I} ^c	-3032.542411	-3049.438969	42.87	37.51
2H/C _{80-II}	-3032.558260	-3049.449500	32.92	30.90
2H/C _{80-III}	-3032.610727	-3049.498738	0.00	0.00
2H/C _{90-I}	-3411.593474	-3430.598601	0.00	0.00
2H/C _{90-II}	-3411.564417	-3430.572261	18.23	16.53
2H/C _{70H_{20-I}}	-2665.796089	-2680.618417	0.00	0.00
2H/C _{70H_{20-II}}	-2665.761804	-2680.586553	21.51	20.00
<i>SW Defect:</i>				
2H/SW-C _{80-I} ^c	-3032.427392	-3049.325586	27.53	23.12
2H/SW-C _{80-II}	-3032.431203	-3049.324438	25.14	23.84
2H/SW-C _{80-III}	-3032.471271	-3049.362433	0.00	0.00
2H/SW-C _{90-I}	-3411.434888	-3430.448252	0.00	0.00
2H/SW-C _{90-II}	-3411.425796	-3430.434404	5.71	8.69
2H/SW-C _{70H_{20-I}}	-2665.691708	-2680.526765	0.00	0.00
2H/SW-C _{70H_{20-II}}	-2665.670510	-2680.500816	13.30	16.28

^a In a.u.

^b In kcal/mol.

^c Adsorption site is on the C–C bond of type I.

ศูนย์วิทยทรัพยากร
จุฬาลงกรณ์มหาวิทยาลัย

Table 4.6 Interaction energy of hydrogen molecule and two hydrogen atoms on rigid structure of pristine and SW-defect SWCNTs calculated at B3LYP/3-21G and B3LYP/6-31G(d) levels of theory using frozen models

Complexes:	$\Delta E_{\text{int}}(\text{H}_2)^a$		$\Delta E_{\text{int}}(2\text{H})^a$	
	B3LYP/3-21G	B3LYP/6-31G(d)	B3LYP/3-21G	B3LYP/6-31G(d)
<i>Pristine:</i>				
2H/C ₈₀ -I ^b	78.89	77.35	-31.55	-32.43
2H/C ₈₀ -II	68.94	70.74	-41.49	-39.04
2H/C ₈₀ -III	36.02	39.84	-74.41	-69.93
2H/C ₉₀ -I	58.51	61.09	-51.92	-48.69
2H/C ₉₀ -II	76.75	77.62	-33.69	-32.16
2H/C ₇₀ H ₂₀ -I	64.52	68.03	-45.92	-41.74
2H/C ₇₀ H ₂₀ -II	86.03	88.03	-24.40	-21.74
<i>SW Defect:</i>				
2H/SW-C ₈₀ -I ^b	55.78	54.47	-54.65	-55.30
2H/SW-C ₈₀ -II	28.25	55.19	-82.19	-54.58
2H/SW-C ₈₀ -III	53.39	31.35	-57.04	-78.42
2H/SW-C ₉₀ -I	70.73	68.36	-39.71	-41.41
2H/SW-C ₉₀ -II	76.43	77.05	-34.00	-32.72
2H/SW-C ₇₀ H ₂₀ -I	79.87	78.10	-30.56	-31.67
2H/SW-C ₇₀ H ₂₀ -II	93.17	94.39	-17.26	-15.39

^a In kcal/mol.

^b Adsorption site is on the C-C bond of type I.

As the interaction energies of adsorption complexes are all positive, their adsorption properties as adsorption energy are not termed. Table 4.6 shows that the adsorption complexes are less stable than their corresponding isolated hydrogen molecule but more stable than their corresponding isolated hydrogen atoms.

ศูนย์วิทยทรัพยากร
จุฬาลงกรณ์มหาวิทยาลัย

4.2 Adsorption mechanism of addition of hydrogen molecule to armchair (5,5) SWCNTs

Reaction mechanism of addition of hydrogen molecule to C-C atoms of the SWCNTs were carried out using the ONIOM(B3LYP/3-21G:AM1) and ONIOM(B3LYP/6-31G(d):AM1) levels of theory. Model of the transition state based on the most stable adsorption complexes of each types of SWCNTs which carried out at the B3LYP/6-31G(d) calculation as mentioned in Chapter 3.

The transition-state structures of hydrogen adsorbed to C-C bond of various SWCNTs are shown in Figure 4.5. Reaction mechanism of hydrogen adsorption at C-C bond at the SWCNT is shown in Figure 4.6. It shows that the adsorption process of hydrogen addition to C-C bond occurs via the transition state, and afford the stable adsorption complex. The transition states of all adsorption processes are verified by their single imaginary vibrational frequencies, see Table 4.7.

Table 4.7 Activation energies and single imaginary vibrational frequencies of hydrogen molecule adsorbed to pristine and SW defect armchair (5,5) SWCNTs, at the ONIOM(B3LYP/6-31G(d):AM1) and ONIOM(B3LYP/3-21G:AM1) (in parenthesis)

Adsorption reaction	$\Delta^\ddagger E^a$	ν_i
<i>Pristine SWCNTs :</i>		
$H_2 + C_{80} \rightarrow TS \rightarrow 2H/C_{80}$	66.23 (66.89)	2802.94i (2808.57i)
$H_2 + C_{90} \rightarrow TS \rightarrow 2H/C_{90}$	70.23 (71.75)	2411.04i (2445.27i)
$H_2 + C_{70}H_{20} \rightarrow TS \rightarrow 2H/C_{70}H_{20}$	79.29 (81.31)	2920.85i (2966.53i)
<i>SW Defect SWCNTs :</i>		
$H_2 + SW-C_{80} \rightarrow TS \rightarrow 2H/SW-C_{80}$	56.13 (53.72)	2471.70i (2488.06i)
$H_2 + SW-C_{90} \rightarrow TS \rightarrow 2H/SW-C_{90}$	73.33 (74.84)	2350.15i (2420.95i)
$H_2 + SW-C_{70}H_{20} \rightarrow TS \rightarrow 2H/SW-C_{70}H_{20}$	89.64 (88.69)	4694.25i (4642.24i)

^a In kcal/mol.

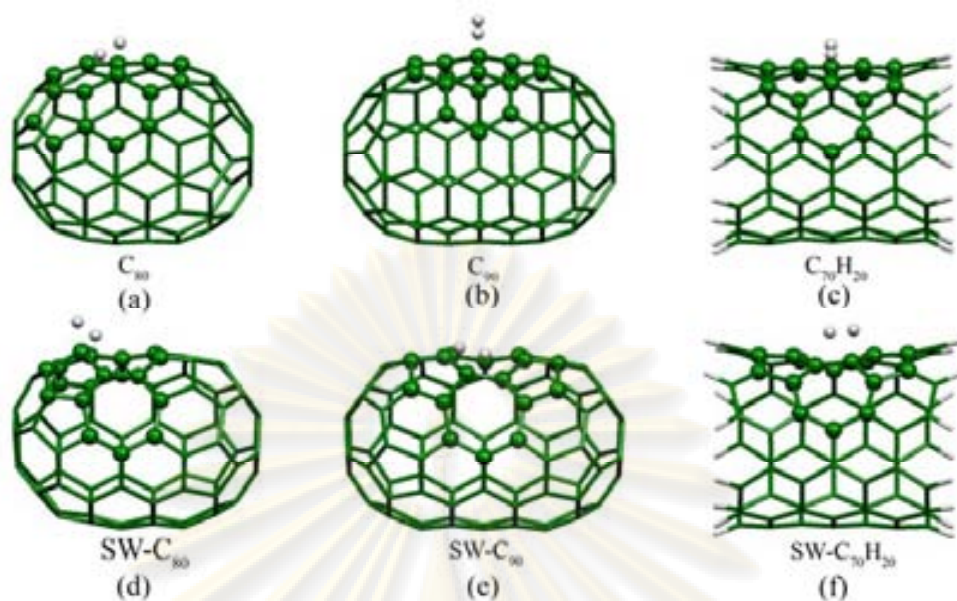


Figure 4.5 Transition-state of structures adsorption process on the pristine (a) cap-ended C_{80} , (b) C_{90} , (c) open-ended $C_{70}H_{20}$ and the SW defect (d) cap-ended SW- C_{80} , (e) SW- C_{90} , (f) open-ended SW- $C_{70}H_{20}$ armchair (5,5) SWCNTs.

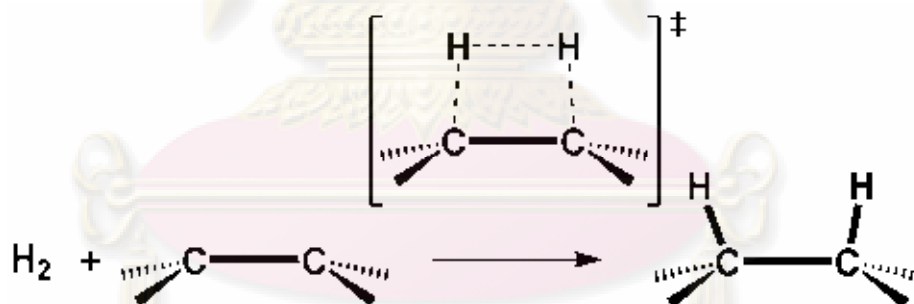


Figure 4.6 Addition of hydrogen molecule to C–C binding site.

4.3 B-doped armchair (5,5) SWCNTs

B-doped Pristine and SW defect armchair (5,5) SWCNTs of cap-ended C_{80} , C_{90} and open-end $C_{70}H_{20}$ as double boron atoms doping were studied using flexible and rigid structure models. Boron doping types can be separated into three types as shown in Figures 3.5 - 3.6 (Chapter 3) and the possible number of their hydrogen adsorption complexes is therefore three configurations.

All geometry optimizations of B-doped SWCNTs and their hydrogen adsorption complexes were carried out at the ONIOM(B3LYP/6-31G(d):AM1) level of theory. Based on the various armchair (5,5) SWCNTs which geometry optimizations were carried out at the same theory, total energies and adsorption energies of adsorption complexes of hydrogen on the armchair (5,5) SWCNTs for flexible and rigid models are shown in Tables A-8 to A-11.

Total energies and the relative stabilities of adsorption complexes of hydrogen on the B-doped type I, II and III armchair (5,5) SWCNTs are shown in Tables A-2 to A-7, respectively. Adsorption configurations of two hydrogen atoms adsorbed on B-doped SWCNTs types I, II and III are shown in Figures 4.7-4.12.

4.3.1 B-doped type I

The adsorption configurations of double hydrogen-atoms on pristine and the SW defect of B-doped armchair (5,5) SWCNTs are shown in Figures 4.7 and 4.8, respectively obtained at the ONIOM(B3LYP/6-31G(d):AM1) levels of theory, two atoms of the hydrogen molecule adsorbed on the C-C binding atoms as mentioned in Chapter 3.

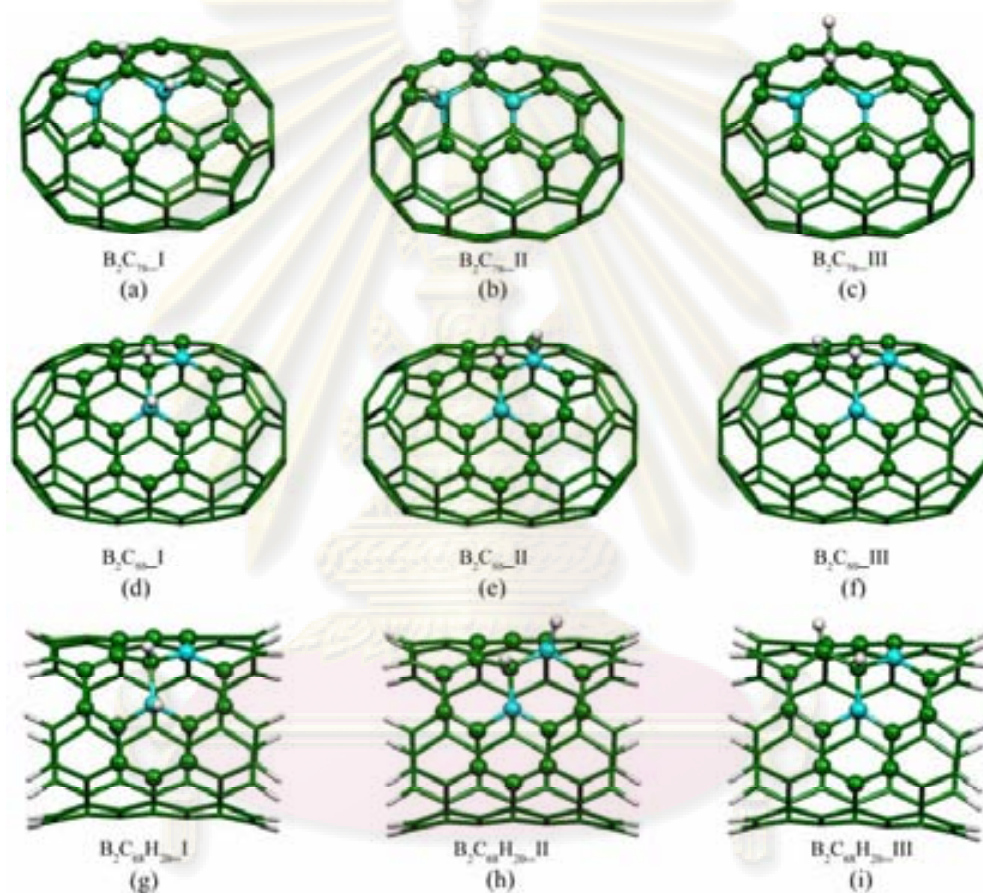


Figure 4.7 Adsorption complexes of two hydrogen-atoms adsorbed on various pristine armchair (5,5) B-doped SWCNTs (type I).

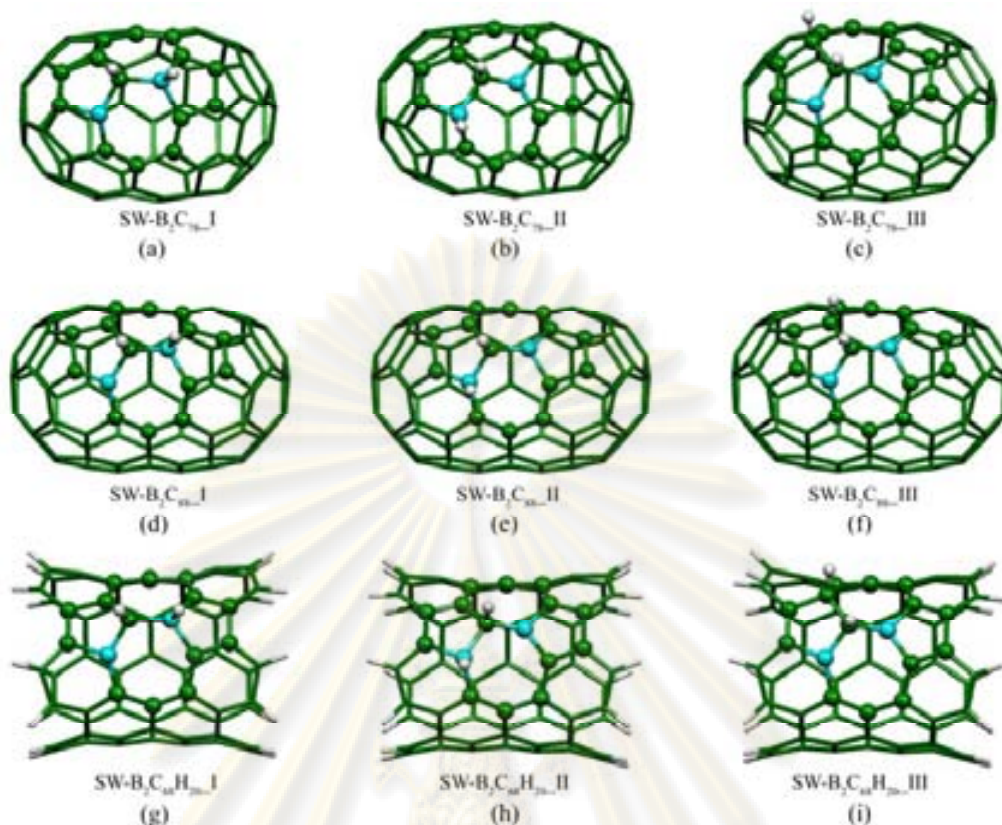


Figure 4.8 Adsorption complexes of two hydrogen-atoms adsorbed on various Stone-Wales defect armchair (5,5) B-doped SWCNTs (type I).

Relative stabilities of adsorption complexes of two hydrogen-atoms on each type of pristine B-doped SWCNTs are in orders: $2\text{H}/\text{B}_2\text{C}_{78_III} > 2\text{H}/\text{B}_2\text{C}_{78_I} > 2\text{H}/\text{B}_2\text{C}_{78_II}$ for B_2C_{78} tubes, $2\text{H}/\text{B}_2\text{C}_{88_II} > 2\text{H}/\text{B}_2\text{C}_{88_III} > 2\text{H}/\text{B}_2\text{C}_{88_I}$ for B_2C_{88} tubes, $2\text{H}/\text{B}_2\text{C}_{68}\text{H}_{20_II} > 2\text{H}/\text{B}_2\text{C}_{68}\text{H}_{20_III} > 2\text{H}/\text{B}_2\text{C}_{68}\text{H}_{20_I}$ for $\text{B}_2\text{C}_{68}\text{H}_{20}$ tubes and relative stabilities of adsorption complexes of two hydrogen-atoms on each type of SW defect B-doped SWCNTs are in orders: $2\text{H}/\text{SW-B}_2\text{C}_{78_III} > 2\text{H}/\text{SW-B}_2\text{C}_{78_II} > 2\text{H}/\text{SW-B}_2\text{C}_{78_I}$ for B_2C_{78} , $2\text{H}/\text{SW-B}_2\text{C}_{88_II} > 2\text{H}/\text{SW-B}_2\text{C}_{88_III} > 2\text{H}/\text{SW-B}_2\text{C}_{88_I}$ for B_2C_{88} , $2\text{H}/\text{SW-B}_2\text{C}_{68}\text{H}_{20_III} > 2\text{H}/\text{SW-B}_2\text{C}_{68}\text{H}_{20_II} > 2\text{H}/\text{SW-B}_2\text{C}_{68}\text{H}_{20_I}$ for $\text{B}_2\text{C}_{68}\text{H}_{20}$.

Adsorption energies of hydrogen molecule adsorbed on B-doped armchair (5,5) SWCNTs of pristine and rigid structure types I are shown in Tables 4.8 and 4.9.

Table 4.8 Adsorption energies of hydrogen molecule and two proton-radicals on various pristine and SW defect armchair (5,5) B-doped SWCNTs (type I)

Complexes :	ΔE_{ads} , ONIOM(B3LYP/6-31G(d):AM1) ^a			
	Pristine SWCNTs		SW Defect SWCNTs	
	H ₂	2H [•]	H ₂	2H [•]
<i>B-doped C₈₀</i> :				
2H/B ₂ C _{78-I} ^b	-45.09	-154.86	-29.73	-139.50
2H/B ₂ C _{78-II}	-41.05	-150.82	-54.50	-164.28
2H/B ₂ C _{78-III}	-50.24	-160.02	-91.35	-201.13
<i>B-doped C₉₀</i> :				
2H/B ₂ C _{88-I}	-46.94	-156.71	-25.57	-135.35
2H/B ₂ C _{88-II}	-42.93	-152.70	-57.43	-167.21
2H/B ₂ C _{88-III}	-51.24	-161.01	-36.05	-145.82
<i>B-doped C₇₀H₂₀</i> :				
2H/B ₂ C ₆₈ H _{20-I}	-43.33	-153.11	-24.16	-133.93
2H/B ₂ C ₆₈ H _{20-II}	-52.20	-161.97	-49.16	-158.94
2H/B ₂ C ₆₈ H _{20-III}	-61.16	-170.93	-71.01	-180.78

^a In kcal/mol.

^b Adsorption site is on the C–C bond of type I.

ศูนย์วิทยทรัพยากร
จุฬาลงกรณ์มหาวิทยาลัย

Table 4.9 Interaction energies of hydrogen molecule and two proton-radicals on various rigid structure of pristine and SW defect armchair (5,5) B-doped SWCNTs (type I)

Complexes :	$\Delta E'_{\text{ads}}$, ONIOM (B3LYP/6-31G(d):AM1) ^a			
	Pristine SWCNTs		SW Defect SWCNTs	
	H ₂	2H [•]	H ₂	2H [•]
<i>B-doped C₈₀:</i>				
2H/B ₂ C _{78-I} ^b	10.25	-99.52	37.30	-72.47
2H/B ₂ C _{78-II}	17.71	-92.06	8.02	-101.75
2H/B ₂ C _{78-III}	17.01	-92.77	-19.28	-129.06
<i>B-doped C₉₀:</i>				
2H/B ₂ C _{88-I}	-3.87	-113.64	68.89	-40.88
2H/B ₂ C _{88-II}	-9.23	-119.00	26.37	-83.41
2H/B ₂ C _{88-III}	-3.86	-113.64	1.47	-108.30
<i>B-doped C₇₀H₂₀:</i>				
2H/B ₂ C ₆₈ H _{20-I}	1.38	-108.39	68.24	-41.53
2H/B ₂ C ₆₈ H _{20-II}	0.05	-109.73	40.38	-69.39
2H/B ₂ C ₆₈ H _{20-III}	1.38	-108.39	56.74	-53.03

^a In kcal/mol.

^b Adsorption site is on the C–C bond of type I.

4.4.2 B-doped type II

The adsorption configurations of double hydrogen-atoms on pristine and the SW defect of B-doped armchair (5,5) SWCNTs are shown in Figures 4.9 and 4.10, respectively. Relative stabilities of adsorption complexes of two hydrogen-atoms on each type of pristine B-doped SWCNTs are in orders: 2H/B₂C_{78-I} > 2H/B₂C_{78-III} > 2H/B₂C_{78-II} for B₂C₇₈, 2H/B₂C_{88-III} > 2H/B₂C_{88-I} > 2H/B₂C_{88-II} for B₂C₈₈, 2H/B₂C₆₈H_{20-III} > 2H/B₂C₆₈H_{20-I} > 2H/B₂C₆₈H_{20-II} for B₂C₆₈H₂₀ and relative stabilities of adsorption complexes of two hydrogen-atoms on each type of SW defect B-doped SWCNTs are in orders: 2H/SW-B₂C_{78-III} > 2H/SW-B₂C_{78-I} > 2H/SW-B₂C_{78-II} for B₂C₇₈, 2H/SW-B₂C_{88-III} > 2H/SW-B₂C_{88-II} > 2H/SW-B₂C_{88-I} for B₂C₈₈, 2H/SW-B₂C₆₈H_{20-III} > 2H/SW-B₂C₆₈H_{20-II} > 2H/SW-B₂C₆₈H_{20-I} for B₂C₆₈H₂₀.

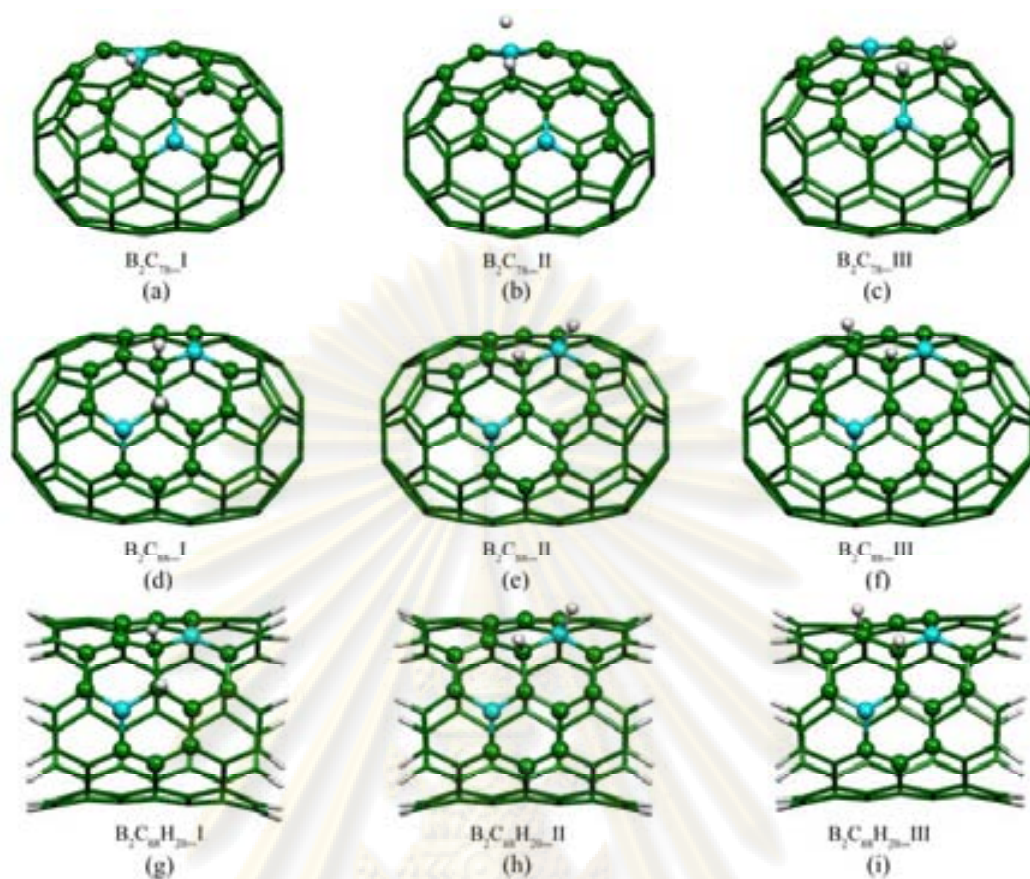


Figure 4.9 Adsorption complexes of two hydrogen-atoms adsorbed on various pristine armchair (5,5) B-doped SWCNTs (type II).

ศูนย์วิทยทรัพยากร
จุฬาลงกรณ์มหาวิทยาลัย

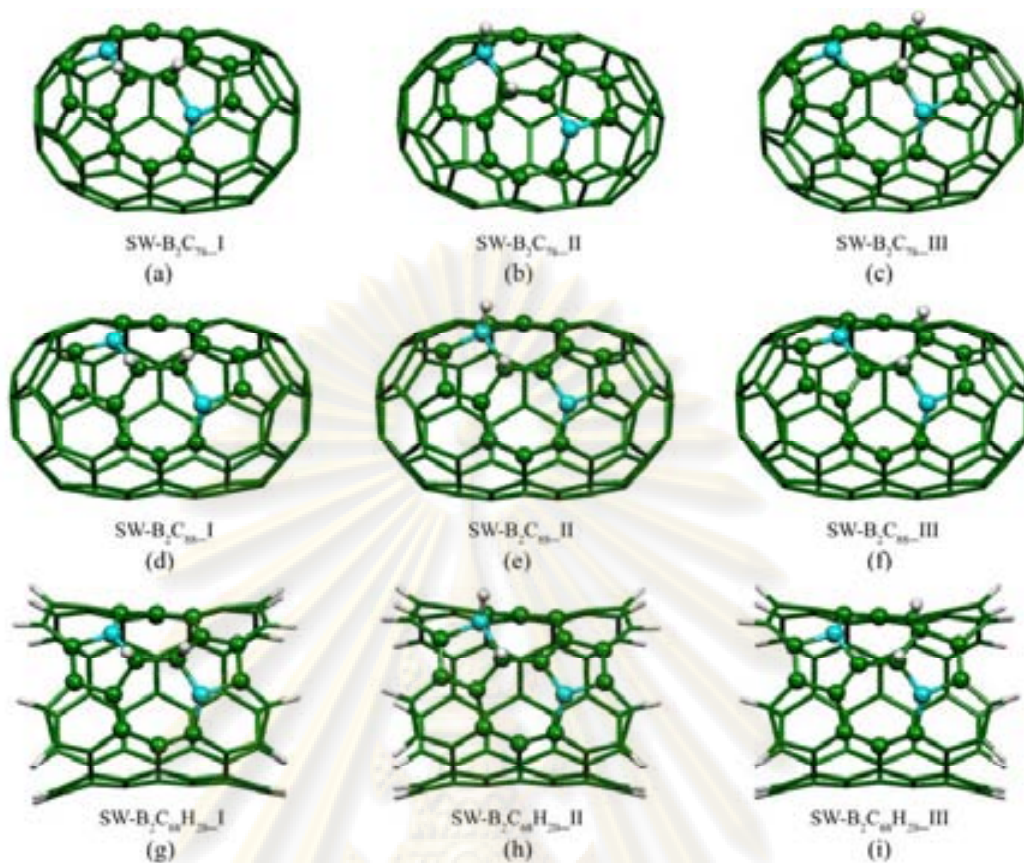


Figure 4.10 Adsorption complexes of two hydrogen-atoms adsorbed on various SW defect armchair (5,5) B-doped SWCNTs (type II).

ศูนย์วิทยทรัพยากร
จุฬาลงกรณ์มหาวิทยาลัย

Adsorption energies of hydrogen molecule adsorbed on B-doped armchair (5,5) SWCNTs of pristine and rigid structure types II are shown in Tables 4.10 and 4.11.

Table 4.10 Adsorption energies of hydrogen molecule and two proton-radicals on various pristine and SW defect armchair (5,5) B-doped SWCNTs (type II)

Complexes :	ΔE_{ads} , ONIOM(B3LYP/6-31G(d):AM1) ^a			
	Pristine SWCNTs		SW Defect SWCNTs	
	H ₂	2H [•]	H ₂	2H [•]
<i>B-doped C₈₀</i> :				
2H/B ₂ C _{78-I} ^b	-63.14	-172.91	-51.03	-160.80
2H/B ₂ C _{78-II}	-38.28	-148.05	-39.38	-149.15
2H/B ₂ C _{78-III}	-71.54	-181.31	-86.81	-196.59
<i>B-doped C₉₀</i> :				
2H/B ₂ C _{88-I}	-28.21	-137.98	-45.92	-155.69
2H/B ₂ C _{88-II}	-28.57	-138.34	-52.09	-161.86
2H/B ₂ C _{88-III}	-68.01	-177.79	-69.88	-179.65
<i>B-doped C₇₀H₂₀</i> :				
2H/B ₂ C ₆₈ H _{20-I}	-54.05	-163.83	-47.49	-157.27
2H/B ₂ C ₆₈ H _{20-II}	-26.44	-136.21	-46.12	-155.89
2H/B ₂ C ₆₈ H _{20-III}	-73.21	-182.98	-81.06	-190.84

^a In kcal/mol.

^b Adsorption site is on the C–C bond of type I.

ศูนย์วิทยทรัพยากร
จุฬาลงกรณ์มหาวิทยาลัย

Table 4.11 Interaction energies of hydrogen molecule and two proton-radicals on to various rigid structures of pristine and SW-defect armchair (5,5) B-doped SWCNTs (type II)

Complexes :	$\Delta E'_{\text{ads}}$, ONIOM (B3LYP/6-31G(d):AM1) ^a			
	Pristine SWCNTs		SW Defect SWCNTs	
	H ₂	2H [•]	H ₂	2H [•]
<i>B-doped C₈₀</i> :				
2H/B ₂ C ₇₈ _I ^b	54.65	-55.12	31.27	-78.50
2H/B ₂ C ₇₈ _II	44.86	-64.92	-0.53	-110.31
2H/B ₂ C ₇₈ _III	97.10	-12.67	29.77	-80.00
<i>B-doped C₉₀</i> :				
2H/B ₂ C ₈₈ _I	51.67	-58.10	78.38	-31.39
2H/B ₂ C ₈₈ _II	21.34	-88.44	-0.52	-110.29
2H/B ₂ C ₈₈ _III	8.55	-101.23	18.91	-90.87
<i>B-doped C₇₀H₂₀</i> :				
2H/B ₂ C ₆₈ H ₂₀ _I	60.09	-49.69	43.04	-66.74
2H/B ₂ C ₆₈ H ₂₀ _II	52.79	-56.99	16.86	-92.92
2H/B ₂ C ₆₈ H ₂₀ _III	10.67	-99.10	37.16	-72.62

^a In kcal/mol.

^b Adsorption site is on the C–C bond of type I.

4.4.3 B-doped type III

The adsorption configurations of double hydrogen-atoms on pristine and the SW defect of B-doped armchair (5,5) SWCNTs are shown in Figures 4.11 and 4.12, respectively. Relative stabilities of adsorption complexes of two hydrogen-atoms on each type of pristine B-doped SWCNTs are in orders: 2H/B₂C₇₈_I > 2H/B₂C₇₈_II > 2H/B₂C₇₈_III for B₂C₇₈, 2H/B₂C₈₈_I > 2H/B₂C₈₈_III > 2H/B₂C₈₈_II for B₂C₈₈, 2H/B₂C₆₈H₂₀_III > 2H/B₂C₆₈H₂₀_I > 2H/B₂C₆₈H₂₀_II for B₂C₆₈H₂₀ and relative stabilities of adsorption complexes of two hydrogen-atoms on each type of SW defect B-doped SWCNTs are in orders: 2H/SW-B₂C₇₈_III > 2H/SW-B₂C₇₈_I > 2H/SW-B₂C₇₈_II for B₂C₇₈, 2H/SW-B₂C₈₈_III > 2H/SW-B₂C₈₈_I > 2H/SW-B₂C₈₈_II for B₂C₈₈, 2H/SW-B₂C₆₈H₂₀_III > 2H/SW-B₂C₆₈H₂₀_I > 2H/SW-B₂C₆₈H₂₀_II for B₂C₆₈H₂₀.

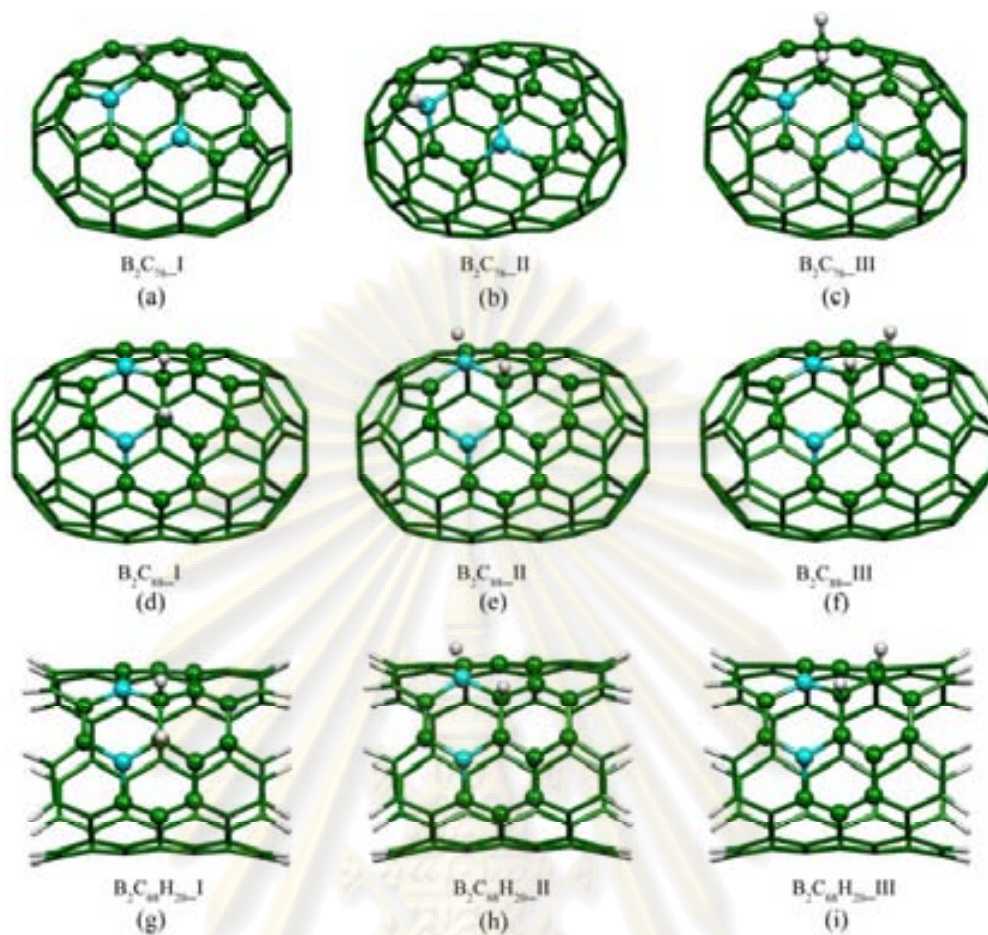


Figure 4.11 Adsorption complexes of two hydrogen-atoms adsorbed on various pristine armchair (5,5) B-doped SWCNTs (type III).

ศูนย์วิทยทรัพยากร
 จุฬาลงกรณ์มหาวิทยาลัย

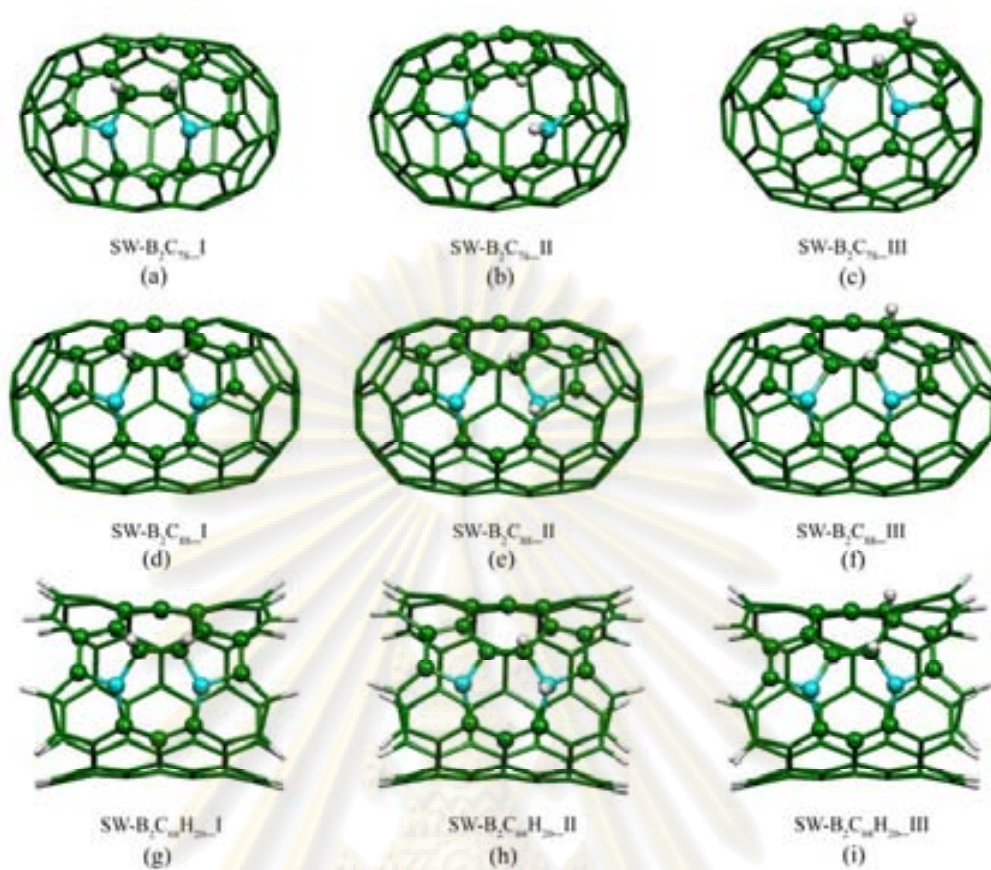


Figure 4.12 Adsorption complexes of two hydrogen-atoms adsorbed on various SW defect armchair (5,5) B-doped SWCNTs (type III).

ศูนย์วิทยทรัพยากร
จุฬาลงกรณ์มหาวิทยาลัย

Adsorption energies of hydrogen molecule adsorbed on B-doped armchair (5,5) SWCNTs of pristine and rigid structure types III are shown in Tables 4.12 and 4.13.

Table 4.12 Adsorption energies of hydrogen molecule and two proton-radicals on various pristine and SW defect armchair (5,5) B-doped SWCNTs (type III)

Complexes :	ΔE_{ads} , ONIOM(B3LYP/6-31G(d):AM1) ^a			
	Pristine SWCNTs		SW Defect SWCNTs	
	H ₂	2H [•]	H ₂	2H [•]
<i>B-doped C₈₀</i> :				
2H/B ₂ C _{78-I} ^b	-78.04	-187.82	-41.92	-151.70
2H/B ₂ C _{78-II}	-84.05	-193.82	-128.27	-238.04
2H/B ₂ C _{78-III}	-53.42	-163.20	-68.64	-178.41
<i>B-doped C₉₀</i> :				
2H/B ₂ C _{88-I}	-39.68	-149.46	-45.69	-155.46
2H/B ₂ C _{88-II}	-14.12	-95.66	-16.68	-126.46
2H/B ₂ C _{88-III}	-74.77	-184.55	-69.74	-179.52
<i>B-doped C₇₀H₂₀</i> :				
2H/B ₂ C ₆₈ H _{20-I}	-21.66	-131.43	-43.44	-153.21
2H/B ₂ C ₆₈ H _{20-II}	-11.14	-120.92	-10.44	-120.21
2H/B ₂ C ₆₈ H _{20-III}	-124.18	-233.95	-71.76	-181.53

^a In kcal/mol.

^b Adsorption site is on the C–C bond of type I.

ศูนย์วิทยทรัพยากร
จุฬาลงกรณ์มหาวิทยาลัย

Table 4.13 Interaction energies of hydrogen molecule and two proton–radicals on to various rigid structure of pristine and SW defect armchair (5,5) B-doped SWCNTs (type III)

Complexes:	ΔE_{ads} , ONIOM(B3LYP/6-31G(d):AM1) ^a			
	Pristine SWCNTs		SW Defect SWCNTs	
	H ₂	2H [•]	H ₂	2H [•]
<i>B-doped C₈₀</i> :				
2H/B ₂ C _{78-I} ^b	21.59	-131.36	55.51	-70.95
2H/B ₂ C _{78-II}	35.89	-145.66	-0.31	-126.77
2H/B ₂ C _{78-III}	11.24	-121.01	10.02	-116.44
<i>B-doped C₉₀</i> :				
2H/B ₂ C _{88-I}	20.34	-89.44	17.62	-92.16
2H/B ₂ C _{88-II}	3.17	-106.61	25.32	-84.45
2H/B ₂ C _{88-III}	35.57	-74.20	17.62	-92.16
<i>B-doped C₇₀H₂₀</i> :				
2H/B ₂ C ₆₈ H _{20-I}	21.66	-88.12	69.90	-39.88
2H/B ₂ C ₆₈ H _{20-II}	5.02	-104.75	36.04	-73.73
2H/B ₂ C ₆₈ H _{20-III}	33.44	-76.34	25.54	-84.24

^a In kcal/mol.

^b Adsorption site is on the C–C bond of type I.

In general, when foreign atom inserted in the nanotube lattice, the nanotube symmetry is altered and its structure and properties consequently change. Boron is used to be nanotube dopants because of its small atomic size and reasonable probability to enter the nanotube lattice, when boron atoms were doped to the SWCNTs they served as an electron acceptor. That makes B-doped SWCNTs not only increase adsorption energy of hydrogen molecule on pristine structure of B-doped SWCNTs but also on rigid structure of boron doped SWCNTs.

Relative adsorption abilities of hydrogen on three different doping types of B-doped SWCNTs are in the decreasing order: type III > II > I.

จุฬาลงกรณ์มหาวิทยาลัย

CHAPTER V

CONCLUSIONS

The reaction energies of chemical adsorption of hydrogen molecule on pristine and the SW defect armchair (5,5) SWCNTs of cap-ended C_{80} , C_{90} and open-ended $C_{70}H_{20}$ and their boron doped can be concluded as follows:

- (a) Hydrogen molecule can be adsorbed only on flexible structure of pristine and SW defect SWCNTs while two hydrogen atom can be chemisorbed on both flexible and rigid structure of pristine and SW defect SWCNTs by adsorption energy of flexible structures are higher than adsorption energy of rigid structure.
- (b) Relative stabilities of adsorption complexes of two hydrogen-atoms on each type of pristine SWCNTs are in order: $2H/C_{80_III} > 2H/C_{80_II} > 2H/C_{80_I}$ for C_{80} , $2H/C_{90_I} > 2H/C_{90_II}$ for C_{90} and $2H/C_{70}H_{20_I} > 2H/C_{70}H_{20_II}$ for $C_{70}H_{20}$ tubes.
- (c) Relative stabilities of adsorption complexes of two hydrogen-atoms on each type of SW defect SWCNTs are in order: $2H/SW-C_{80_III} > 2H/SW-C_{80_II} > SW-C_{80_I}$ for $SW-C_{80}$, $2H/SW-C_{90_I} > 2H/SW-C_{90_II}$ for $SW-C_{90}$ and $2H/SW-C_{70}H_{20_I} > 2H/SW-C_{70}H_{20_II}$ for $SW-C_{70}H_{20}$ tubes.
- (d) Addition mechanism of hydrogen molecule to C-C atoms of the SWCNTs shows that hydrogen molecule dissociations produce the two hydrogen radicals before formation of C-H bond.
- (e) Doping boron atoms can increase adsorption energy of both flexible and rigid structure of the SW defect and pristine armchair (5,5) SWCNTs.
- (f) All computational results obtained by the B3LYP/3-21G are in good agreement with by the B3LYP/6-31G(d).

Suggestions for future work

The high levels of theory such as B3LYP/3-21G and B3LYP/6-31G(d) should be employed to calculate in the adsorption mechanism of hydrogen addition to C-C bond of (5,5) SWCNTs and the calculations with the high theory for the hydrogen adsorption on the B-doped (5,5) SWCNTs are suggested to obtain their more accurate results.



ศูนย์วิจัยทรัพยากร
จุฬาลงกรณ์มหาวิทยาลัย

REFERENCES

- [1] Ross, D.K. Hydrogen storage: The major technological barrier to the development of hydrogen fuel cell cars. *Vacuum* 80 (2006): 1084-89.
- [2] Zhao, J.; Buldum, A.; Han, J.; Lu, J.P. Gas molecule adsorption on nanotubes and their bundles. *Nanotechnology* 13 (2002): 195-200.
- [3] Dillon, A.C.; Jones, K.M.; Bekkedahl, T.A.; Kiang, C.H.; Bethune, D.S.; Heben, M.J.; Storage of hydrogen in single-walled carbon nanotubes. *Nature* 386 (1997): 377-9.
- [4] Nikitin, A.; Ogasawara, H.; Mann, D.; Denecke, R.; Zhang, Z.; Dai, H.; Cho, K.; Nilsson, A. Hydrogenation of single-walled carbon nanotubes. *Phys. Rev. Lett.* 95 (2005): 225507/1-4.
- [5] Ye, Y.; Ahn, C.C.; Witham, C.; Fultz, B.; Liu, J.; Rinzler, A.G.; Colbert, D.; Smith, K.A.; Smalley, R.E. Hydrogen adsorption and cohesive energy of single-walled carbon nanotubes. *Appl. Phys. Lett.* 74 (1999): 2307-9.
- [6] Liu, C.; Fan, Y.Y.; Liu, M.; Cong, H.T.; Cheng, H.M.; Dresselhaus, M.S. Hydrogen storage in single-walled carbon nanotubes at room temperature. *Science* 286 (1999): 1127-9.
- [7] Chen, P.; Wu, X.; Lin, J.; Tan, K.L. High H₂ uptake by alkali-doped carbon nanotubes under ambient pressure and moderate temperatures. *Science* 285 (1999): 91-3.
- [8] Wang, Q.; Johnson, J.K.J. Optimization of carbon nanotube arrays for hydrogen adsorption. *J. Phys. Chem. B* 103 (1999): 4809-13.
- [9] Barone, V.; Heyd, J.; Scuseria, S.E.J. Interaction of atomic hydrogen with single-walled carbon nanotubes: A density functional theory study. *J. Chem. Phys.* 120 (2004): 7169-73.
- [10] Li, J.; Furuta, T.; Goto, H.; Ohashi, T.; Fujiwara, Y.; Yip, S.J. Theoretical evaluation of hydrogen storage capacity in pure carbon nanostructures. *J. Chem. Phys.* 119 (2003): 2376-85.
- [11] Arellano, J.S.; Molina, L.M.; Rubio, A.; Lopez, M.J.; Alonso, A.J. Interaction of molecular and atomic hydrogen with (5,5) and (6,6) single-wall carbon nanotubes. *J. Chem. Phys.* 117 (2002): 2281-88.

- [12] Bauschlicher Jr., C.W.; So, C.R. High coverages of hydrogen on (10,0), (9,0) and (5,5) carbon nanotubes. *Nano. Lett.* 2 (2002): 337–41.
- [13] Rafii-Tabar, H. Computational modeling of thermo-mechanical and transport properties of carbon nanotubes. *Physics Report* 390 (2004): 235-452.
- [14] Saito, R.; Fujita, M.; Dresselhaus, M.S. Electronic structure of chiral graphene tubules. *Appl. Phys. Lett.* 60 (18) 1992: 2204-06.
- [15] Curtarolo, S.; Gatica, S.M.; Cole, M.W. Uptake of gases in bundles of carbon nanotubes. *Phys. Rev. B* 62 (2000): 2173-80.
- [16] Zhao, J.; Buldum, A.; Han, J.; Lu, J.P. Gas molecule adsorption in carbon nanotubes and nanotube bundles. *Nanotechnology* 13(2002): 195-200.
- [17] Calbi, M.M.; Toigo, F.; Cole, M.W. Dilation-induced phases of gases absorbed within a bundle of carbon nanotubes. *Phys. Rev. Lett* 8 (2001): 5062-65.
- [18] Darkrim, F.L.; Malbrunot, P.; Tartaglia, G.P. Review of hydrogen storage by adsorption in carbon nanotubes. *Int. J. Hydrogen Energy* 27 (2002): 193–202.
- [19] Yang, H.T; Yang, L.; Chen, J.; Dong, J. Antiresonance effect due to Stone–Wales defect in carbon nanotubes. *Appl. Phys. Lett.* 325 (2004): 287–93.
- [20] Zhou, L.G.; Shi, S.Q. Formation energy of Stone–Wales defects in carbon nanotubes. *Appl. Phys. Lett.* 83 (2003): 1222–4.
- [21] Jiang, H.; Feng, X.Q.; Huang, Y.; Hwang, K.C.; Wu, P.D. Defect nucleation in carbon nanotubes under tension and torsion: Stone–Wales transformation. *Comput. Methods Appl. Mech. Engrg.* 193 (2004): 3419–29.
- [22] Seifert, G. Hydrogen on and in carbon nanostructures. *Solid State Ion* 168 (2004): 265–9.
- [23] Sankaran, M.; Viswanathan, B. Hydrogen storage in boron substituted carbon nanotubes. *Carbon* 45 (2007): 1628-1635.
- [24] Zhen, Z.; Xueping, G.; Jie, Y.; Deying, S. Doping effects of B and N on hydrogen adsorption in single-walled carbon nanotubes through density functional calculations. *Carbon* 44 (2006): 939-947.
- [25] Wu, X.B.; Chen, P.; Lin, J.; Tan, K.L. Hydrogen uptake by carbon nanotubes. *Int. J. Hydrogen Energy* 25 (2000): 261-5.

- [26] Bettinger, H.F. The reactivity of defects at the sidewalls of single-walled carbon nanotubes: The Stone-Wales defect. *J. Phys. Chem. B* 109 (2005): 6922-4.
- [27] Zhen, Z.; Jijun, Z.; Zhongfang, C.; Xueping, G.; Tianying, Y.; Bin, W.; Paul von, R. Comparative study of hydrogen adsorption on carbon and BN nanotubes. *J. Phys. Chem. B* 110 (2006): 13363-9.
- [28] Gayathri, V.; Geetha, R. Hydrogen adsorption in defected carbon nanotubes. *Adsorption* 13 (2007): 53-9.
- [29] Dinadayalane, T.C.; Leszczynski, J. Stone-Wales defects with two different orientations in (5,5) single-walled carbon nanotubes: A theoretical study. *Chem. Phys. Lett.* 434 (2007): 86-91.
- [30] Dinadayalane, T.C.; Kaczmarek, A.; Lukaszewicz, J.; Leszczynski, J. Chemisorption of hydrogen atoms on the sidewalls of armchair single-walled carbon nanotubes. *J. Phys. Chem. C* 111 (2007): 7376-83.
- [31] Foresman, J.B. Exploring chemistry with electronic structure methods. Revision D.02, Pittsburg, PA: Gaussian, 1996.
- [32] Jensen, F. Introduction to computational chemistry. Chichester: John Wiley & Sons, 1999.
- [33] Becke, D. A. Density-Functional Thermochemistry .3. the Role of Exact exchange. *J. Chem. Phys.* 98 (1993): 5648-52
- [34] Lewars, E. Computational chemistry: Introduction to the theory and applications of molecular and quantum mechanics. Ontario: Trent University: Peter-borough, 2003.
- [35] Dapprich, S.; Komaro, I.; Byun, K.S.; Marokuma, K.; Frisch, M.J. A new ONIOM implementation in Gaussian 98. Part I. The calculation of energies, gradients, vibrational frequencies and electronic field derivatives. *J. of Molecular structure(Theochem)* 461-2 (1999) 1-21.
- [36] Levine, I. N. Quantum chemistry. New York: Prentice-Hall, 2000.
- [37] Han S.S.; Lee H.M. Adsorption properties of hydrogen on (10,0) single-walled carbon nanotube through density functional theory. *Carbon* 42 (2004): 2169-77.
- [38] Frisch MJ et al., J. A. Gaussian 03. Revision B.03. Pittsburgh PA: Gaussian, 2003.

- [39] Schaftenaar, G. MOLDEN 4.2 CAOS/CAMM. Nijmegen, Netherlands: Center Nijmegen, Toernooiveld, 1991.
- [40] Flükiger, P.; Lüthi, P. H.; Portmann, S.; Weber, J. MOLEKEL 4.3. Manno (Switzerland): Swiss Center for Scientific Computing, 2000.



ศูนย์วิทยทรัพยากร
จุฬาลงกรณ์มหาวิทยาลัย

APPENDIX



ศูนย์วิทยทรัพยากร
จุฬาลงกรณ์มหาวิทยาลัย

APPENDIX A

Table A-1 Total energy of the isolated bare tubes of pristine and SW-defect SWCNTs calculated by method B3LYP/3-21G and B3LYP/6-31G(d)

Complexes:	Total Energy (E_{total}) ^a	
	B3LYP/3-21G	B3LYP/6-31G(d)
<i>Pristine:</i>		
C ₈₀ _isolated	-3031.497517	-3048.386745
C ₉₀ _isolated	-3410.516111	-3429.520467
C ₇₀ H ₂₀ _isolated	-2664.728293	-2679.551355
<i>Defect:</i>		
SW-C ₈₀ _isolated	-3031.345674	-3048.236913
SW-C ₉₀ _isolated	-3410.376985	-3429.381710
SW-C ₇₀ H ₂₀ _isolated	-2664.648379	-2679.475749

^a In a.u.**Table A-2** Total energy and relative energy of various pristine and SW-defect armchair (5,5) B-doped SWCNTs (type I)

Complexes	Pristine SWCNTs		SW Defect SWCNTs	
	Total Energy (E_{total}) ^a	Relative energy (ΔE_{rel}) ^b	Total Energy (E_{total}) ^a	Relative energy (ΔE_{rel}) ^b
<i>B-doped C₈₀:</i>				
2H/B ₂ C ₇₈ -I ^c	-588.775532	0.28	-590.311129	49.89
2H/B ₂ C ₇₈ -II	-588.764141	7.43	-590.353476	23.32
2H/B ₂ C ₇₈ -III	-588.775980	0.00	-590.390640	0.00
<i>B-doped C₉₀:</i>				
2H/B ₂ C ₈₈ -I	-588.637528	13.81	-588.475586	40.49
2H/B ₂ C ₈₈ -II	-588.659529	0.00	-588.540109	0.00
2H/B ₂ C ₈₈ -III	-588.642016	10.99	-588.499994	25.17
<i>B-doped C₇₀H₂₀:</i>				
2H/B ₂ C ₆₈ H ₂₀ -I	-589.679365	11.17	-589.577860	51.13
2H/B ₂ C ₆₈ H ₂₀ -II	-589.697159	0.00	-589.632301	16.97
2H/B ₂ C ₆₈ H ₂₀ -III	-589.686438	6.73	-589.659348	0.00

^a In a.u.^b In kcal/mol.^c Adsorption site is on the C-C bond of type I.

Table A-3 Total energy and relative energy of rigid structures of pristine and SW-defect armchair (5,5) B-doped SWCNTs (type I)

Complexes	Pristine SWCNTs		SW Defect SWCNTs	
	Total Energy (E_{total}) ^a	Relative energy (ΔE_{rel}) ^b	Total Energy (E_{total}) ^a	Relative energy (ΔE_{rel}) ^b
<i>B-doped C₈₀</i> :				
2H/B ₂ C _{78-I} ^c	-588.719555	29.50	-590.246854	56.59
2H/B ₂ C _{78-II}	-588.720680	28.80	-590.293518	27.30
2H/B ₂ C _{78-III}	-588.766572	0.00	-590.337031	0.00
<i>B-doped C₉₀</i> :				
2H/B ₂ C _{88-I}	-588.622581	5.36	-588.398767	42.52
2H/B ₂ C _{88-II}	-588.631127	0.00	-588.466530	0.00
2H/B ₂ C _{88-III}	-588.583432	29.93	-588.438213	17.77
<i>B-doped C₇₀H₂₀</i> :				
2H/B ₂ C ₆₈ H _{20-I}	-589.651826	0.00	-589.501170	66.90
2H/B ₂ C ₆₈ H _{20-II}	-589.607777	27.64	-589.607777	0.00
2H/B ₂ C ₆₈ H _{20-III}	-589.593169	36.81	-589.593169	9.17

^a In a.u.^b In kcal/mol.^c Adsorption site is on the C–C bond of type I.**Table A-4** Total energy and relative energy of various pristine and SW-defect armchair (5,5) B-doped SWCNTs (type II)

Complexes	Pristine SWCNTs		SW Defect SWCNTs	
	Total Energy (E_{total}) ^a	Relative energy (ΔE_{rel}) ^b	Total Energy (E_{total}) ^a	Relative energy (ΔE_{rel}) ^b
<i>B-doped C₈₀</i> :				
2H/B ₂ C _{78-I} ^c	-591.658367	0.00	-588.663200	32.80
2H/B ₂ C _{78-II}	-591.600870	36.08	-588.655056	37.91
2H/B ₂ C _{78-III}	-591.639930	11.57	-588.715462	0.00
<i>B-doped C₉₀</i> :				
2H/B ₂ C _{88-I}	-588.603718	42.46	-588.476292	33.41
2H/B ₂ C _{88-II}	-588.598093	45.99	-588.503868	16.11
2H/B ₂ C _{88-III}	-588.671376	0.00	-588.529540	0.00
<i>B-doped C₇₀H₂₀</i> :				
2H/B ₂ C ₆₈ H _{20-I}	-589.655791	38.80	-589.580580	36.38
2H/B ₂ C ₆₈ H _{20-II}	-589.637086	50.54	-589.594711	27.52
2H/B ₂ C ₆₈ H _{20-III}	-589.717629	0.00	-589.638563	0.00

^a In a.u.^b In kcal/mol.^c Adsorption site is on the C–C bond of type I.

Table A-5 Total energy and relative energy of rigid structures of pristine and SW-defect armchair (5,5) B-doped SWCNTs (type II)

Complexes	Pristine SWCNTs		SW Defect SWCNTs	
	Total Energy (E_{total}) ^a	Relative energy (ΔE_{rel}) ^b	Total Energy (E_{total}) ^a	Relative energy (ΔE_{rel}) ^b
<i>B-doped C₈₀</i> :				
2H/B ₂ C _{78-I} ^c	-591.574251	9.79	-588.595485	31.80
2H/B ₂ C _{78-II}	-591.589853	0.00	-588.646169	0.00
2H/B ₂ C _{78-III}	-591.506600	52.24	-588.597871	30.31
<i>B-doped C₉₀</i> :				
2H/B ₂ C _{88-I}	-588.543197	43.13	-588.365802	78.90
2H/B ₂ C _{88-II}	-588.591543	12.79	-588.491545	0.00
2H/B ₂ C _{88-III}	-588.611926	0.00	-588.460584	19.43
<i>B-doped C₇₀H₂₀</i> :				
2H/B ₂ C ₆₈ H _{20-I}	-589.573447	49.41	-589.508216	26.18
2H/B ₂ C ₆₈ H _{20-II}	-589.585078	42.12	-589.549940	0.00
2H/B ₂ C ₆₈ H _{20-III}	-589.652194	0.00	-589.517590	20.30

^a In a.u.^b In kcal/mol.^c Adsorption site is on the C–C bond of type I.**Table A-6** Total energy and relative energy of various pristine and SW-defect armchair (5,5) B-doped SWCNTs (type III)

Complexes	Pristine SWCNTs		SW Defect SWCNTs	
	Total Energy (E_{total}) ^a	Relative energy (ΔE_{rel}) ^b	Total Energy (E_{total}) ^a	Relative energy (ΔE_{rel}) ^b
<i>B-doped C₈₀</i> :				
2H/B ₂ C _{78-I} ^c	-591.678628	0.00	-588.660137	39.75
2H/B ₂ C _{78-II}	-591.632305	29.07	-588.702602	13.10
2H/B ₂ C _{78-III}	-591.607222	44.81	-588.723478	0.00
<i>B-doped C₉₀</i> :				
2H/B ₂ C _{88-I}	-588.684252	0.00	-588.496812	34.06
2H/B ₂ C _{88-II}	-588.624268	37.64	-588.490274	38.16
2H/B ₂ C _{88-III}	-588.681193	1.92	-588.551090	0.00
<i>B-doped C₇₀H₂₀</i> :				
2H/B ₂ C ₆₈ H _{20-I}	-589.718876	8.13	-589.590312	36.38
2H/B ₂ C ₆₈ H _{20-II}	-589.664951	41.97	-589.568526	50.06
2H/B ₂ C ₆₈ H _{20-III}	-589.731833	0.00	-589.648295	0.00

^a In a.u.^b In kcal/mol.^c Adsorption site is on the C–C bond of type I.

Table A-7 Total energy and relative energy of rigid structures of pristine and SW-defect armchair (5,5) B-doped SWCNTs (type III)

Complexes	Pristine SWCNTs		SW Defect SWCNTs	
	Total Energy (E_{total}) ^a	Relative energy (ΔE_{rel}) ^b	Total Energy (E_{total}) ^a	Relative energy (ΔE_{rel}) ^b
<i>B-doped C₈₀:</i>				
2H/B ₂ C _{78-I} ^c	-591.547097	14.30	-588.583453	55.82
2H/B ₂ C _{78-II}	-591.569886	0.00	-588.672409	0.00
2H/B ₂ C _{78-III}	-591.530597	24.65	-588.655940	10.33
<i>B-doped C₉₀:</i>				
2H/B ₂ C _{88-I}	-588.616444	17.17	-588.477308	0.00
2H/B ₂ C _{88-II}	-588.643806	0.00	-588.465030	7.70
2H/B ₂ C _{88-III}	-588.592167	32.40	-588.477308	0.00
<i>B-doped C₇₀H₂₀:</i>				
2H/B ₂ C ₆₈ H _{20-I}	-589.652679	16.64	-589.496977	44.36
2H/B ₂ C ₆₈ H _{20-II}	-589.679192	0.00	-589.550927	10.50
2H/B ₂ C ₆₈ H _{20-III}	-589.633909	28.42	-589.567667	0.00

^a In a.u.^b In kcal/mol.^c Adsorption site is on the C-C bond of type I.**Table A-8** Total energy and relative energy of pristine perfect and SW-defect SWCNTs calculated by method ONIOM(B3LYP/6-31G(d):AM1)

Complexes:	Pristine SWCNTs		SW Defect SWCNTs	
	Total Energy (E_{total}) ^a	Relative energy (ΔE_{rel}) ^b	Total Energy (E_{total}) ^a	Relative energy (ΔE_{rel}) ^b
2H/C _{80-I} ^c	-615.246441	24.14	-615.153933	0.00
2H/C _{80-II}	-615.248800	22.66	-615.116451	23.52
2H/C _{80-III}	-615.284904	0.00	-615.123919	18.83
2H/C _{90-I}	-615.176324	0.00	-615.031889	0.00
2H/C _{90-II}	-615.134481	26.26	-614.958356	46.14
2H/C ₇₀ H _{20-I}	-616.220097	0.00	-616.138681	0.00
2H/C ₇₀ H _{20-II}	-616.189702	19.07	-616.057789	50.76

^a In a.u.^b In kcal/mol.^c Adsorption site is on the C-C bond of type I.

Table A-9 Adsorption energy of hydrogen molecule and two hydrogen atom to pristine perfect and SW-defect SWCNTs calculated by method ONIOM(B3LYP/6-31G(d):AM1)

Complexes:	Pristine SWCNTs		SW Defect SWCNTs	
	2H ^a	H ₂ ^a	2H ^a	H ₂ ^a
2H/C _{80-I} ^b	-32.52	-142.29	-51.91	-161.68
2H/C _{80-II}	-33.66	-143.43	-53.86	-163.64
2H/C _{80-III}	-52.55	-162.32	-38.87	-148.65
2H/C _{90-I}	-58.05	-167.82	-49.27	-159.04
2H/C _{90-II}	-42.47	-152.24	-2.04	-111.81
2H/C ₇₀ H _{20-I}	-52.06	-161.83	-49.14	-158.91
2H/C ₇₀ H _{20-II}	-48.18	-157.96	-17.83	-127.60

^a In kcal/mol.

^b Adsorption site is on the C–C bond of type I.

Table A-10 Total energy and relative energy of rigid structures of pristine and SW-defect SWCNTs calculated by method ONIOM(B3LYP/6-31G(d):AM1)

Complexes:	Pristine SWCNTs		SW Defect SWCNTs	
	Total Energy (E _{total}) ^a	Relative energy (ΔE _{rel}) ^b	Total Energy (E _{total}) ^a	Relative energy (ΔE _{rel}) ^b
2H/C _{80-I} ^c	-615.149544	30.41	-615.072768	11.01
2H/C _{80-II}	-615.160582	23.49	-615.007342	52.07
2H/C _{80-III}	-615.198011	0.00	-615.090313	0.00
2H/C _{90-I}	-615.083622	0.00	-614.944193	0.00
2H/C _{90-II}	-615.016228	42.29	-614.917590	16.69
2H/C ₇₀ H _{20-I}	-616.123381	0.00	-616.044333	0.00
2H/C ₇₀ H _{20-II}	-616.053958	43.56	-615.950598	58.82

^a In a.u.

^b In kcal/mol.

^c Adsorption site is on the C–C bond of type I.

Table A-11 Adsorption energy of hydrogen molecule and two hydrogen atom to rigid structure of pristine and SW-defect SWCNTs calculated by method ONIOM(B3LYP/6-31G(d):AM1)

Complexes:	Pristine SWCNTs		SW Defect SWCNTs	
	2H ^a	H ₂ ^a	2H ^a	H ₂ ^a
2H/C _{80-I} ^b	75.34	-34.44	45.36	-64.41
2H/C _{80-II}	68.41	-41.36	86.42	-23.36
2H/C _{80-III}	44.92	-64.85	34.35	-75.42
2H/C _{90-I}	48.57	-61.20	58.40	-51.37
2H/C _{90-II}	90.86	-18.91	75.09	-34.68
2H/C ₇₀ H _{20-I}	56.72	-53.05	67.00	-42.77
2H/C ₇₀ H _{20-II}	100.29	-9.49	125.82	16.05

^a In kcal/mol.

^b Adsorption site is on the C-C bond of type I.

ศูนย์วิทยทรัพยากร
จุฬาลงกรณ์มหาวิทยาลัย

VITA

NAME: Ms. Kwanchanok Donsamer

BIRTH DATE: December 7th, 1983

BIRTH PLACE: Surin, Thailand

EDUCATION: 2002-2005: B.Sc. (Industrial Chemistry), Kasetsart University, Thailand
2006-2008: M.Sc. (Petrochemistry and Polymer Science), Chulalongkorn University, Thailand

ADDRESS: 85/84 Changwattana Rd., Pakred, Nonthaburi 11120, Thailand

Tel: 089-107-1983

E-MAIL: k_donsamer@yahoo.com

PRESENTATION: Kwanchanok Donsamer, Vithaya Ruangpornvisuti, Chemisorption of hydrogen on pristine and Stone–Wales defect armchair (5,5) SWCNTs of cap-ended C₈₀, C₉₀ and open-ended C₇₀H₂₀ and their boron-doped SWCNTs (Poster Session): 10th National Graduate Research Conference, 11-12 September 2008. Sukhothai Thammathirat Open University, Nonthaburi, Thailand